

“A Study of Flow of Biofluids”

A Thesis

Submitted to



University of Kota, Kota

for the award of the degree

Doctor of Philosophy

in

Mathematics

(Faculty of Science)

By

Manoj Kumar Gupta

Department of Mathematics

Government College, Kota (Rajasthan)

Under the Supervision of:

Dr. Manish Gaur

Department of Mathematics

Govt. College, Kota (Rajasthan)

University of Kota, Kota (Rajasthan)

2015

ACKNOWLEDGEMENT

The entire investigations and the observations taken in the research work have been completely carried out by me under the guidance of Dr. Manish Gaur, Department of Mathematics, Government College, Kota (Rajasthan). I am highly indebted and grateful to him for his constant encouragements, vigorous supervisions and the great patience with which he answered my all queries and cleared my doubts without which I would not be able to successfully complete my thesis.

I would also like to express my heartiest gratitude from the deepest core of my heart to Dr. Arun Kumar, Department of Mathematics, Government College, Kota (Rajasthan) for his kind valuable suggestions which helped me a lot in preparing the summery reports and giving shape to my thesis.

I also acknowledge my gratitude to the Principal, Government College, Kota (Rajasthan) for providing all the facilities to me required to carry out the research work.

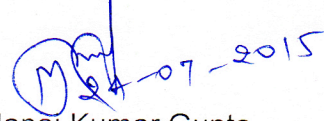
I am heartily grateful to the staff and the faculty members, my seniors and my fellow research scholars of the Department of Mathematics, Government College, Kota (Rajasthan) for their constant encouragement.

I also take this opportunity to give thanks to the officials of libraries of Government College, Kota (Rajasthan), University of Kota, Kota (Rajasthan), central libraries of I.I.T., Delhi and I.I.T., Kanpur which helped me greatly to find the relevant literatures.

Many heartiest thanks are due to my all the friends and well wishers who consistently inspired me to touch the new academic heights but I would like to take this opportunity to thank specially Mr. Santosh Dubey, Mr. Pradeep Varshaney, Mr. Abhishek Divoliya, Mr. Dharmendra Singh Sengar, Mr. Shivendra Singh Patel, Mr. Vijay Singh Sengar, Mr. Gandharva Singh Tomar, Mrs. Antima Patel, Mr. Sachin Kumar Gupta, Mr. Alok Gupta, Dr. Narendra Kumar, Dr. G.C. Shukla, Mr. Yashpal Yadav, Mr. Shalabh Agrawal, Mr. Avaneesh Kumar, Mr. Yatendra Singh Pundhir and Mr. Tarun Mathur.

This acknowledgement will be incomplete without owing my heartiest sincere gratitude to the Almighty God for His blessings and to my loving parents Mr. Ram Awatar Gupta and Mrs. Champa Gupta, my wife Mrs. Sarika Gupta, my son Master Krish Kumar Gupta and my all relatives who always encouraged, showed firm faith in me and irrigated the plant of my success with the water of their well wishes.

Kota



Manoj Kumar Gupta,
Ph.D. Scholar,
Department of Mathematics,
Government College, Kota
Rajasthan.

In the loving memories of my

Grand Father

Late Shri Ram Saran Prasad

Grand Mother

Late Smt. Bela Devi

Maternal Grand Mother

Late Smt. Shyama Devi

&

Elder Sister

Late Ms. Sudha Gupta

who left us untimely.

Dedicated to

My Parents

Mr. Ram Awatar Gupta

and

Mrs. Champa Gupta

who dreamed an Excellence for me

&

My Wife

Mrs. Sarika Gupta

and

Son

Master Krish Kumar Gupta

who inspired me to put a step forward to
realize my parents' dream.

LIST OF RESEARCH PAPERS PUBLISHED

The present thesis entitled **“A Study of Flow of Biofluids”** consists of the following research papers published in various international journals:

1. **“A Casson fluid model for the steady flow through a stenosed blood vessel”**, British J. Math. Comp. Sc., Vol. 4, Issue 11, pp. 1629 – 1641, 2014.
2. **“Slip effects on steady flow through a stenosed blood artery”**, Int. J. Sci. Engg. Res., Vol. 5, Issue 2, pp. 753 – 758, 2014.
3. **“Unsteady slip flow of blood through constricted artery”**, Adv. Appl. Sci. Res., Vol. 6, Issue 1, pp. 49 – 58, 2015.
4. **“Biomagnetic steady flow through an axisymmetric Stenosed artery”**, IJIAS, Vol. 8, No. 1, pp. 394 – 407, 2014.
5. **“Steady slip blood flow through a stenosed porous artery”**, Adv. Appl. Sci. Res., Vol. 5, Issue 5, pp. 249 – 259, 2014.

SUPERVISOR'S CERTIFICATE

It is certified that

- (i) The thesis entitled "A STUDY OF FLOW OF BIOFLUIDS" submitted by Mr. **Manoj Kumar Gupta** is an original piece of research work carried out by him under my supervision.
- (ii) The literary presentation is satisfactory and the thesis is in a form suitable for publication.
- (iii) The work evidences the capacity of the candidate for critical examination and independent judgment.
- (iv) He has put in at least 200 days of attendance every year.

Date: 24-07-2015



Dr. Manish Gaur
Department of Mathematics
Government College
Kota (Rajasthan).

INDEX

Chapter	Title	Page No.
1.	Introduction	1 - 13
2.	A Casson Fluid Model for the Steady Flow through a Stenosed Blood Vessel	14 - 33
3.	Slip Effects on Steady Flow through a Stenosed Blood Artery	34 - 50
4.	Unsteady Slip Flow of Blood through Constricted Artery	51 - 68
5.	Biomagnetic Steady Flow through an Axisymmetric Stenosed Artery	69 - 88
6.	Steady Slip Blood Flow through a Stenosed Porous Artery	89 - 106
7.	References	107 - 118

CHAPTER - 1
Introduction

Biomathematics:

The term “Biomathematics” which in general stands for the Mathematical Biosciences; has a deep root and its literature can be found in abundance in different journals with varying areas. Some other terms such as Theoretical Biology, Mathematical Biology or Mathematical Life Sciences are also in practice. But the term “Biomathematics” is the most appropriate term as it covers a wider area.

This subject has been contributed by mathematicians, statisticians, physicists, zoologists, botanists, computer experts, physiologists, demographers, medical scientists and engineers etc.

Various models in Biomathematics are studied. Some of them are mentioned below:

- i. Demographic Models
- ii. Genetic Models
- iii. Models in Epidemiology
- iv. Mathematical Models for Synovial Joints
- v. Mathematical Models in Pharmacokinetics
- vi. Optimization Models in Biological and Medical Sciences
- vii. Mathematical Models for Blood Flow

In addition to the above mentioned models in biosciences, there are still many areas which need to be treated mathematically and our mathematical bioscientists are constantly trying to open up new areas of biosciences to have a better and deep understanding of various life forms.

Areas of Biomathematics:

In the process of expanding the areas of Biomathematics, the researchers have not restricted themselves only to the existing mathematical techniques. Rather they are now using a number of new mathematical techniques developed during the last few decades, to understand the already studied areas of mathematical biosciences. In order to make a universally acceptable model in Biomathematics, we take both the results and processes of mathematical modelling. Biomathematics has a number of disciplines e.g. Bioengineering, Mathematical Physiology, Biophysics, Mathematical Zoology, Mathematical Botany, Demography, Mathematical Genetics and Mathematical Biomechanics.

Bioengineering is concerned with the design of the appliances used in medical sciences like artificial limbs, heart – lung machines, dialysers etc.

Mathematical Physiology is the study of the conduction of current in nervous system, brain models, exchange of oxygen and carbon dioxide in human system etc.

Biophysics is the study of applications of physical concepts in biological systems using the mathematical approaches.

Mathematical Zoology deals with the micro-organism and its role in fermentation technology, population growth, removal of unwanted elements, removal of pollutants, bioconversion of solar energy etc.

Mathematical Botany is the study of problems regarding growth of cells, growth and shape of plants, nutrition intakes by plants, growth of forests etc.

Demography which is also popularly known as the **Population Dynamics**, deals with growth of population, population dispersal, effects of immigration and mixing of population, effect of age factor on the size of population etc.

Mathematical Genetics is the study of transfer of genetic features from one generation to another one carried through the action of genes.

Mathematical Biomechanics is categorized into two categories. In **Biosolid Mechanics**, stresses and strains in bones and muscles are studied while **Biofluid Dynamics** is the study of the flow of biofluids in living bodies.

Classes of Fluids:

The constitutive equations of the fluid are the functional relations between the six components of the stress tensor τ and the rate of strain tensor e which depend upon the fluid under consideration. Therefore the fluids are categorized in the following two classes given as:

(i) Newtonian Fluids:

A fluid is called a Newtonian fluid when its viscosity remains unchanged with the rate of deformation e .

The tangential stress tensor of such a viscous Newtonian fluid is given as

$$\tau = \mu e$$

(ii) Non – Newtonian Fluids:

A fluid is called a non – Newtonian fluid when its viscosity changes with the rate of deformation i.e. the coefficient of viscosity becomes the function of strain tensor e .

Various Non – Newtonian Fluid Models:

Several models have been introduced for the non – Newtonian behavior of fluids. A few of them with their constitutive equations are mentioned below:

(i) Bingham Plastic:

$$\tau = \mu e + \tau_0 \quad \text{for } \tau \geq \tau_0$$

$$e = 0 \quad \text{for } \tau \leq \tau_0$$

(ii) Ellis Fluid:

$$e = A\tau + B\tau^n \quad \text{for } \tau \geq \tau_0$$

(iii) Herschel – Bulkley Fluid:

$$\tau = \mu e^n + \tau_0 \quad \text{for } \tau \geq \tau_0$$

$$e = 0 \quad \text{for } \tau \leq \tau_0$$

(iv) Power – Law Fluid:

$$\tau = \mu e^n \quad \text{for } \tau \geq \tau_0$$

$$e = 0 \quad \text{for } \tau \leq \tau_0$$

where

$n < 1$ gives pseudo – plastic power – law fluid.

$n > 1$ gives dilatant power – law fluid.

$n = 1$ gives Newtonian viscous fluid.

(v) Prandtl Fluids:

$$\tau = A \sin^{-1}(e/c)$$

where τ_0 represents the yield stress.

(J.N. Kapur, 1985)

Casson Fluid:

Casson fluid is a non – Newtonian fluid which can be defined as a shear thinning fluid. It is assumed that the fluid has a zero viscosity at an infinite shear rate and an infinite viscosity at zero shear rate (N. Casson, 1959; R.K. Dash, 1996). Also the Casson fluid has a yield stress below which there is no flow with the following constitutive equations:

$$\tau^{1/2} = \mu^{1/2} e^{1/2} + \tau_0^{1/2} \quad \text{for } \tau \geq \tau_0$$

$$e = 0 \quad \text{for } \tau \leq \tau_0$$

where τ_0 is the yield stress.

After a number of experiments performed on blood with varying blood parameters (G.W.S. Blair, 1959; S.E. Charm et al., 1965; E.W. Merrill et al., 1965), it can be concluded that the blood flowing through small vessels (D.A. McDonald, 1974) behaves like a Casson fluid (N. Casson, 1959; Y.C. Fung, 1981) at a low rate of shear.

Composition and Functions of Blood:

Blood is composed of a suspension of cells like red blood cells (RBCs) or erythrocytes, white blood cells (WBCs) or leucocytes and platelets or thrombocytes in an aqueous solution of pale yellow

colour known as plasma. This plasma has about 90% water by weight, 7% some dissolved proteins like albumin, globulin, fibrinogen etc., 1% inorganic substances and 1% other organic substances (Y.C. Fung, 1981).

The red blood cells occupy about 50% of the total blood volume in an average man (Y.C. Fung, 1981). There are approximately 5×10^9 cells in one milliliter of healthy human blood of which 95% parts are covered by red blood cells. The red cells have the shape of a biconcave disc. They transport the oxygen from the lungs to all the other cells of the body as well as remove the carbon dioxide originated by the metabolic processes in the body. They carry oxygen by binding it with hemoglobin. (J.N. Kapur, 1985). Hemoglobin is a form of iron oxides which is present at a unique high concentration in the mature red blood cells (E.E. Tzirtzilakis, 2005)

The average life span of a red cell is approximately 120 days and the total number of erythrocytes dying per second is around 2.4×10^6 . The average volume of a red cell is 90μ cubic metre and its surface area is about 140μ square meter (J.N. Kapur, 1985).

The white blood cells cover about one – sixth or 1% of the blood volume (J.N. Kapur, 1985). There are about 5000 to 8000 white blood cells per mm^3 (Y.C. Fung, 1981). The white blood cells are classified in mainly two categories as granulocytes and agranulocytes. The granulocytes contain neutrophils, eosinophils, and basophils while agranulocytes contain monocytes and lymphocytes. The leukocytes help us to protect our body from the infections and remove the dead cells and tissue debris (L. Sherwood, 2010).

The platelets constitute about 5% of the total blood volume (J.N. Kapur, 1985). There are about 250,000 to 300,000 platelets

per mm^3 (Y.C. Fung, 1981). The platelets are very small parts (2 to 4 μm in diameter) of bone marrow cells produced by shedding off the outer edges of extraordinarily large (up to 60 μm in diameter) bone marrow cells known as megakaryocytes. One megakaryocyte produces approximately 1000 platelets. An average life of a platelet is of about 10 days. Platelets help to stop bleeding by forming a temporary plug whenever there is a leakage in the blood vessel due to any reason. Platelets also dissolve the blood clots when they are not required any longer (L. Sherwood, 2010).

Viscosity of Blood:

The blood is neither homogeneous nor Newtonian but the plasma in the state of isolation can be regarded as a Newtonian fluid whose viscosity is approximately 1.2 times of that of water which keeps on increasing with growing age (J.N. Kapur, 1985, J.N. Mazumdar, 1992).

The effective viscosity of the whole blood depends upon the shear rate and mostly on the hematocrit which represents a percentage of red blood cells in the total blood volume. The hematocrit is around 45% for men and 42% for women. According to the Fahraeus - Lindqvist effect (R. Fahraeus, 1929; R. Fahraeus and T. Lindqvist, 1931; J.H. Barbee et al. 1971), the blood viscosity also depends upon the radii of the capillaries when their diameters are less than 300 μ metre (J.N. Kapur, 1985). The apparent viscosity decreases with decreasing blood vessel diameter (Y.C. Fung, 1981).

Blood Flow Properties:

The blood flow problems in the engineering situations have been observed more complex in comparison to the general fluid problems which are due to the following reasons:

- (i) The unusual growth in the Reynold number.
- (ii) The uncommon changes in the curvatures of the blood arteries which give ways to the secondary flows for high Reynold numbers.
- (iii) Some unusual pulsatility in the blood flows because of the rhythmic actions of the heart.
- (iv) A large number of tree – like blood vessels originated from the bifurcations.
- (v) Some unexpected fluid properties arising from the different shapes of the cells and the distortions from passing through the arteries of the diameters less than their own (J.N. Kapur, 1985).

Some Other Biofluids:

1. Peristaltic Fluid:

When a progressive wave of area expansion and contraction travels along the wall of a flexible tube, the fluid of the tube is known as the peristaltic fluid. The neuro – muscular properties of a tubular smooth muscle are responsible for the motion in the peristaltic fluid. It may be Newtonian or non – Newtonian. The fluid flow can occur in either one layer or two layers i.e. a core layer and a peripheral layer. (J.N. Kapur, 1985).

2. Synovial Fluid:

The synovial fluid is a shear – dependent viscous fluid which is filled in a synovial joint cavity which is a space between two mating globular bones with ends covered with a soft sponge like material known as articular cartilage (J.N. Kapur, 1985). The fluid has hyaluronic acid which is a polysaccharide combined with protein

(Y.C. Fung, 1981). It is a light yellow coloured clear dialyzate of blood plasma having a concentration of 3.5 mg/gm hyaluronic acid molecules with a molecular weight 500,000 and the molecular length of order $5 \times 10^{-5} - 10^{-4}$ cm. The behaviour of the fluid is like that of a pseudo – plastic fluid (J.N. Kapur, 1985). The fluid is more viscous than blood due to the presence of hyaluronic acid (Y.C. Fung, 1981). Its effective viscosity keeps on varying between 100 P at 10^{-2} per sec and 10 cP at 100 per sec and depends upon the concentration of the molecules of the hyaluronic acid.

The main function of the synovial fluid is to lubricate the articulating joints so that the friction between the articular cartilage can be reduced while movement.

Generally the synovial fluid is better represented by a power – law fluid of constitutive equation $\tau = \mu e^n$ where $\mu = 4.5$ dynes-sec/cm² and $n = 0.37$.

In a diseased synovial joint, the synovial fluid is no longer a non – Newtonian fluid as the articular cartilage becomes rough and cracked. (J.N. Kapur, 1985).

Survey of literature

So far various aspects of biofluids have been extensively studied by research workers. The arterial stenosis is a common problem which the whole globe is facing. In the arterial stenosis the walls get swelled due to some unwanted fatty and fibrous tissues in the lumen of the wall which ultimately narrows the blood vessels causing different cerebral and cardiovascular problems. Various flow features through the constricted arteries under different circumstances and parameters have been studied so far.

J.R. Womersley (1955) studied the method for the calculation of velocity, rate of flow and viscous drag in arteries when the pressure

gradient is known and found a phase lag between the motion of the liquid and the pressure gradient which causes it. R.H. Haynes et al. (1959) discussed the role of the non-Newtonian behaviour of blood and concluded that the flow features of blood in perfused vascular beds are linear in the physiological working range due to which the distensibility of the vessels decides the shape of the pressure – flow curves. G.W.S. Blair (1959) gave an equation for the blood flow, plasma and serum through narrow glass tubes and observed that the larger suspended particles of blood passing through the tubes accumulate in the center making a plasma region near the walls. E.W. Merrill et al. (1963) studied the non – Newtonian rheology of human blood and found that the yield stress in the human blood exists due to the plasma protein fibrinogen. E.W. Merrill et al. (1965) investigated the pressure flow relations of human blood passing through straight and curved glass and plastic tubes. S.E. Charm et al. (1965) represented the viscometry of human blood by a number of empirical equations and used the Casson's equation to calculate the shear strength of blood. C.E. Huckaback et al. (1968) presented a generalized approach for modelling the blood flow through arteries and used the model to calculate the localized arterial wall elasticity. G.E. Saito et al. (1975) discussed the significance of viscoelasticity in arterial blood flow models and concluded that the arterial walls in single large artery models may be taken purely elastic. C.S. Peskin (1977) analyzed the blood flow in the heart numerically in the presence of moving immersed boundaries which include the muscular heart valve. B.B. Gupta et al. (1982) developed a three layer semi – empirical model for blood flow and other particular suspensions in narrow tubes with a thin cell - free layer, cell depleted one and a central core with uniform cell concentration. V.K. Sud et al. (1985) studied the flow variables of blood flow in single large arteries by subjecting it to the pulsating pressure gradient and externally – imposed body accelerations. N.

Rudraiah (1985) investigated the steady laminar flow of blood through a parallel plate channel bounded below by a porous layer of finite thickness and bounded above by a rigid impermeable plate moving with a uniform velocity and concluded that the finite thickness of porous layer affects the blood flow only for larger values of viscosity factor and small values of the porous parameter. R.E. Larson et al. (1986) studied the microscopic axial flow through infinite and semi – infinite lattices of cylindrical inclusions and examined the influence of lattice geometry and inclusion shape on the permeability and surface flow. R.E. Larson et al. (1987) studied the microscopic transverse flow through infinite and semi – infinite periodic lattices of cylindrical inclusions. J.C. Misra et al. (1988) gave a mathematical analysis of blood flow under a periodic acceleration field under two cases: in one case, the arterial wall is taken as the orthotropic elastic cylindrical membrane and in another case, the wall tissues are taken to exhibit the experimentally observed material damping properties. P. Chaturani et al. (1990) discussed a Casson fluid model for the pulsatile nature of blood flow under an action of periodic body acceleration. Y.I. Cho et al. (1991) investigated the effects of the non – Newtonian viscosity of blood on a flow through a coronary arterial casting and observed that this effect on the overall pressure drop is significant for a flow with Reynolds number 100 or less. J.M. Huyghe et al. (1992) described a porous medium model of the beating left ventricle which included the torsion around the axis of symmetry of ventricle, transmural variation of fiber angle and redistribution of intracoronary blood in the myocardial wall. B. Das et al. (1995) studied the non – Newtonian flow of blood in an arteriosclerotic blood vessel with rigid permeable walls and found that the wall permeability significantly affects the flow resistance and wall shear stress. R.K. Dash et al. (1997) investigated the influence of yield stress on the flow variables of Casson fluid in a homogeneous porous medium

bounded by a circular tube and concluded that the minimum pressure gradient to start the flow is independent of the permeability of the porous medium and is equal to the yield stress of the fluid. R. Usha et al. (1999) presented a particle fluid suspension model for the pulsatile blood flow under the effect of periodic body acceleration and found that the amplitude of instantaneous flow rate due to body acceleration decreases with decrease in the tube radius. P. Nardinocchi et al. (2005) developed a continuum model for a vascular segment to investigate the blood – vessel interactions in a finite arterial segment of the cardiovascular tree. Y. Huo et al. (2006) presented a Womersely type mathematical model to study the pulsatile blood flow in diastole in the absence of vessel tone in the entire coronary arterial tree. N. Westerhof et al. (2006) discussed the mechanical aspects of cross talk between cardiac muscle and coronary vasculature including the extracellular matrix and noticed that the influence of cardiac muscle on the coronary vasculature depends upon the changes in muscle length but seems to be very small. J. Jung et al. (2006) simulated the blood flow patterns and particulate build up by applying the multiphase non – Newtonian principle of dense suspension hemodynamics in a realistic right coronary artery having various cross – sections and found that the increase in the initial plasma viscosity causes the decrease in wall shear stress. J. Chen et al. (2006) applied the Carreau– Yasuda model to study the pulsatile non – Newtonian blood flow in a bifurcation model with a non- planar daughter branch and showed that the non – planarity deflects the blood flow from the inner wall of the vessel to the outer wall. F. Song et al. (2007) used the microcirculation method or porous flow model to study the blood and tissue liquid flow and showed that the more threshold stress causes the greater flow resistance. V.P. Srivastava (2007) proposed a two – fluid theoretical model with a core region of suspension of all the erythrocytes in plasma and a peripheral layer

of cell-free plasma in small diameter tubes. P.K. Mandal et al. (2007) studied the influence of externally imposed periodic body accelerations on unsteady pulsatile flow of a power – law fluid through a stenosed artery of elastic walls. J. Spaan et al. (2008) studied the coronary structure which is responsible for the blood circulation through the heart muscle and observed that the perfusion of the myocardium can be affected by the microvascular diseases or by the arterial stenosis. V.M. Calo et al. (2008) used a multiphysics mathematical model to represent the blood flow and drug transport in patient specific coronary arteries taking arterial walls as a linear poroelastic medium and drug delivery as a scalar advection – diffusion equation. D.S. Sankar et al. (2010) studied the two – fluid model to discuss the unsteady blood flow through stenosed tapered arteries with the suspension of all the erythrocytes as a Herschel – Bulkley fluid in the core region and the plasma in the peripheral layer and found that the flow rate decreases with the increase in the tapering angle. J.C. Misra et al. (2011) developed a mathematical model to study the blood flow through a porous artery with two stenoses under the influence of externally imposed magnetic field. I.M. Eldesoky (2012) discussed the slip effects on the unsteady pulsatile flow of blood through porous medium under externally applied periodic body accelerations and magnetic field and observed that the Knudsen number of slip condition greatly affects the blood flow. S. Pramanik (2014) investigated the flow and heat transfer of a Casson fluid towards an exponentially permeable stretching surface with thermal radiation which enhances the effective thermal diffusivity.

CHAPTER - 2

A Casson Fluid Model for the Steady Flow through a Stenosed Blood Vessel

A CASSON FLUID MODEL FOR THE STEADY FLOW THROUGH A STENOSED BLOOD VESSEL

2.1 Introduction

Many researchers have now established this fact that stenosis is causing a number of deaths in several countries and this problem needs to be dealt seriously. In a stenosed artery, the wall thickens because of an abnormal development along the lumen of the wall which in turn; affects the hemodynamic behaviour of the blood flow. According to medical experts, the blood vessel narrows when the macrophage white blood cells gather near the arterial wall; and the fat and cholesterol from the macrophages are not sufficiently removed by the High Density Lipoproteins. It has been observed that the blood behaves like a Newtonian fluid at high shear rate and it behaves like a non – Newtonian fluid at low shear rate due to which it requires a certain yield stress for smooth flow. So far various mathematical models have been proposed by many researchers to study the different features of the blood.

S. Rodbard (1966) studied the dynamics of blood flow in stenotic lesions. D.F. Young (1968) analyzed the effect of an axially symmetric time-dependent growth into the lumen of a tube of constant cross-section on the steady flow of a Newtonian fluid. P. Chaturani and D. Biswas (1983) made a theoretical study of blood flow through stenosed artery with slip velocity at wall. S. Chakravarty (1987) studied the effects of stenosis on the flow behaviour of blood in an artery. N.P. Smith et al. (2002) presented an anatomically based model of transient coronary blood flow through an artery with mild stenosis viz. two – layered model for different shapes of stenosis and slip velocity at the wall. B.K. Mishra

et al. (2008) studied the effect of resistance parameter on uniform and non – uniform portion of artery for non – Newtonian fluid model of blood flow through an arterial stenosis. B. Singh et al. (2010) explored blood flow through an artery having radially non – symmetric mild stenosis by taking blood as a power law fluid and D. Biswas et al. (2011) represented a non – Newtonian model for the steady flow of blood through a stenosed artery by assuming blood as a Herschel – Bulkley fluid and a slip velocity near the arterial wall. S.S. yadav et al. (2012) suggested a Bingham plastic model to discuss the blood flow characteristics through a generalized atherosclerotic artery with multiple stenosis.

2.2 Mathematical Formulation

Consider a laminar, steady and incompressible blood flow through a cylindrical artery; which is stenosed in an axially symmetric manner. The geometry of the artery is given by figure 2.0:

Let the radius of the artery is $\bar{R}(\bar{z})$ in the stenotic region and \bar{R}_0 in the non – stenotic region which can be given as (Young, 1968):

$$\bar{R}(\bar{z}) = \begin{cases} \bar{R}_0 - \frac{\bar{h}}{2} \left[1 + \cos \frac{2\pi}{\bar{l}_s} (\bar{z}_1 + \bar{l}_s - \bar{z}) \right] & ; \bar{z}_1 \leq \bar{z} \leq \bar{z}_1 + \bar{l}_s \\ \bar{R}_0 & ; \text{otherwise} \end{cases} \quad (2.2.1)$$

where \bar{h} , \bar{l}_s and \bar{z}_1 represent the maximum height, length and the position of the stenosis in the artery whose whole length is \bar{l} . Also, let \bar{r} and \bar{z} are the radial and axial coordinates.

In this study the blood is considered to behave like a Casson fluid.

Under the above assumptions, the equations of motion for the blood can be written as

$$-\frac{\partial \bar{p}}{\partial \bar{z}} + \frac{1}{\bar{r}} \frac{\partial}{\partial \bar{r}} (\bar{r} \bar{\tau}_c) = 0 \quad (2.2.2)$$

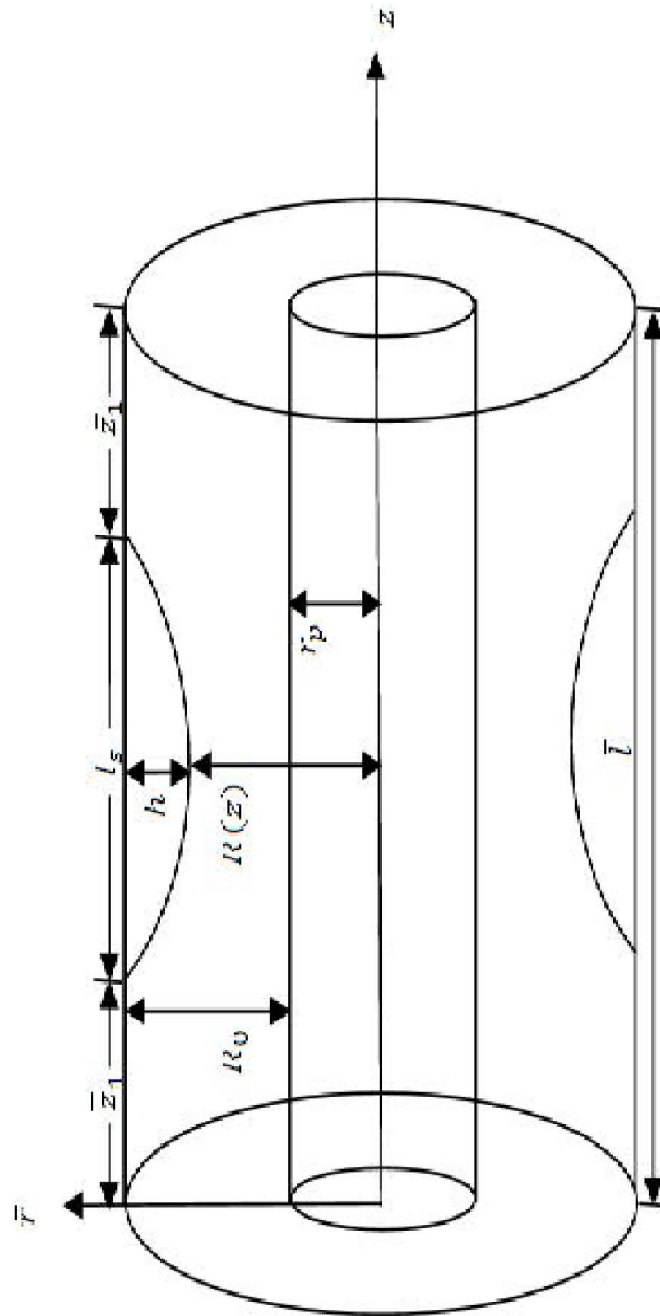


Figure 2.0: Geometry of the Stenosed Artery

$$\frac{\partial \bar{p}}{\partial \bar{r}} = 0 \quad (2.2.3)$$

where \bar{p} represents the pressure at any point and $\bar{\tau}_c$ denotes the shear stress of the blood. The constitutive equation of a Casson fluid can be simplified as

$$F(\bar{\tau}_c) = -\frac{\partial \bar{v}_c}{\partial \bar{r}} = \frac{1}{\bar{k}_c} (\bar{\tau}_c^{1/2} - \bar{\tau}_0^{1/2})^2 \quad \text{for } \bar{\tau}_c \geq \bar{\tau}_0 \quad (2.2.4)$$

$$\frac{\partial \bar{v}_c}{\partial \bar{r}} = 0 \quad \text{for } \bar{\tau}_c \leq \bar{\tau}_0 \quad (2.2.5)$$

where \bar{v}_c represents the axial velocity of blood, $\bar{\tau}_0$ stands for the yield stress and \bar{k}_c is the viscosity of the fluid. The equations (2.2.2) to (2.2.5) are applied to the following boundary conditions:

$$\left. \begin{array}{l} \bar{v}_c = \bar{v}_s \\ \bar{\tau}_c = \text{Finite value} \end{array} \right\} \begin{array}{l} \text{at } \bar{r} = \bar{R}(\bar{z}) \\ \text{at } \bar{r} = 0 \end{array} \quad (2.2.6)$$

where \bar{v}_s denotes the slip velocity in the axial direction.

Introducing following non – dimensional quantities:

$$\begin{aligned} R(z) &= \frac{\bar{R}(\bar{z})}{\bar{R}_0}, \quad z = \frac{\bar{z}_1 + \bar{l}_s - \bar{z}}{\bar{l}_s}, \quad r = \frac{\bar{r}}{\bar{R}_0}, \quad \frac{\partial p}{\partial z} = \frac{\partial \bar{p}}{\partial \bar{z}}, \quad \tau_c = \frac{\bar{\tau}_c}{\bar{p}_0 \bar{R}_0 / 2}, \\ \tau_0 &= \frac{\bar{\tau}_0}{\bar{p}_0 \bar{R}_0 / 2}, \quad H = \frac{\bar{h}}{\bar{R}_0}, \quad v_c = \frac{\bar{v}_c}{\bar{p}_0 \bar{R}_0^2 / 2 \bar{k}_c}, \quad v_s = \frac{\bar{v}_s}{\bar{p}_0 \bar{R}_0^2 / 2 \bar{k}_c}, \end{aligned} \quad (2.2.7)$$

where \bar{p}_0 represents absolute typical pressure gradient.

Using the above non – dimensional scheme, the radius of the stenotic region of the artery becomes

$$\begin{aligned} \bar{R}(\bar{z}) &= \begin{cases} \bar{R}_0 - \frac{\bar{h}}{2}(1 + \cos 2\pi z) & ; 0 \leq z \leq 1 \\ \bar{R}_0 & ; \text{otherwise} \end{cases} \\ \Rightarrow R(z) &= \begin{cases} 1 - H \cos^2 \pi z & ; 0 \leq z \leq 1 \\ 1 & ; \text{otherwise} \end{cases} \end{aligned} \quad (2.2.8)$$

The equations of the motion in the non – dimensional form are

$$-2 \frac{\partial p}{\partial z} + \frac{1}{r} \frac{\partial}{\partial r} (r \tau_c) = 0 \quad (2.2.9)$$

$$\frac{\partial p}{\partial r} = 0 \quad (2.2.10)$$

Constitutive equations of Casson fluid in the non – dimensional form are

$$-\frac{\partial v_c}{\partial r} = (\tau_c^{1/2} - \tau_0^{1/2})^2 \quad \text{for } \tau_c \geq \tau_0 \quad (2.2.11)$$

$$\frac{\partial v_c}{\partial r} = 0 \quad \text{for } \tau_c \leq \tau_0 \quad (2.2.12)$$

The dimensionless boundary conditions (2.2.6) are

$$\left. \begin{array}{l} v_c = v_s \\ \tau_c = \text{Finite value} \end{array} \right\} \begin{array}{l} \text{at } r = R(z) \\ \text{at } r = 0 \end{array} \quad (2.2.13)$$

Applying the condition (2.2.13) to the equation (2.2.9), we can write the expressions for the shear stress τ_c and wall shear stress τ_R given as

$$\tau_c = -r \frac{\partial p}{\partial z} \quad (2.2.14)$$

$$\tau_R = -R(z) \frac{\partial p}{\partial z} \quad (2.2.15)$$

From equations (2.2.14) and (2.2.15),

$$\frac{\tau_c}{\tau_R} = \frac{r}{R} \quad (2.2.16)$$

where $R = R(z)$

2.3 Method of Solution

Integrating equation (2.2.11) using equations (2.2.13) and (2.2.15), we get the velocity function for $r_p \leq r \leq R(z)$ where $r_p = \frac{\bar{r}_p}{R_0}$ is the dimensionless radius of the plug flow region, given as

$$v_c = v_s + \frac{R}{2\tau_R} \left[(\tau_R^2 - \tau_c^2) - \frac{8}{3}\tau_0^{1/2}(\tau_R^{3/2} - \tau_c^{3/2}) + 2\tau_0(\tau_R - \tau_c) \right] \quad (2.3.1)$$

within plug flow region i.e. $0 \leq r \leq r_p$, $\tau_c = \tau_0$ at $r = r_p$

Then equation (2.3.1) gives the plug flow velocity as

$$v_p = v_s + \frac{R}{2\tau_R} \left[\tau_R^2 - \frac{1}{3}\tau_0^2 - \frac{8}{3}\tau_0^{1/2}\tau_R^{3/2} + 2\tau_0\tau_R \right] \quad (2.3.2)$$

The volumetric flow rate in the dimensionless form for the region $0 \leq r \leq R(z)$ can be obtained as

$$\begin{aligned} Q &= 4 \int_0^R rv(r)dr \\ &= 4 \int_0^{r_p} rv_p dr + 4 \int_{r_p}^R rv_c dr \end{aligned}$$

Hence

$$Q = 2R^2v_s + \frac{2R^3}{\tau_R^3} \left(\frac{1}{4}\tau_R^4 - \frac{4}{7}\tau_0^{1/2}\tau_R^{7/2} + \frac{1}{3}\tau_0\tau_R^3 - \frac{1}{84}\tau_0^4 \right) \quad (2.3.3)$$

If $\tau_0 \ll \tau_R$ i.e. $\frac{\tau_0}{\tau_R} \ll 1$, then equation (2.3.3) takes the form

$$Q = 2R^2v_s + \frac{R^3}{2} \left(\tau_R - \frac{16}{7}\tau_0^{1/2}\tau_R^{1/2} + \frac{4}{3}\tau_0 \right) \quad (2.3.4)$$

which gives us the wall shear stress for the artery with stenosis as

$$\tau_R = \left[\frac{8}{7}\tau_0^{1/2} + \left\{ \frac{2}{R^3} (Q - 2R^2v_s) - \frac{4}{147}\tau_0 \right\}^{1/2} \right]^2 \quad (2.3.5)$$

When there is no stenosis i.e. $R(z) = R_0$ then the wall shear stress for the non – stenotic artery is given as

$$\tau_N = \left[\frac{8}{7} \tau_0^{1/2} + \left\{ \frac{2}{R_0^3} (Q - 2R_0^2 v_s) - \frac{4}{147} \tau_0 \right\}^{1/2} \right]^2 \quad (2.3.6)$$

Using equation (2.3.5) in equation (2.2.15), we get the pressure gradient as

$$\frac{\partial p}{\partial z} = -\frac{1}{R} \left[\frac{8}{7} \tau_0^{1/2} + \left\{ \frac{2}{R^3} (Q - 2R^2 v_s) - \frac{4}{147} \tau_0 \right\}^{1/2} \right]^2 \quad (2.3.7)$$

2.4 Results and Discussion

The velocity profile for the axial velocity in the non – plug flow region has been obtained in equation (2.3.1) and results are analyzed graphically in figures 2.1(a), 2.1(b), 2.2(a) and 2.2(b).

Figure 2.1(a) shows the variations of the axial velocity along the axial distance z for the different values of the shear stress τ_c and wall yield stress τ_0 with some fixed values like $\tau_R = 0.070$ and $v_s = 0.0$ i.e. no slip condition. It is clear that the axial velocity increases and after a certain point, it starts decreasing and again increases along the axial distance z . The axial velocity slows down when there is a decrease in the yield stress.

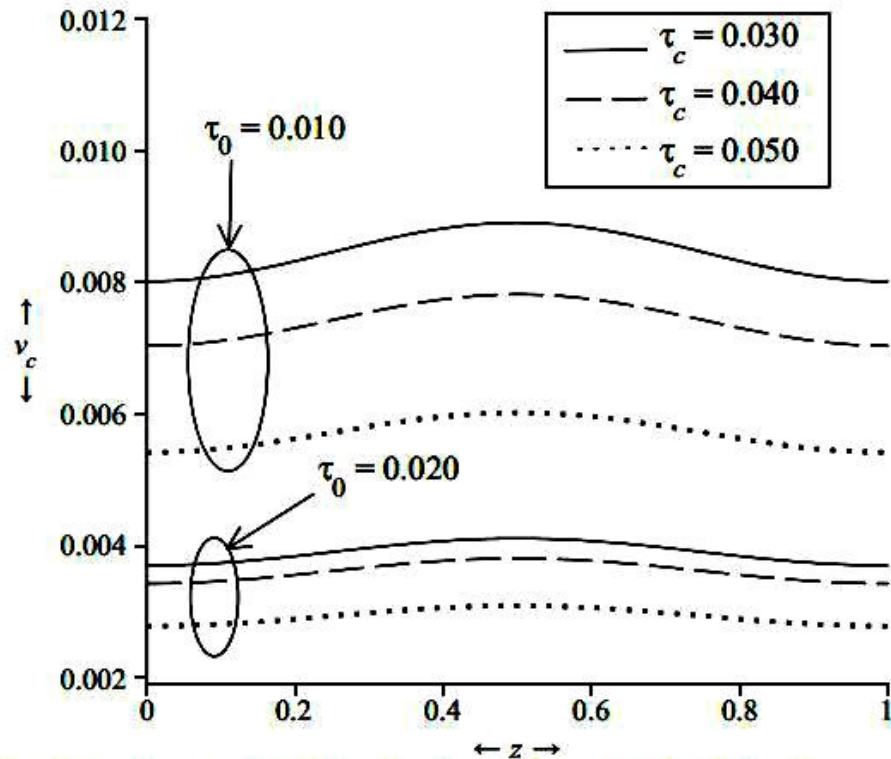


Figure 2.1 (a): Variation of Axial velocity Along Axial Distance for Different Values of the Shear Stress τ_c and Yield Stress τ_0 with some fixed values $\tau_R = 0.070$, $v_s = 0.0$, $H = 0.1$

In Figure 2.1(b), the variations of the axial velocity along the radial distance $R(z)$ have been shown for the different values of the shear stress τ_c and wall yield stress τ_0 taking $\tau_R = 0.070$ and $v_s = 0.0$. It is clear that the axial velocity decreases with the increase in shear stress but it decreases rapidly with the increase in yield stress. The axial velocity is greater for the greater radius of the stenosis region of the artery.

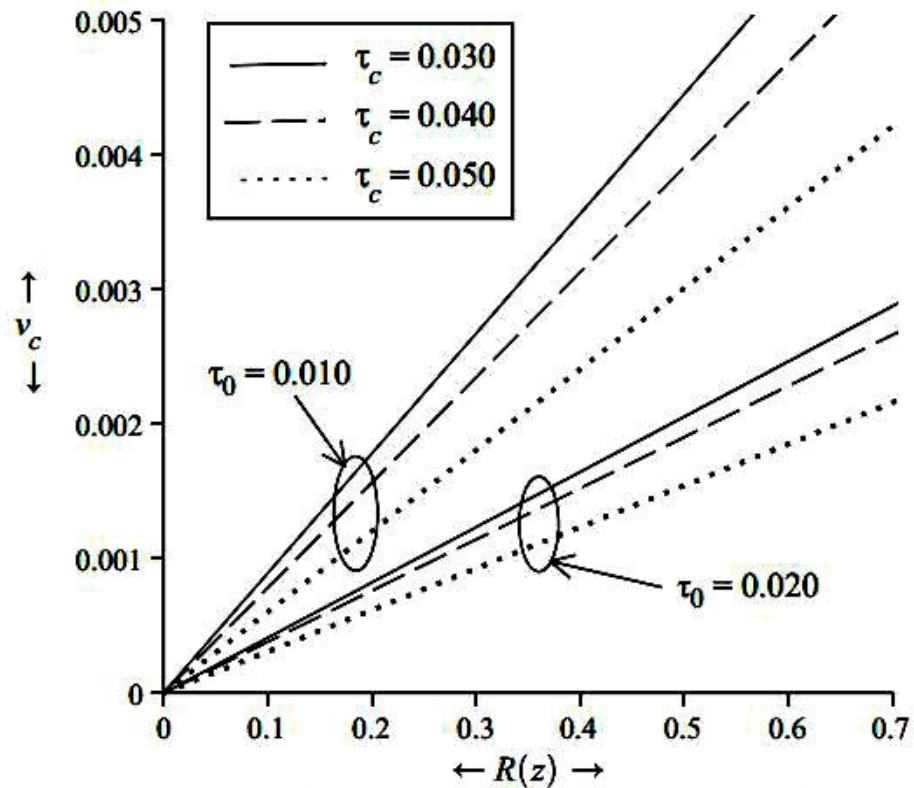


Figure 2.1 (b): Variation of Axial velocity Along Radial Distance for Different Values of the Shear Stress τ_c and Yield Stress τ_0 with some fixed values $\tau_R = 0.070$ and $v_s = 0.0$

Figure 2.2(a) shows the variations of the axial velocity along the axial distance z for different values of shear stress τ_R and slip velocity v_s with $\tau_0 = 0.010$ and $\tau_R = 0.070$. It shows that the axial velocity fluctuates i.e. increases and after certain point decreases and again starts increasing along the axial distance z . The axial velocity increases with the increase in slip velocity.

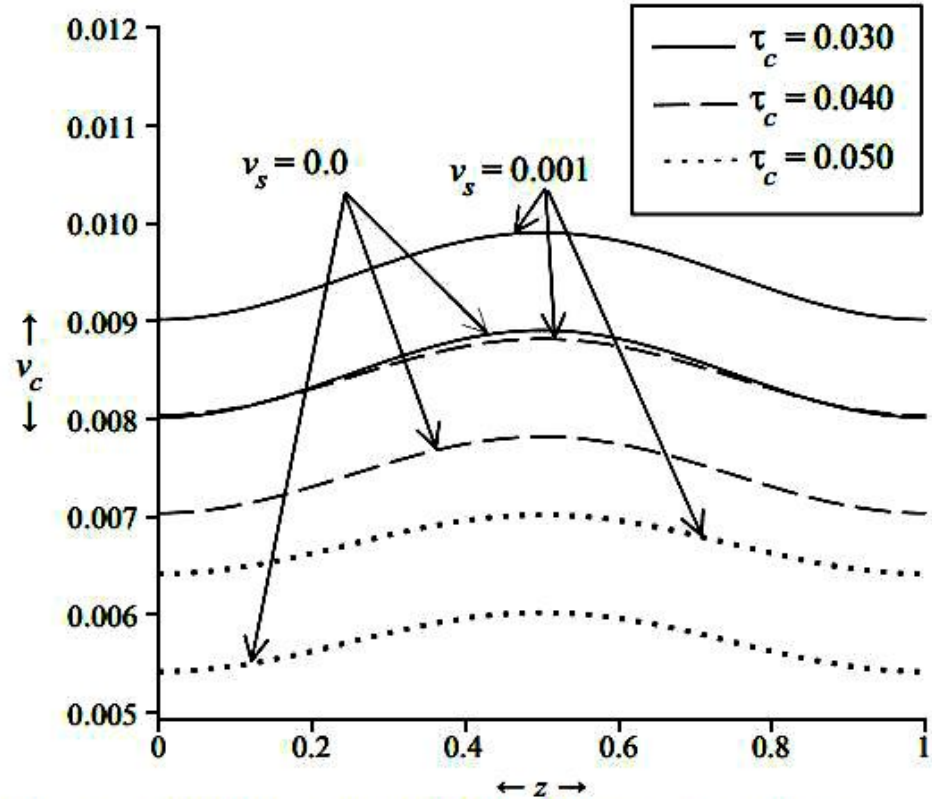


Figure 2.2 (a): Variation of Axial velocity Along Axial Distance for Different Values of the Shear Stress τ_c and Slip Velocity v_s with some fixed values $\tau_0 = 0.010$, $\tau_R = 0.070$, $H = 0.1$

Figure 2.2(b) shows the variations of the axial velocity along radial distance $R(z)$ for the different values of the shear stress τ_c and slip velocity v_s fixing some values as $\tau_0 = 0.010$ and $\tau_R = 0.070$. It is observed that there is an increase in the axial velocity with a decrease in shear stress.

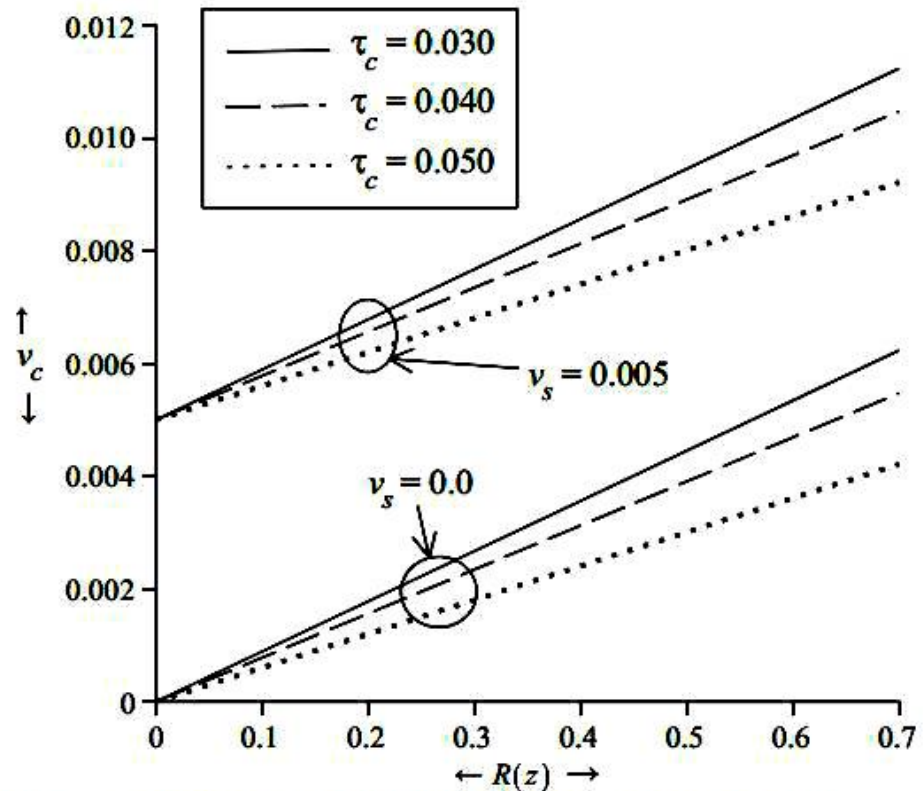


Figure 2.2 (b): Variation of Axial velocity Along Radial Distance for Different Values of the Shear Stress τ_c and Slip Velocity v_s with Some Fixed Values $\tau_0 = 0.010$ and $\tau_R = 0.070$

The axial velocity for the plug flow region obtained through equation (2.3.2) has been graphically presented in figure 2.3(a). It shows the variations of the plug flow velocity along the axial distance z for the various values of the yield stress τ_0 and slip velocity v_s with a fixed value $\tau_R = 0.070$. The plug flow velocity has wave – like variations along the axial distance z . Also the plug flow velocity increases when the slip velocity increases and it decreases for an increase in the yield stress.

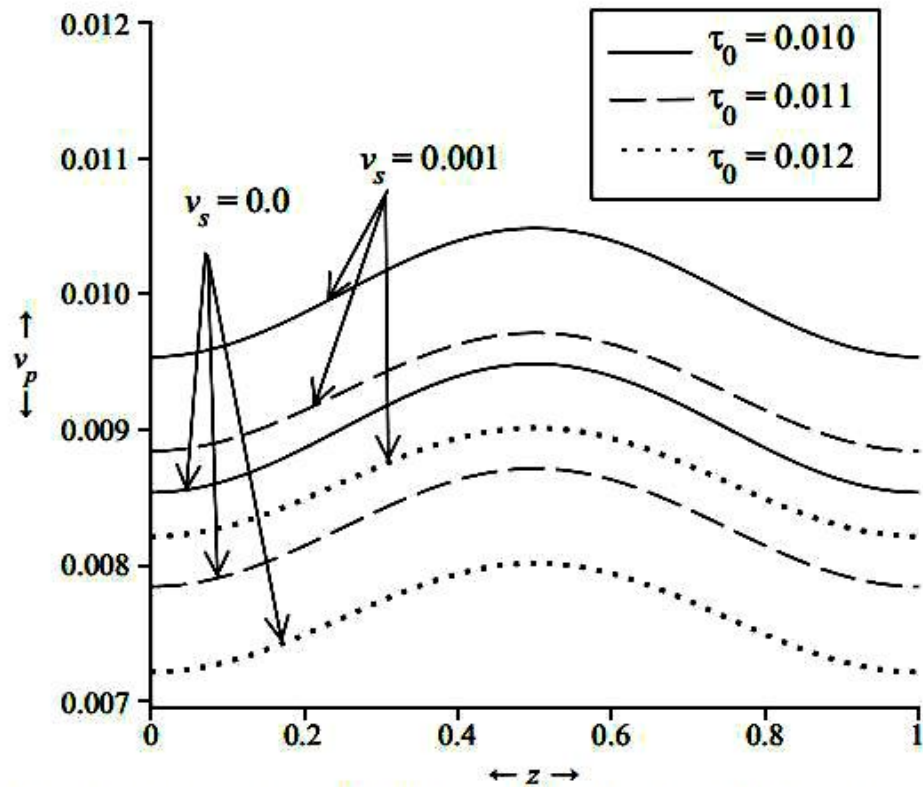


Figure 2.3 (a): Variation of Plug Flow velocity Along Axial Distance for Different Values of the Yield Stress τ_0 and Slip Velocity v_s with some fixed values $\tau_R = 0.070, H = 0.1$

Figure 2.3(b) shows the variations of the plug flow velocity with the change in radial distance $R(z)$ for the different values of the yield stress τ_0 and slip velocity v_s with $\tau_R = 0.070$. The graph also clarifies the fact that the axial velocity in the plug flow region increases due to an increase in slip velocity but the increase in yield stress decreases the plug flow velocity rapidly.

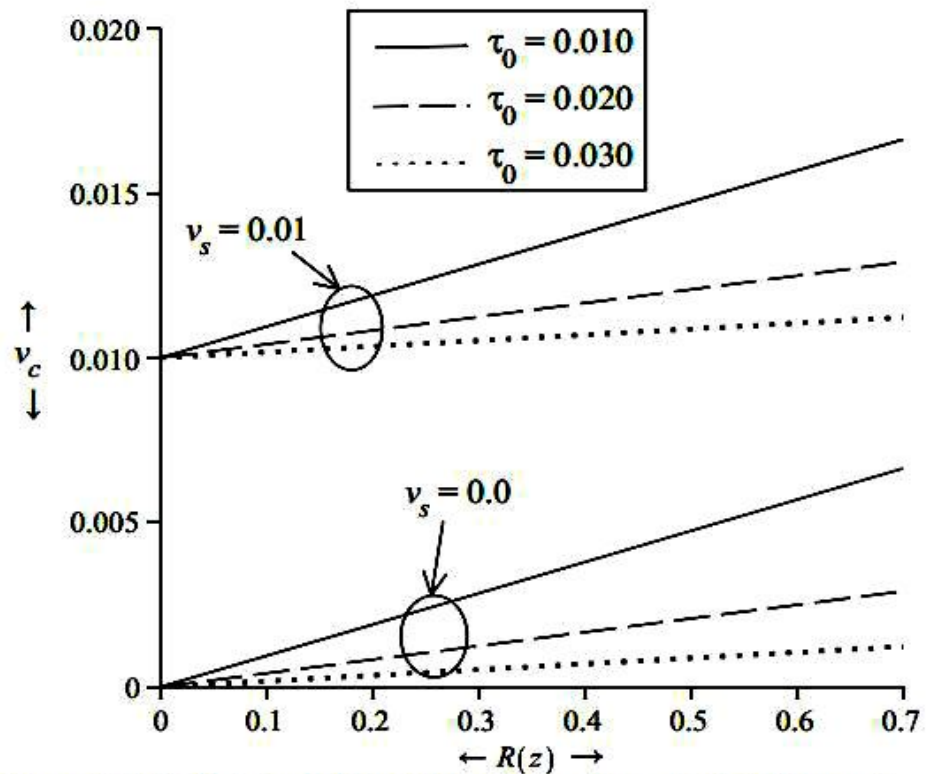


Figure 2.3 (b): Variation of Plug Flow velocity Along Radial Distance for Different Values of the Yield Stress τ_0 and Slip Velocity v_s with some fixed values $\tau_R = 0.070$.

Figure 2.4(a) shows the variations of the volumetric flow rate derived in equation (2.3.4) along the radial distance $R(z)$ for the various values of the yield stress τ_0 and slip velocity v_s with $\tau_R = 0.070$. The volumetric flow rate increases as the slip velocity increases but it decreases with increase in yield stress.

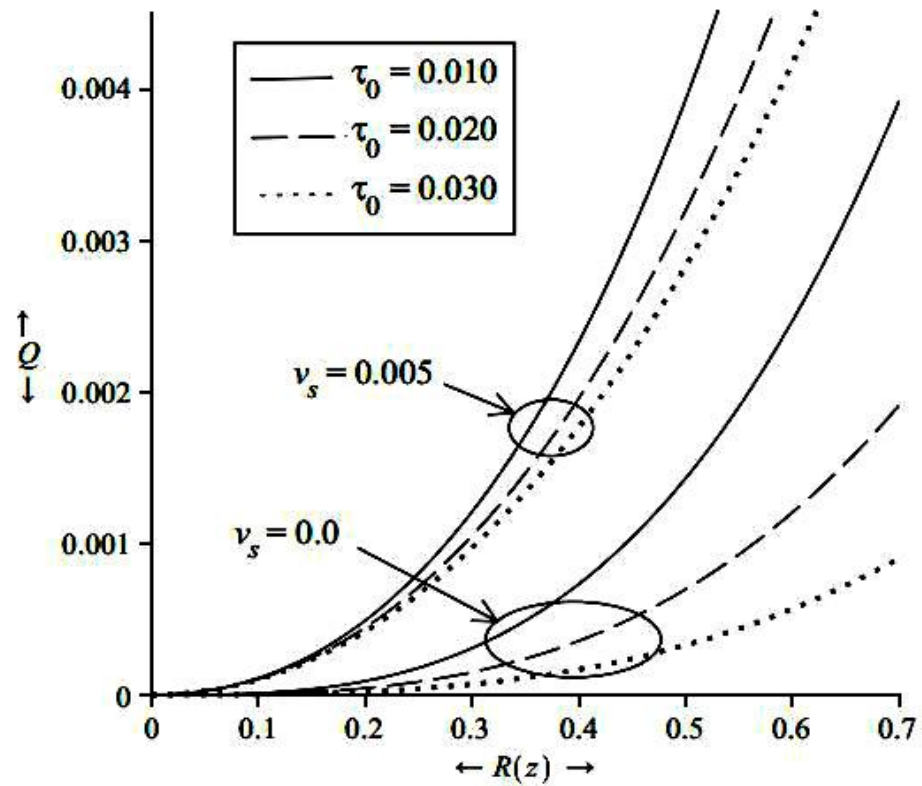


Figure 2.4 (a): Variation of Volumetric Flow Rate Along Radial Distance for Different Values of the Yield Stress τ_0 and Slip Velocity v_s with Some Fixed Values $\tau_R = 0.070$.

Figure 2.4(b) shows the changes in the volumetric flow rate along the height H of the stenosis for the different values of the yield stress τ_0 and wall slip velocity v_s with $\tau_R = 0.070$. It is observed that the volumetric flow rate decreases as the height of the stenosis increases but the volumetric flow rate increases with increase in slip velocity.

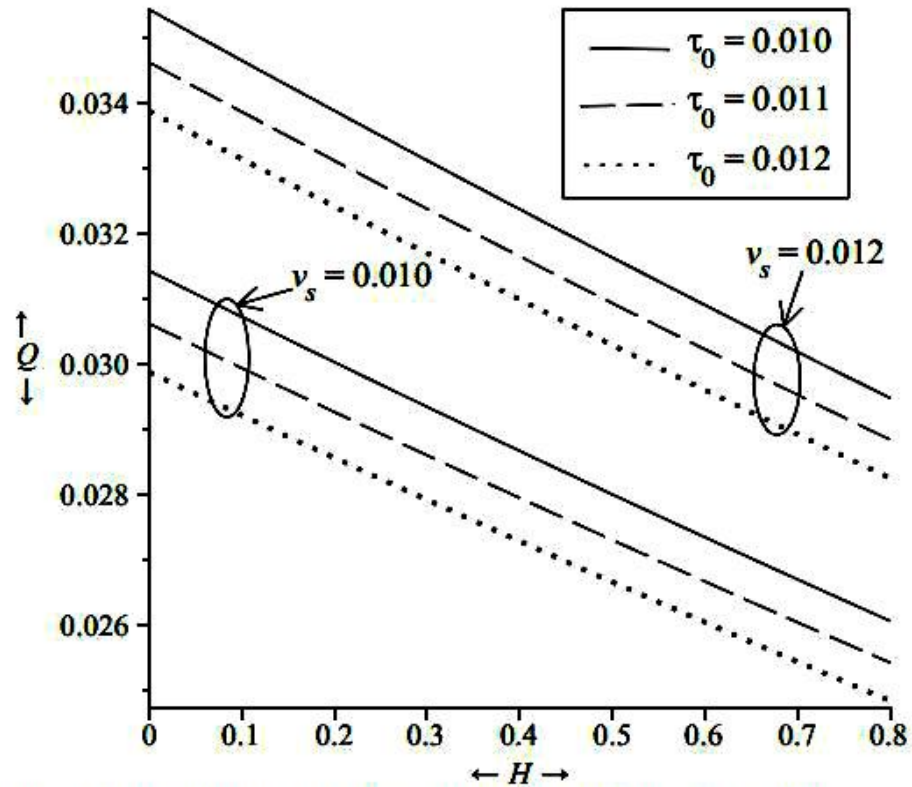


Figure 2.4 (b): Variation of Volumetric Flow Rate Along the Stenosis Height for Different Values of the Yield Stress τ_0 and Slip Velocity v_s with Some Fixed Value $\tau_R = 0.070$.

Figure 2.5(a) shows variations of the wall shear stress obtained in equation (2.3.5) along the radial distance $R(z)$ for the different values of the yield stress τ_0 and slip velocity v_s with $Q = 1$. It shows that the wall stress decreases as the slip velocity increases and increases with the increase in yield stress.

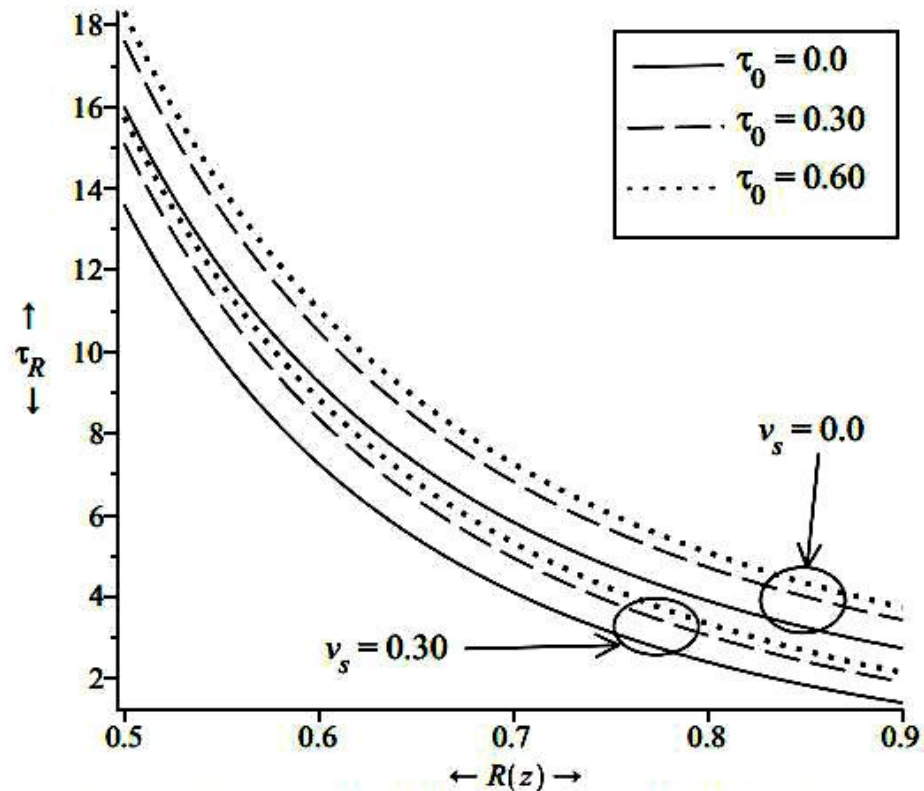


Figure 2.5 (a): Variation of Wall Shear Stress Along Radial Distance for Different Values of the Yield Stress τ_0 and Slip Velocity v_s with some fixed value $Q=1$.

In figure 2.5(b), the changes in the wall shear stress are plotted against the height H of the stenosis for the different values of the yield stress τ_0 and wall slip velocity v_s with a fixed value $Q = 1$. It shows that the wall shear stress increases continuously as the height of the stenosis increases but goes on decreasing when the yield stress increases. The wall shear stress decreases as the slip velocity increases.

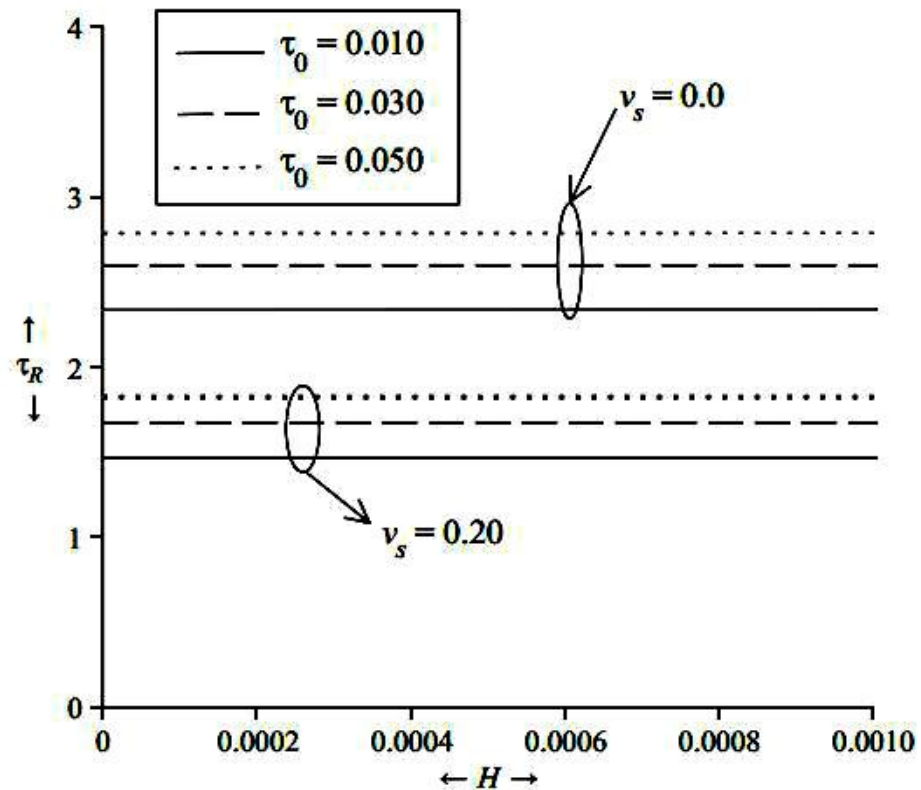


Figure 2.5 (b): Variation of Wall Shear Stress Along the Stenosis Height for Different Values of the Yield Stress τ_0 and Slip Velocity v_s with some fixed value $Q = 1$

Figure 2.6(a) shows the variations of the pressure gradient obtained in equation (2.3.7) along the radial distance $R(z)$ for various values of the yield stress τ_0 and slip velocity v_s assuming a fixed value $Q = 1$. Figure also shows that the pressure gradient increases with the increase in slip velocity with a slower rate for higher values of the yield stress.

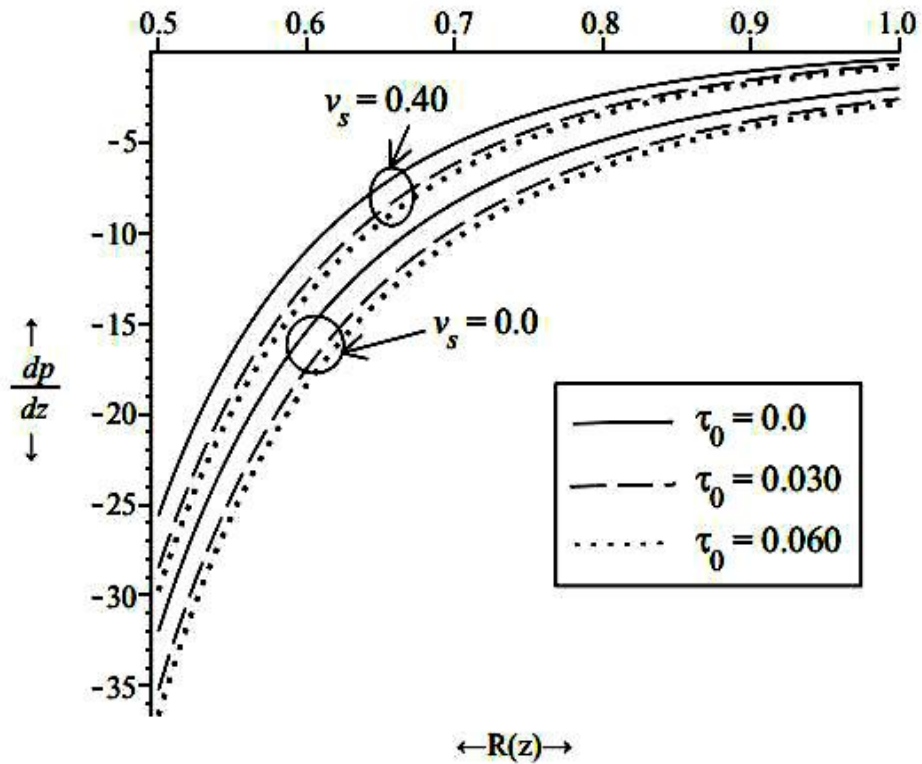


Figure 2.6 (a): Variation of Pressure Gradient Along Radial Distance $R(z)$ for Different Values of Yield Stress τ_0 and Slip Velocity v_s with Some fixed Value $Q = 1$.

Figure 2.6(b) shows the variations of the pressure gradient along the height H of the stenosis. These variations are plotted for the various values of the yield stress τ_0 and wall slip velocity v_s with a fixed value $Q = 1$. It is observed that the pressure gradient decreases as the height of the stenosis increases but it increases when the slip velocity increases.

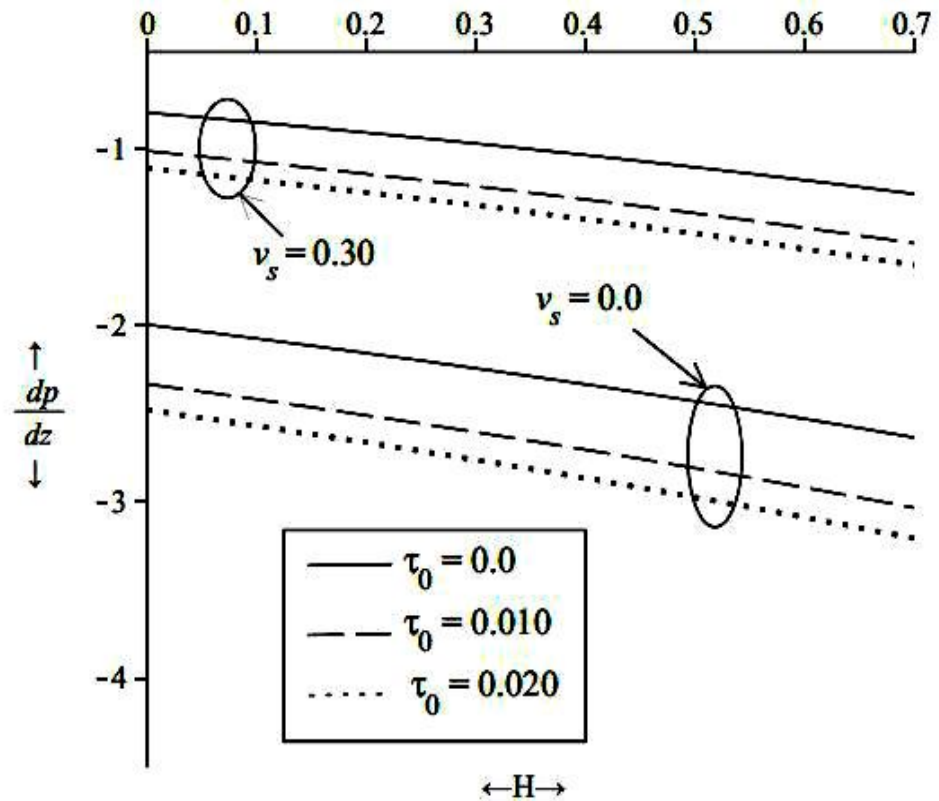


Figure 2.6 (b): Variation of Pressure Gradient Along the Stenosis Height for Different Values of the Yield Stress τ_0 and Slip Velocity v_s with Some Fixed Value $Q = 1$.

2.5 Conclusion

This chapter makes a theoretical study regarding the various blood flow properties through a stenosed artery assuming blood as a Casson fluid. It shows that the axial velocity increases due to an increase in slip velocity but it decreases as the shear stress and yield stress increase along the radial distance $R(z)$. The yield stress slows down the axial velocity in both plug flow as well as non – plug flow regions. The volumetric flow rate increases when the slip velocity increases but it begins to decrease when the yield stress increases. The wall stress decreases with increase in slip velocity and increases with increase in yield stress. The pressure gradient grows with a growth in slip velocity and yield stress. The effects of the stenosis on other flow properties like volumetric flow rate, wall shear stress and pressure gradient have also been studied and the analysis shows that these flow properties decrease as the height of the stenosis increases.

CHAPTER - 3

Slip Effects on Steady Flow through a Stenosed Blood Artery

SLIP EFFECTS ON STEADY FLOW THROUGH A STENOSED BLOOD ARTERY

3.1 Introduction

It is now a well proved fact that stenosis has become a serious threat to the life which needs an immediate attention. The artery becomes stenosed when its wall becomes fatty due to abnormal development along the lumen of the wall. Because of this stenosis the hemodynamic behaviour of the blood flow is badly affected. The stenosis of the artery gives rise to many medical problems like stroke, heart attack and serious circulatory disorders.

Many researchers have proved that the blood behaves like a Newtonian fluid at high shear rate and it behaves like a non – Newtonian fluid at low shear rate. Y. Nubar (1971) studied the blood flow, slip and viscometry and the study showed that the viscosity indications would exhibit a flow dependent behaviour of much the same pattern as the actual indications supplied by the usual viscometers if the slip function is of plausible form. M.D. Deshpande et al. (1976) discussed the steady laminar flow through modelled vascular stenosis and compared the theoretical results with available experimental values. J.B. Shukla et. al. (1980) analyzed the effects of stenosis on non – Newtonian flow of the blood in an artery and showed that the increments in the size of the stenosis produce small increments in the flow resistance and wall shear stress as the blood shows a non – Newtonian behaviour. K. Haldar (1985) studied the effects of stenosis shape on blood flow resistance and proved that the variations in the stenosis shape may decrease the flow resistance but the symmetric stenosis gives maximum resistance to flow. L.M. Srivastava (1985) also discussed the flow of couple stress fluid through stenotic blood vessels and

showed that the flow resistance and wall shear stress in case of mild stenosis of non – Newtonian blood are increased over those with no stenosis by 60% and 62% respectively in comparison to the Newtonian fluid. J.C. Misra et al. (1993) presented a non – Newtonian model for blood flow through arteries under stenotic conditions and gave a qualitative analysis for the frequency variations of flow rate at various points of the artery, phase velocities and transmission per wavelength. J.C. Misra et al. (2007) discussed the role of slip velocity in blood flow through stenosed arteries considering the blood as a Herschel – Bulkley fluid and investigated the influence of the slip at the wall of the vessel with mild, moderate and severe stenoses. D. Biswas et al. (2011) gave a non – Newtonian model to study the steady blood flow through a stenosed artery taking blood as a Herschel – Bulkley fluid and observed that axial velocity, flow rate increase with slip and decrease with yield stress. A. Sinha et al. (2013) studied the effects of externally imposed periodic body acceleration on blood flow taking slip velocity on the arterial wall with time-dependent stenosis.

3.2 Mathematical Formulation

Laminar steady flow of an incompressible Casson fluid through a cylindrical artery having axially symmetric stenosis is considered. The geometry of the artery is described in figure 2.0.

Let $\bar{R}(\bar{z})$ be the radius of the artery in the stenotic region and \bar{R}_0 in the non – stenotic area given as (Young, 1968):

$$\bar{R}(\bar{z}) = \begin{cases} \bar{R}_0 - \frac{\bar{h}}{2} \left[1 + \cos \frac{2\pi}{\bar{l}_s} (\bar{z}_1 + \bar{l}_s - \bar{z}) \right] & ; \bar{z}_1 \leq \bar{z} \leq \bar{z}_1 + \bar{l}_s \\ \bar{R}_0 & ; \text{otherwise} \end{cases} \quad (3.2.1)$$

where \bar{h} , \bar{l}_s and \bar{z}_1 are the maximum height, length and the location of the stenosis in the artery with whole length \bar{l} . Also, let \bar{r} and \bar{z} are the radial and axial coordinates.

With above considerations, the equations of motion for the blood can be given as

$$-\frac{\partial \bar{p}}{\partial z} + \frac{1}{\bar{r}} \frac{\partial}{\partial \bar{r}} (\bar{r} \bar{\tau}_c) = 0 \quad (3.2.2)$$

$$\frac{\partial \bar{p}}{\partial \bar{r}} = 0 \quad (3.2.3)$$

Here \bar{p} denotes the pressure at any point and $\bar{\tau}_c$ gives the shear stress of Casson fluid with the following simplified constitutive equations:

$$F(\bar{\tau}_c) = -\frac{\partial \bar{v}_c}{\partial \bar{r}} = \frac{1}{\bar{k}_c} (\bar{\tau}_c^{1/2} - \bar{\tau}_0^{1/2})^2 \quad \text{for } \bar{\tau}_c \geq \bar{\tau}_0 \quad (3.2.4)$$

$$\frac{\partial \bar{v}_c}{\partial \bar{r}} = 0 \quad \text{for } \bar{\tau}_c \leq \bar{\tau}_0 \quad (3.2.5)$$

where \bar{v}_c is the axial velocity of fluid, $\bar{\tau}_0$ represents the yield stress and \bar{k}_c is the fluid viscosity.

The flow is subject to slip boundary conditions as follows:

$$\left. \begin{array}{l} \bar{v}_c = \bar{\beta} \frac{\partial \bar{v}_c}{\partial \bar{r}} \\ \bar{\tau}_c = \text{Finite value} \end{array} \right\} \begin{array}{l} \text{at } \bar{r} = \bar{R}(\bar{z}) \\ \text{at } \bar{r} = 0 \end{array} \quad (3.2.6)$$

where $\bar{\beta}$ represents the slip length in the axial direction

Using following non – dimensional quantities:

$$\begin{aligned} R(z) &= \frac{\bar{R}(\bar{z})}{\bar{R}_0}, \quad z = \frac{\bar{z}_1 + \bar{l}_s - \bar{z}}{\bar{l}_s}, \quad r = \frac{\bar{r}}{\bar{R}_0}, \quad H = \frac{\bar{h}}{\bar{R}_0}, \quad \frac{\partial p}{\partial z} = \frac{\partial \bar{p} / \partial \bar{z}}{\bar{p}_0}, \quad \tau_c = \frac{\bar{\tau}_c}{\bar{p}_0 \bar{R}_0 / 2}, \\ \tau_0 &= \frac{\bar{\tau}_0}{\bar{p}_0 \bar{R}_0 / 2}, \quad v_c = \frac{\bar{v}_c}{\bar{p}_0 \bar{R}_0^2 / 2 \bar{k}_c}, \quad \beta = \frac{\bar{\beta}}{\bar{R}_0}. \end{aligned} \quad (3.2.7)$$

where \bar{p}_0 is the absolute typical pressure gradient.

The non – dimensional radius of the stenotic area of the artery is

$$R(z) = \begin{cases} 1 - H \cos^2 \pi z & ; 0 \leq z \leq 1 \\ 1 & ; \text{otherwise} \end{cases} \quad (3.2.8)$$

The non – dimensional forms of the equations of the motion (3.2.2) and (3.2.3) are

$$-2 \frac{\partial p}{\partial z} + \frac{1}{r} \frac{\partial}{\partial r} (r \tau_c) = 0 \quad (3.2.9)$$

$$\frac{\partial p}{\partial r} = 0 \quad (3.2.10)$$

The constitutive equations (3.2.4) and (3.2.5) of the Casson fluid in the dimensionless forms, can be written as

$$-\frac{\partial v_c}{\partial r} = (\tau_c^{1/2} - \tau_0^{1/2})^2 \quad \text{for } \tau_c \geq \tau_0 \quad (3.2.11)$$

$$\frac{\partial v_c}{\partial r} = 0 \quad \text{for } \tau_c \leq \tau_0 \quad (3.2.12)$$

The non – dimensional boundary conditions are

$$\left. \begin{array}{l} v_c = \beta \frac{\partial v_c}{\partial r} \\ \tau_c = \text{Finite value} \end{array} \right\} \begin{array}{l} \text{at } r = R(z) \\ \text{at } r = 0 \end{array} \quad (3.2.13)$$

Using boundary conditions (3.2.13) in equation (3.2.9), we get the expressions for the shear stress τ_c and wall shear stress τ_R in the following forms:

$$\tau_c = -r \frac{\partial p}{\partial z} \quad (3.2.14)$$

$$\tau_R = -R(z) \frac{\partial p}{\partial z} \quad (3.2.15)$$

From equations (3.2.14) and (3.2.15),

$$\frac{\tau_c}{\tau_R} = \frac{r}{R} \quad (3.2.16)$$

where $R = R(z)$

3.3 Method of Solution

Integrating equation (3.2.11) using equations (3.2.13) to (3.2.15), the velocity profile for $r_p \leq r \leq R(z)$, where $r_p = \frac{\bar{r}_p}{R_0}$ is the non – dimensional radius of the plug flow region, is

$$v_c = \frac{R}{2\tau_R} \left[(\tau_R^2 - \tau_c^2) - \frac{8}{3}\tau_0^{1/2}(\tau_R^{3/2} - \tau_c^{3/2}) + 2\tau_0(\tau_R - \tau_c) \right] - \beta(\tau_R^{1/2} - \tau_0^{1/2})^2 \quad (3.3.1)$$

Within pug flow region i.e. $0 \leq r \leq r_p$, $\tau_c = \tau_0$ at $r = r_p$.

Then from equation (3.3.1), the plug flow velocity is

$$v_p = \frac{R}{2\tau_R} \left(\tau_R^2 - \frac{1}{3}\tau_0^2 - \frac{8}{3}\tau_0^{1/2}\tau_R^{3/2} + 2\tau_0\tau_R \right) - \beta(\tau_R^{1/2} - \tau_0^{1/2})^2 \quad (3.3.2)$$

The non – dimensional volumetric flow rate for the region $0 \leq r \leq R(z)$ is calculated as

$$\begin{aligned} Q &= 4 \int_0^R rv(r)dr \\ &= 4 \int_0^{r_p} rv_p dr + 4 \int_{r_p}^R rv_c dr \end{aligned}$$

Hence

$$Q = \frac{2R^3}{\tau_R^3} \left(\frac{1}{4}\tau_R^4 - \frac{4}{7}\tau_0^{1/2}\tau_R^{7/2} + \frac{1}{3}\tau_0\tau_R^3 - \frac{1}{84}\tau_0^4 \right) - 2R^2\beta(\tau_R^{1/2} - \tau_0^{1/2})^2 \quad (3.3.3)$$

If $\tau_0 \ll \tau_R$ i.e. $\frac{\tau_0}{\tau_R} \ll 1$, then equation (3.3.3) becomes

$$Q = \frac{R^3}{2} \left(\tau_R - \frac{16}{7}\tau_0^{1/2}\tau_R^{1/2} + \frac{4}{3}\tau_0 \right) - 2R^2\beta(\tau_R^{1/2} - \tau_0^{1/2})^2 \quad (3.3.4)$$

which can also be used to get the wall shear stress for the stenosed artery given as

$$\tau_R = \left[\frac{4}{7} \left(\frac{2R-7\beta}{R-4\beta} \right) \tau_0^{1/2} + \left\{ \frac{2Q}{R^2(R-4\beta)} + \frac{16}{49} \frac{(2R-7\beta)^2}{(R-4\beta)^2} \tau_0 - \frac{4}{3} \left(\frac{R-3\beta}{R-4\beta} \right) \tau_0 \right\}^{1/2} \right]^2 \quad (3.3.5)$$

For an artery without stenosis i.e. $R(z) = R_0$, the wall shear stress is given as

$$\tau_R = \left[\frac{4}{7} \left(\frac{2R_0-7\beta}{R_0-4\beta} \right) \tau_0^{1/2} + \left\{ \frac{2Q}{R_0^2(R_0-4\beta)} + \frac{16}{49} \frac{(2R_0-7\beta)^2}{(R_0-4\beta)^2} \tau_0 - \frac{4}{3} \left(\frac{R_0-3\beta}{R_0-4\beta} \right) \tau_0 \right\}^{1/2} \right]^2 \quad (3.3.6)$$

Now using equation (3.3.5) in equation (3.2.15), we can compute the pressure gradient as

$$\frac{\partial p}{\partial z} = -\frac{1}{R} \left[\frac{4}{7} \left(\frac{2R-7\beta}{R-4\beta} \right) \tau_0^{1/2} + \left\{ \frac{2Q}{R^2(R-4\beta)} + \frac{16}{49} \frac{(2R-7\beta)^2}{(R-4\beta)^2} \tau_0 - \frac{4}{3} \left(\frac{R-3\beta}{R-4\beta} \right) \tau_0 \right\}^{1/2} \right]^2 \quad (3.3.7)$$

3.4 Results and Discussion

The velocity profile for the axial velocity in the non – plug flow region has been obtained in equation (3.3.1) and results are analyzed using graphs in figures 3.1(a) and 3.1(b).

Figure 3.1(a) shows the variations of the axial velocity along the axial distance z for the different values of the shear stress τ_c and slip length β with some fixed values $\tau_R = 0.070$, $\tau_0 = 0.010$ and $H = 0.1$. It is clear that the axial velocity first increases and then decreases after attaining a maximum value along the axial distance z . It also clarifies that the axial velocity increases whenever the velocity slip β increases and it decreases for the increasing values of the shear stress.

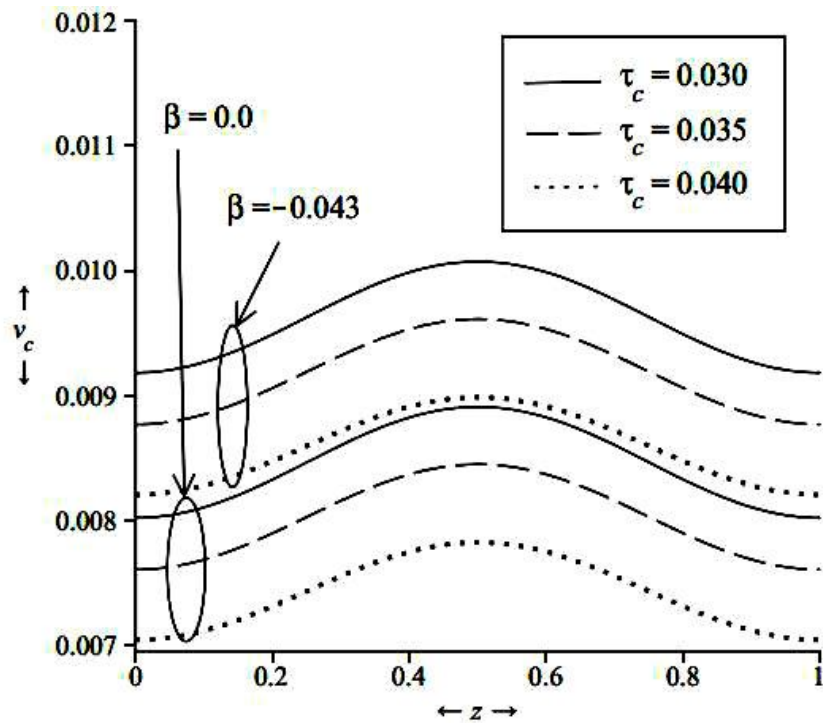


Figure 3.1 (a): Variation of Axial Velocity Along Axial Distance for Different Values of the Shear Stress τ_c and Slip Length β with Some Fixed Values $\tau_R = 0.070$, $\tau_0 = 0.010$, $H = 0.1$

Figure 3.1(b) shows the variations of the axial velocity along the radial distance $R(z)$ for the different values of the shear stress τ_c and slip length β with some fixed values $\tau_R = 0.070$ and $\tau_0 = 0.010$. Graph shows that the axial velocity is increasing along the radial distance. Also, the axial velocity increases when the velocity slip increases and it decreases as the shear stress increases.

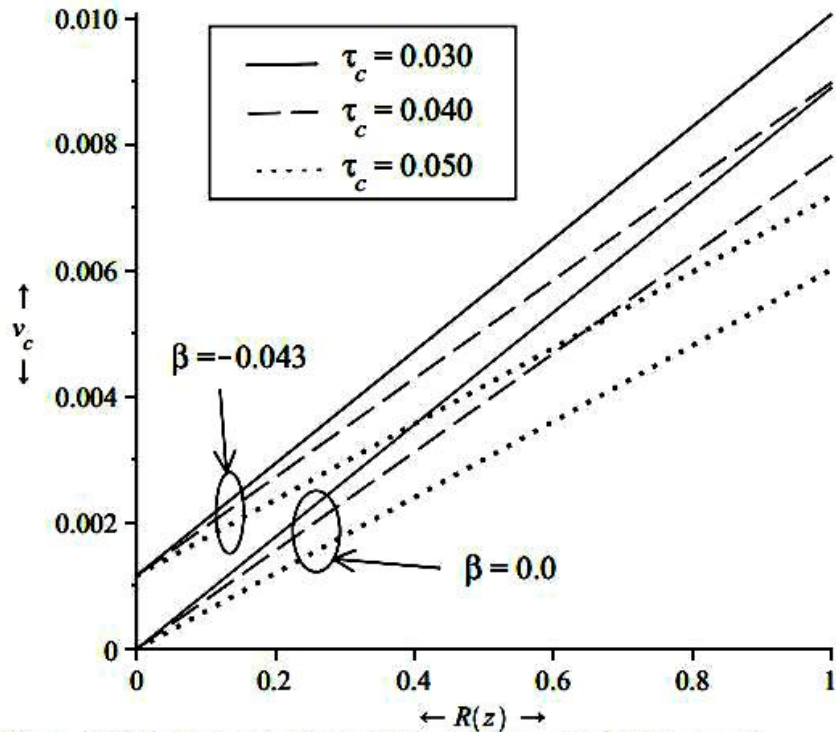


Figure 3.1 (b): Variation of Axial Velocity Along Radial Distance for Different Values of the Shear Stress τ_c and Slip Length β with Some Fixed Values $\tau_R = 0.070$, $\tau_0 = 0.010$.

The axial velocity for the plug flow region obtained through equation (3.3.2) has been analyzed in figure 3.2(a) which shows the variations of the plug flow velocity along the axial distance z taken for the different values of the yield stress τ_0 and slip length β with fixed values $\tau_R = 0.070$ and $H = 0.1$. It is observed here that the plug flow velocity is showing wavy variations along the axial distance z . Also the plug flow velocity increases as the velocity slip increases and it decreases when the yield stress increases.

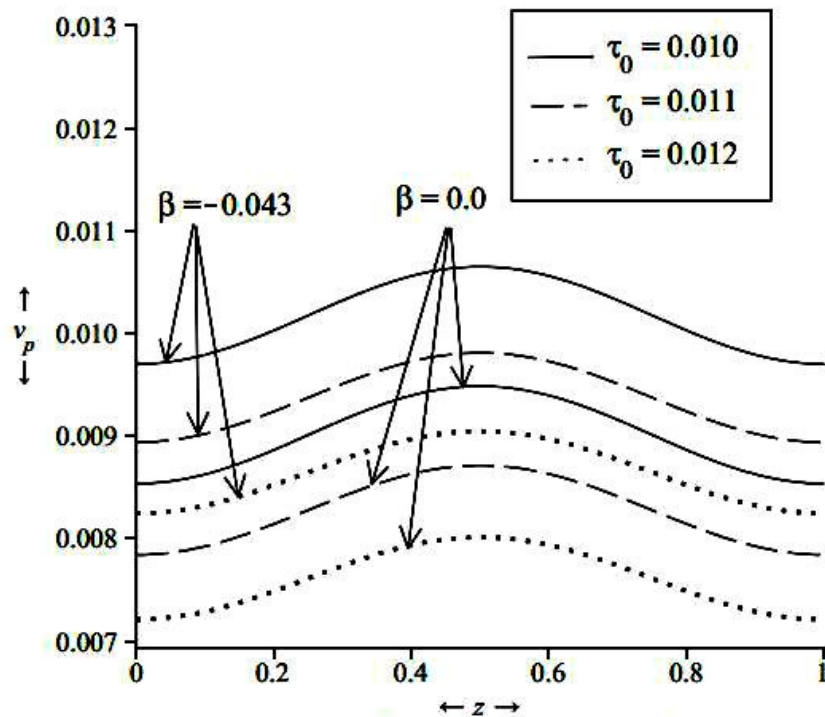


Figure 3.2 (a): Variation of Plug Flow Velocity Along Axial Distance for Different Values of the Yield Stress τ_0 and Slip Length β with Some Fixed Values $\tau_R = 0.070$, $H = 0.1$.

Figure 3.2(b) shows the variations of the axial velocity along radial distance $R(z)$ for the different values of the yield stress τ_0 and slip length β with other fixed values $\tau_R = 0.070$. It shows that the plug flow velocity increases along the radial distance and it decreases when the yield stress increases. Also the plug flow velocity increases as the velocity slip increases. It is to be noted here that for the greater values of the yield stress, the plug flow velocity increases slowly as the velocity slip increases as compared to the lower values of the yield stress.

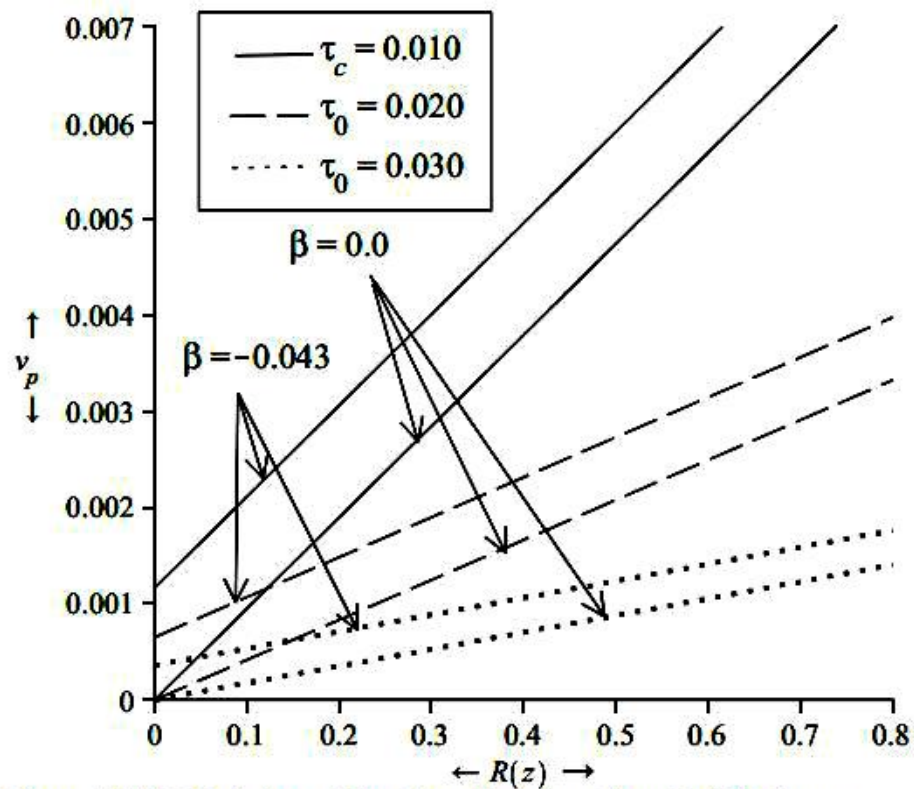


Figure 3.2 (b): Variation of Plug Flow Velocity Along Radial Distance for Different Values of the Yield Stress τ_0 and Slip Length β with Some Fixed Fixed Values $\tau_R = 0.070$.

The volumetric flow rate derived through equation (3.3.4) has been graphically presented in figures 3.3(a) and 3.3(b). Figure 3.3(a) shows the variations of the volumetric flow rate along the radial distance $R(z)$ for the various values of the yield stress τ_0 and slip length β with a fixed value $\tau_R = 0.070$. Clearly the volumetric flow rate increases along the radial distance. It is observed that the volumetric flow rate increases as the velocity slip increases but it decreases when the yield stress increases. Also, the volumetric flow rate increases at a little slower rate for the greater values of the yield stress.

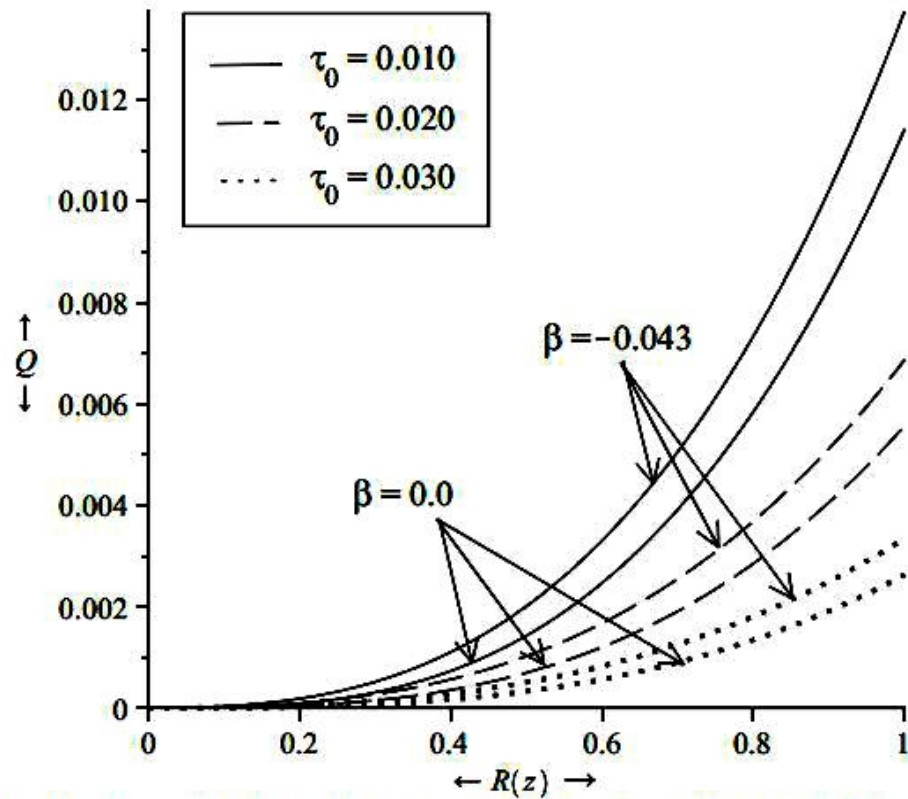


Figure 3.3(a): Variation of Volumetric Flow Rate Along Radial Distance for Different Values of the Yield Stress τ_0 and Slip Length β with Some Fixed Value $\tau_R = 0.070$.

Figure 3.3(b) presents the variations of the volumetric flow rate are shown along the height of the stenosis H for the different values of the yield stress τ_0 and wall slip length β with fixed values $\tau_R = 0.070$ and $z = 0.4$. It is obvious that the volumetric flow rate slows down along the height of the stenosis with increments in yield stress but it increases when the slip length increases.

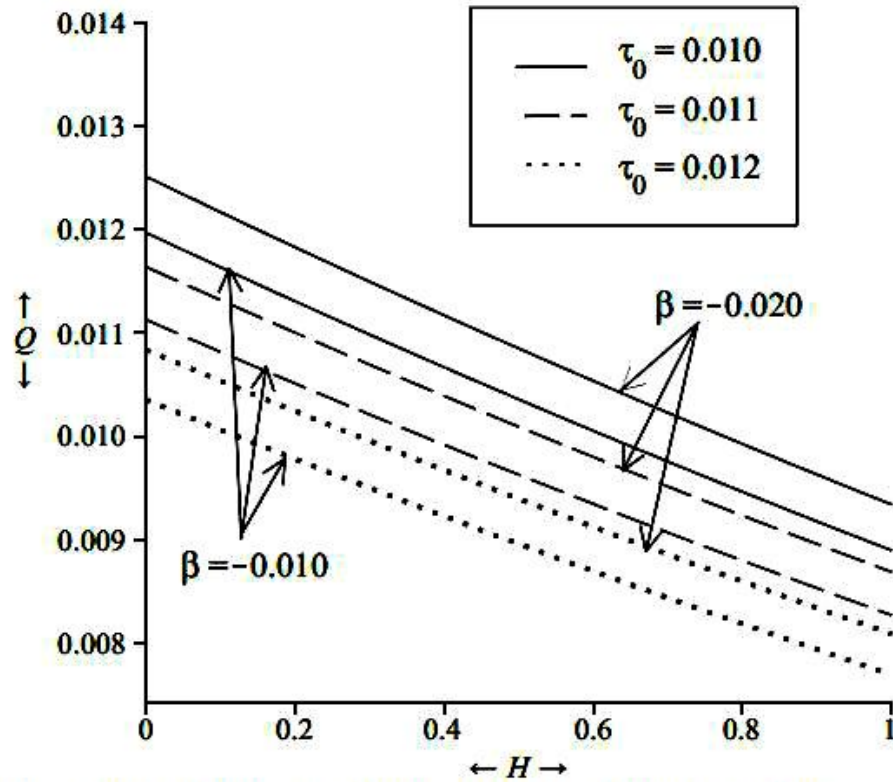


Figure 3.3(b): Variation of Volumetric Flow Rate Along the Stenosis Height for Different Values of the Yield Stress τ_0 and Slip Length β with Some Fixed Value $\tau_R = 0.070, z = 0.4$.

Figure 3.4(a) explains the variations of the wall shear stress obtained in equation (3.3.5) along the radial distance $R(z)$ for the different values of the slip length β with a fixed value $Q = 1$. It shows that the wall shear stress decreases along the radial distance. Also the wall shear stress decreases when velocity slip increases.

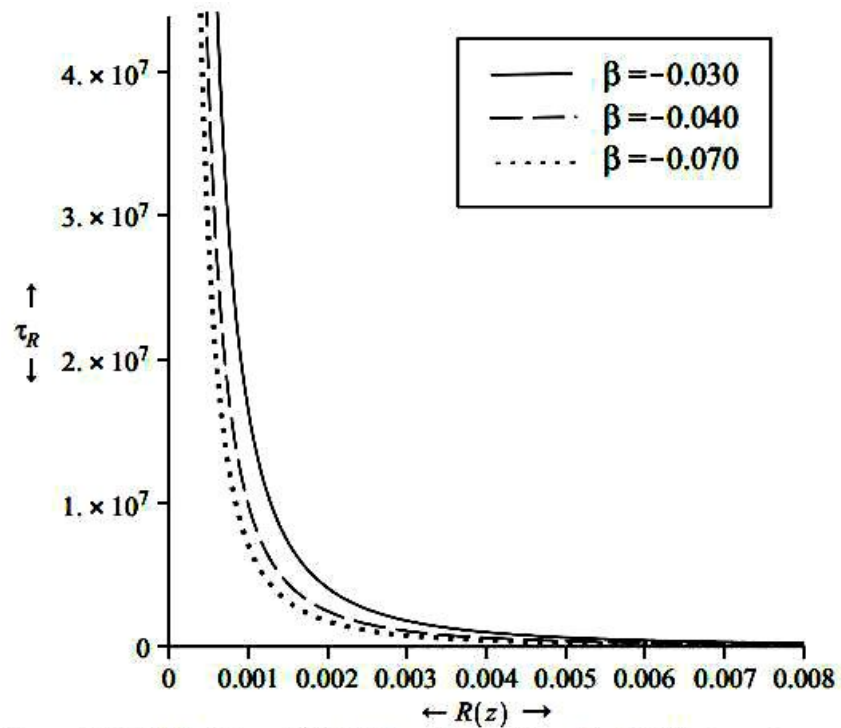


Figure 3.4(a): Variation of Wall Shear Stress Along Radial Distance for Different Values of the Slip Length β with Some Fixed Values $Q = 1$ and Yield Stress τ_0 .

Figure 3.4(b) shows the variations of the wall shear stress along the height of the stenosis H for the different values of the yield stress τ_0 and wall slip length β with some fixed values $Q = 1$ and $z = 0.4$. It is clear that the wall shear stress increases along the height of the stenosis. Also the wall shear stress increases as the yield stress increases and it decreases when the velocity slip increases.

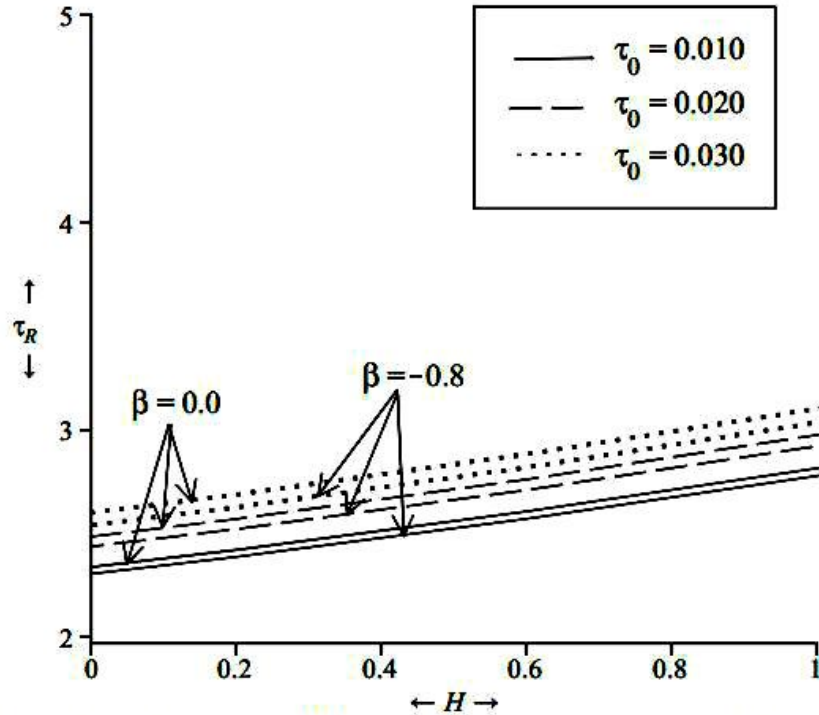


Figure 3.4(b): Variation of Wall Shear Stress Along the Stenosis Height for Different Values of the Yield Stress τ_0 and Slip Length β with Some Fixed Values $Q = 1, z = 0.4$.

The variations of the pressure gradient obtained in equation (3.3.7) are shown in figures 3.5(a) and 3.5(b). Figure 3.5(a) shows that the variations of the pressure gradient along the radial distance $R(z)$ for the different values of the slip length β with a fixed value $Q = 1$. The pressure gradient increases along the radial distance and it increases with the increase in velocity slip.

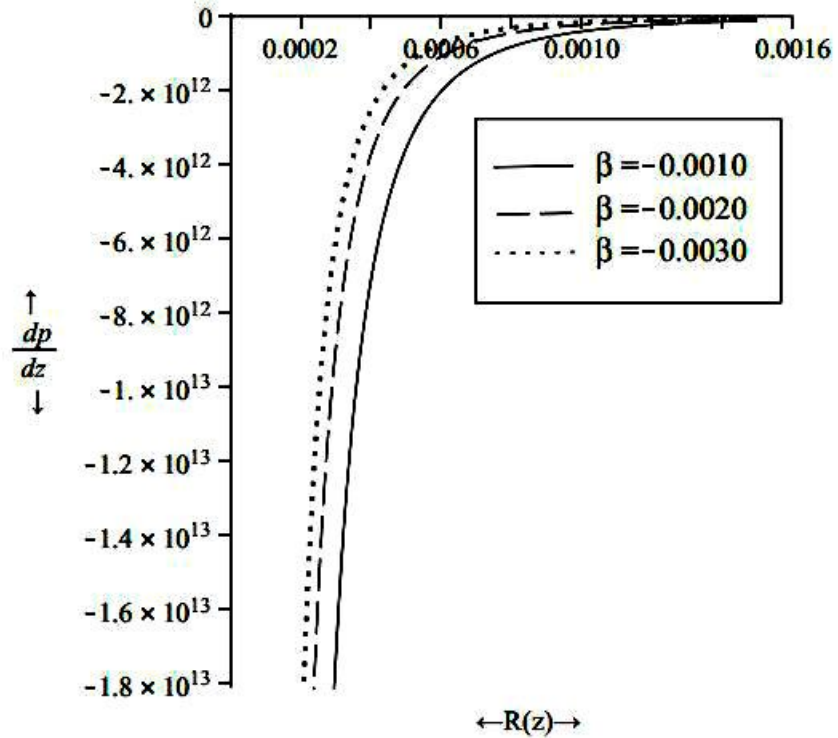


Figure 3.5(a): Variation of Pressure Gradient Along Radial Distance $R(z)$ for Different Values of Slip Length β with Some fixed Value $Q = 1$.

Figure 3.5(b) gives the variations of the pressure gradient along the height of the stenosis H for the various values of the yield stress τ_0 and wall slip length β with some fixed values $Q = 1$ and $z = 0.4$. It is observed that the pressure gradient decreases greatly along the height of the stenosis. Also the pressure gradient decreases whenever the yield stress increases and it increases as the velocity slip increases.

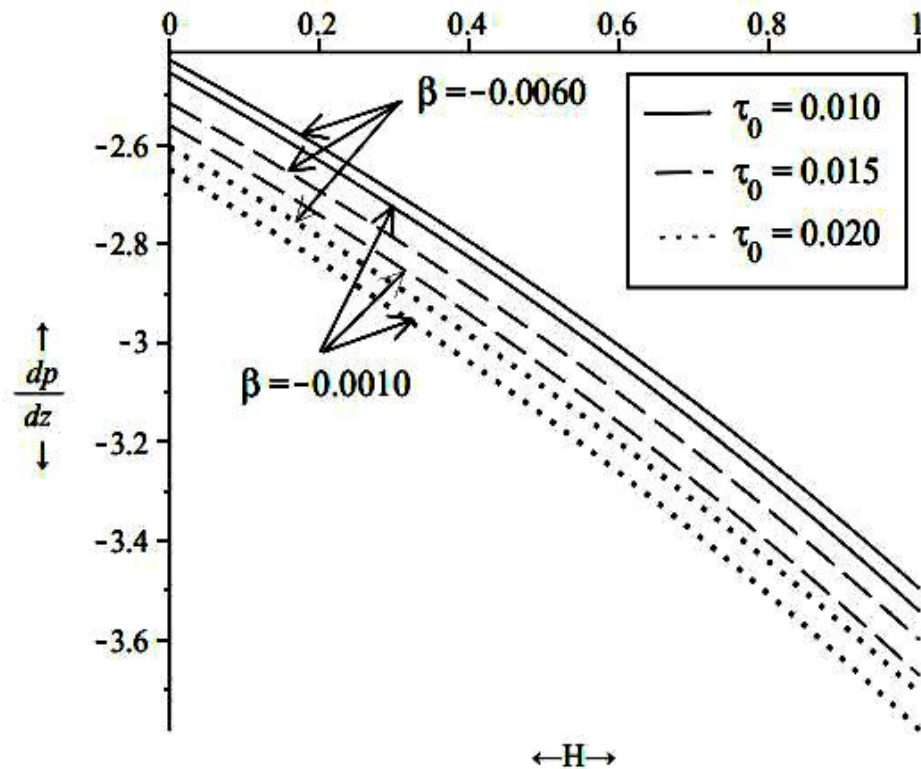


Figure 3.5(b): Variation of Pressure Gradient Along the Stenosis Height for Different Values of the Yield Stress τ_0 and Slip Length β with Some Fixed Value $Q = 1, z = 0.4$.

3.5 Conclusion

This chapter is an attempt to present the theoretical observations of the different flow features by considering a stenosed artery with blood behaving like a Casson fluid. The results are explained analytically and graphically by choosing some suitable parameters. The graphical analysis of the study reveals that the axial velocity is showing the wave like variations along the axial distance z and for increments in velocity slip, it increases in both plug flow and non – plug flow domains. Also the axial velocity increases along the radial distance as the slip length increases in both plug flow and non – plug flow regions. The volumetric flow rate increases along the radial distance as the velocity slip increases. The axial velocity and the volumetric flow rate decrease when the yield stress increases. It is observed that the plug flow velocity and the volumetric flow rate increase gradually for the greater values of the yield stress as compared to the lower yield stress. The wall shear stress decreases and the pressure gradient increases along the radial distance as the velocity slip increases. The analysis regarding the effect of the stenosis over other flow properties like volumetric flow rate, wall shear stress and pressure gradient has also been done. The volumetric flow rate and the pressure gradient decrease when the yield stress increases but they increase with increments in velocity slip along the height of the stenosis. Also the wall shear stress increases as the yield stress increases and it decreases when the velocity slip increases along the height of the stenosis.

CHAPTER - 4

Unsteady Slip Flow of Blood through Constricted Artery

UNSTEADY SLIP FLOW OF BLOOD THROUGH CONSTRICTED ARTERY

4.1. Introduction

The hemodynamic behaviour of flows through the constricted arteries have always drawn attention of the researchers as it puts the health at risk which sometimes proves fatal. One basic reason of the constriction of the artery is the deposits of fatty and fibrous tissues in the arterial wall which restricts the normal blood flow through the artery. Many research workers have made valuable contributions to understand the various flow properties through the constricted arteries.

A.C. Burton (1966) made several experiments to study the effects of whole body accelerations on human bodies and presented empirical data regarding the relations between blood flows and the radii of the blood vessels. D.F. Young (1968) discussed the effect of an axially symmetric time-dependent stenotic growth into the lumen of a tube of constant cross-section over the steady flow of a Newtonian fluid. P. Chaturani et al. (1986) studied the pulsatile flow of a Casson fluid through stenosed arteries with application to blood flow. S. Chakravarty et al. (1994) presented a mathematical model for the blood flow through an overlapping time-dependent arterial stenosis by taking the experimentally established viscoelastic properties of the blood and deformability of the arterial wall. A.V. Mernone (2002) et al. performed a mathematical study of peristaltic transport of a Casson fluid and found the analytical and numerical solutions for the zeroth and first order in stream function. H. Jung et al. (2004) studied the asymmetric flows of non – Newtonian fluids in symmetric stenosed artery and discussed the characteristics of pulsatile blood flow. R.N. Pralhad et al. (2004) modelled the arterial

stenosis and studied its application in blood diseases assuming blood as a couple – stress fluid. K.Y. Volokh (2006) studied the stresses in growing soft tissues and showed that the uniform volumetric growth can lead to the deposits of residual stresses in blood arteries due to the material anisotropy. T. Ishikawa (2007) performed the numerical simulation of a low- hematocrit blood flow in a small artery with stenosis and showed that the erythrocytes are considerably deformed around the stenosis. S.U. Siddiqui et al. (2010) studied pulsatile flow of blood through stenosed arteries and found that the width of the plug core region increases with increasing value of yield stress at any time. Author in previous chapter 2, presented a Casson fluid model for the steady flow through a stenosed blood vessel in which the author showed that the axial velocity, volumetric flow rate and pressure gradient increase with the increase in slip velocity and decrease with growth in yield stress. Author studied the slip effects on steady flow through a stenosed blood artery and showed that axial velocity, volumetric flow rate and pressure gradient decrease along the radial distance as the slip length increases but the wall shear stress increases with increase in slip length in chapter 3.

4.2. Mathematical Formulation

Consider an incompressible blood with a laminar unsteady flow through a cylindrical blood artery which is stenosed with an axially symmetric stenosis. The geometrical diagram of the stenosis is shown by figure 2.0.

Let $\bar{R}(\bar{z})$ be the radius of the vessel in the constricted region and \bar{R}_0 in the non – stenotic area given as (Young, 1968):

$$\bar{R}(\bar{z}) = \begin{cases} \bar{R}_0 - \frac{\bar{h}}{2} \left[1 + \cos \frac{2\pi}{\bar{l}_s} (\bar{z}_1 + \bar{l}_s - \bar{z}) \right] & ; \bar{z}_1 \leq \bar{z} \leq \bar{z}_1 + \bar{l}_s \\ \bar{R}_0 & ; \text{otherwise} \end{cases} \quad (4.2.1)$$

where \bar{h} , \bar{l}_s and \bar{z}_1 are the maximum height, length and the location of the stenosis in the vessel of the length \bar{l} . Also, let \bar{r} and \bar{z} represent the radial and axial coordinates.

Here the blood is assumed to behave like a Casson fluid.

Considering the above assumptions, the equations of motion for the blood can be written as

$$\bar{\rho} \frac{\partial \bar{v}_c}{\partial \bar{t}} = -\frac{\partial \bar{p}}{\partial \bar{z}} + \frac{1}{\bar{r}} \frac{\partial}{\partial \bar{r}} (\bar{r} \bar{\tau}_c) \quad (4.2.2)$$

$$\frac{\partial \bar{p}}{\partial \bar{r}} = 0 \quad (4.2.3)$$

Where $\bar{\rho}$ denotes the density of blood, \bar{p} is the pressure at any point at time \bar{t} and $\bar{\tau}_c$ is the shear stress. The constitutive equations for Casson fluid are:

$$F(\bar{\tau}_c) = -\frac{\partial \bar{v}_c}{\partial \bar{r}} = \frac{1}{\bar{k}_c} (\bar{\tau}_c^{1/2} - \bar{\tau}_y^{1/2})^2 \quad \text{for } \bar{\tau}_c \geq \bar{\tau}_y \quad (4.2.4)$$

$$\frac{\partial \bar{v}_c}{\partial \bar{r}} = 0 \quad \text{for } \bar{\tau}_c \leq \bar{\tau}_y \quad (4.2.5)$$

Here \bar{v}_c gives the axial velocity of blood, $\bar{\tau}_y$ represents the yield stress and \bar{k}_c is the fluid viscosity. The equations (4.2.2) to (4.2.5) are governed with the following boundary conditions:

$$\left. \begin{array}{l} \bar{v}_c = \bar{v}_s \\ \bar{\tau}_c = \text{Finite value} \end{array} \right\} \begin{array}{l} \text{at } \bar{r} = \bar{R}(\bar{z}) \\ \text{at } \bar{r} = 0 \end{array} \quad (4.2.6)$$

where \bar{v}_s is the slip velocity in the axial direction.

The pressure gradient is a function of \bar{z} and \bar{t} , hence it can be expressed as

$$\frac{\partial \bar{p}}{\partial \bar{z}} (\bar{z}, \bar{t}) = \bar{p}_0(\bar{z}) + \bar{p}_1(\bar{z}) \cos(\bar{\omega} \cdot \bar{t}) \quad (4.2.7)$$

Here \bar{p}_0 is the steady – state amplitude and \bar{p}_1 is the fluctuating amplitude of the pressure gradient with a period $\bar{\omega} = 2\pi\bar{f}$ where \bar{f} is the pulse frequency.

Applying the following non – dimensional quantities:

$$R(z) = \frac{\bar{R}(z)}{\bar{R}_0}, \quad z = \frac{\bar{z}_1 + \bar{l}_s - \bar{z}}{\bar{l}_s}, \quad r = \frac{\bar{r}}{\bar{R}_0}, \quad \tau_c = \frac{\bar{\tau}_c}{\bar{p}_0 \bar{R}_0 / 2}, \quad \tau_y = \frac{\bar{\tau}_y}{\bar{p}_0 \bar{R}_0 / 2},$$

$$v_c = \frac{\bar{v}_c}{\bar{p}_0 \bar{R}_0^2 / 2k_c}, \quad v_s = \frac{\bar{v}_s}{\bar{p}_0 \bar{R}_0^2 / 2k_c}, \quad H = \frac{\bar{h}}{\bar{R}_0}, \quad \alpha^2 = \frac{\bar{\omega} \bar{p}_0 \bar{R}_0^2}{k_c}, \quad t = \bar{\omega} \bar{t}, \quad e = \frac{\bar{p}_1}{\bar{p}_0}$$

(4.2.8)

where e represents the amplitude of the flow and α defines the pulsatile Reynold number which is also known as the Womersley parameter.

Hence the dimensionless radius of the stenotic area of the artery is

$$R(z) = \begin{cases} 1 - H \cos^2 \pi z & ; 0 \leq z \leq 1 \\ 1 & ; \text{otherwise} \end{cases} \quad (4.2.9)$$

The non – dimensional form of equation of the motion (4.2.2) is

$$\alpha^2 \frac{\partial v_c}{\partial t} = -2\phi + \frac{1}{r} \frac{\partial}{\partial r} (r\tau_c) \quad (4.2.10)$$

where $\phi \equiv \phi(t) = 1 + e \cos t$

The non – dimensional constitutive equations of Casson fluid are

$$-\frac{\partial v_c}{\partial r} = (\tau_c^{1/2} - \tau_y^{1/2})^2 \quad \text{for } \tau_c \geq \tau_y \quad (4.2.11)$$

$$\frac{\partial v_c}{\partial r} = 0 \quad \text{for } \tau_c \leq \tau_y \quad (4.2.12)$$

The dimensionless boundary conditions are

$$\left. \begin{aligned} v_c &= v_s \\ \tau_c &= \text{Finite value} \end{aligned} \right\} \begin{aligned} &\text{at } r = R(z) \\ &\text{at } r = 0 \end{aligned} \quad (4.2.13)$$

4.3. Method of Solution

In order to get the required solutions of the problem, the perturbation method is used for which $\alpha^2 \ll 1$ is taken to maintain the non – Newtonian nature of the blood in which a plug flow region is developed through the constricted arteries in small blood vessels like coronary arteries. Then the axial velocity v_c , plug flow velocity v_p , shear stress τ_c and the plug core radius r_p can be expressed in the powers of α^2 given as

$$v_c = v_{c0} + \alpha^2 v_{c1} + \alpha^4 v_{c2} + \dots \quad (4.3.1)$$

$$v_p = v_{p0} + \alpha^2 v_{p1} + \alpha^4 v_{p2} + \dots \quad (4.3.2)$$

$$\tau_c = \tau_{c0} + \alpha^2 \tau_{c1} + \alpha^4 \tau_{c2} + \dots \quad (4.3.3)$$

$$r_p = r_{p0} + \alpha^2 r_{p1} + \alpha^4 r_{p2} + \dots \quad (4.3.4)$$

where $r_p = \frac{\bar{r}_p}{R_0}$ is the non – dimensional radius of the plug core.

Using equations (4.3.1) & (4.3.3) in equation (4.2.10), we get

$$\frac{\partial v_{c0}}{\partial t} = \frac{1}{r} \frac{\partial}{\partial r} (r \tau_{c1}) \quad (4.3.5)$$

$$\frac{\partial}{\partial r} (r \tau_{c0}) = 2r\phi \quad (4.3.6)$$

Substituting equations (4.3.1) & (4.3.3) in equation (4.2.11), we have

$$-\frac{\partial v_{c0}}{\partial r} = \tau_{c0} + \tau_y - 2\tau_y^{1/2} \cdot \tau_{c0}^{1/2} \quad (4.3.7)$$

$$-\frac{\partial v_{c1}}{\partial r} = \tau_{c1} \left[1 - \left(\frac{\tau_y}{\tau_{c0}} \right)^{1/2} \right] \quad (4.3.8)$$

Using equation (4.3.1), the boundary conditions (4.2.13) reduce to

$$\left. \begin{array}{l} v_{c0} = v_s \\ v_{c1} = 0 \end{array} \right\} \quad \text{at } r = R \quad (4.3.9)$$

where $R = R(z)$

Integrating equation (4.3.6) and using condition (4.2.13), we get

$$\tau_{c0} = r\phi \quad (4.3.10)$$

Using equation (4.3.10), equation (4.3.7) on integration yields

$$v_{c0} = \frac{1}{2}\phi(R^2 - r^2) - \frac{4}{3}\tau_y^{1/2}\phi^{1/2}(R^{3/2} - r^{3/2}) + \tau_y(R - r) + v_s \quad (4.3.11)$$

The expression for v_{p0} is obtained by putting $r = r_{p0}$ in equation (4.3.11) given as

$$v_{p0} = \frac{1}{2}\phi(R^2 - r_{p0}^2) - \frac{4}{3}\tau_y^{1/2}\phi^{1/2}(R^{3/2} - r_{p0}^{3/2}) + \tau_y(R - r_{p0}) + v_s \quad (4.3.12)$$

Integrating equation (4.3.5) using equation (4.3.11) and (4.2.13), we get

$$\tau_{c1} = \frac{1}{2}\phi' \left(\frac{1}{2}R^2r - \frac{1}{4}r^3 \right) - \frac{2}{3}\tau_y^{1/2}\phi'\phi^{-1/2} \left(\frac{1}{2}R^{3/2}r - \frac{2}{7}r^{5/2} \right) \quad (4.3.13)$$

where $\phi' = \frac{\partial\phi}{\partial t}$

Applying equations (4.3.10) and (4.3.13) in equation (4.3.8) and then integrating, we obtain

$$\begin{aligned}
v_{c1} = & \frac{1}{2}\phi' \left(\frac{3}{16}R^4 - \frac{1}{4}R^2r^2 + \frac{1}{16}r^4 \right) \\
& - \frac{2}{3}\tau_y^{1/2}\phi'\phi^{-1/2} \left(\frac{33}{196}R^{7/2} - \frac{1}{4}R^{3/2}r^2 + \frac{4}{49}r^{7/2} \right) \\
& - \frac{1}{2}\tau_y^{1/2}\phi'\phi^{-1/2} \left(\frac{11}{42}R^{7/2} - \frac{1}{3}R^2r^{3/2} + \frac{1}{14}r^{7/2} \right) \\
& + \frac{2}{3}\tau_y\phi'\phi^{-1} \left(\frac{5}{21}R^3 - \frac{1}{3}R^{3/2}r^{3/2} + \frac{2}{21}r^3 \right)
\end{aligned} \tag{4.3.14}$$

Substitution of $r = r_{p1}$ in equation (4.3.14) yields the expression for v_{p1} given as

$$\begin{aligned}
v_{p1} = & \frac{1}{2}\phi' \left(\frac{3}{16}R^4 - \frac{1}{4}R^2r_{p1}^2 + \frac{1}{16}r_{p1}^4 \right) \\
& - \frac{2}{3}\tau_y^{1/2}\phi'\phi^{-1/2} \left(\frac{33}{196}R^{7/2} - \frac{1}{4}R^{3/2}r_{p1}^2 + \frac{4}{49}r_{p1}^{7/2} \right) \\
& - \frac{1}{2}\tau_y^{1/2}\phi'\phi^{-1/2} \left(\frac{11}{42}R^{7/2} - \frac{1}{3}R^2r_{p1}^{3/2} + \frac{1}{14}r_{p1}^{7/2} \right) \\
& + \frac{2}{3}\tau_y\phi'\phi^{-1} \left(\frac{5}{21}R^3 - \frac{1}{3}R^{3/2}r_{p1}^{3/2} + \frac{2}{21}r_{p1}^3 \right)
\end{aligned} \tag{4.3.15}$$

Thus the total axial velocity distribution for the region $r_p \leq r \leq R(z)$ is $v_c = v_{c0} + \alpha^2 v_{c1}$ (Neglecting terms of higher powers of α^2)

$$\begin{aligned}
\Rightarrow v_c = & \frac{1}{2}\phi(R^2 - r^2) - \frac{4}{3}\tau_y^{1/2}\phi^{1/2}(R^{3/2} - r^{3/2}) + \tau_y(R - r) \\
& + v_s + \alpha^2 \left[\frac{1}{2}\phi' \left(\frac{3}{16}R^4 - \frac{1}{4}R^2r^2 + \frac{1}{16}r^4 \right) \right. \\
& - \frac{2}{3}\tau_y^{1/2}\phi'\phi^{-1/2} \left(\frac{33}{196}R^{7/2} - \frac{1}{4}R^{3/2}r^2 + \frac{4}{49}r^{7/2} \right) \\
& - \frac{1}{2}\tau_y^{1/2}\phi'\phi^{-1/2} \left(\frac{11}{42}R^{7/2} - \frac{1}{3}R^2r^{3/2} \right. \\
& \left. \left. + \frac{1}{14}r^{7/2} \right) + \frac{2}{3}\tau_y\phi'\phi^{-1} \left(\frac{5}{21}R^3 - \frac{1}{3}R^{3/2}r^{3/2} + \frac{2}{21}r^3 \right) \right]
\end{aligned} \tag{4.3.16}$$

The plug flow velocity distribution for the region $0 \leq r \leq r_p$ is

$$\begin{aligned}
v_p = & \frac{1}{2} \phi (R^2 - r_{p0}^2) - \frac{4}{3} \tau_y^{1/2} \phi^{1/2} (R^{3/2} - r_{p0}^{3/2}) + \tau_y (R - r_{p0}) \\
& + v_s + \alpha^2 \left[\frac{1}{2} \phi' \left(\frac{3}{16} R^4 - \frac{1}{4} R^2 r_{p1}^2 + \frac{1}{16} r_{p1}^4 \right) \right. \\
& - \frac{2}{3} \tau_y^{1/2} \phi' \phi^{-1/2} \left(\frac{33}{196} R^{7/2} - \frac{1}{4} R^{3/2} r_{p1}^2 + \frac{4}{49} r_{p1}^{7/2} \right) \\
& - \frac{1}{2} \tau_y^{1/2} \phi' \phi^{-1/2} \left(\frac{11}{42} R^{7/2} - \frac{1}{3} R^2 r_{p1}^{3/2} + \frac{1}{14} r_{p1}^{7/2} \right) \\
& \left. + \frac{2}{3} \tau_y \phi' \phi^{-1} \left(\frac{5}{21} R^3 - \frac{1}{3} R^{3/2} r_{p1}^{3/2} + \frac{2}{21} r_{p1}^3 \right) \right]
\end{aligned}
\tag{4.3.17}$$

The shear stress τ_c is given as

$$\tau_c = r\phi + \alpha^2 \left[\frac{1}{2} \phi' \left(\frac{1}{2} R^2 r - \frac{1}{4} r^3 \right) - \frac{2}{3} \tau_y^{1/2} \phi' \phi^{-1/2} \left(\frac{1}{2} R^{3/2} r - \frac{2}{7} r^{5/2} \right) \right]
\tag{4.3.18}$$

The wall shear stress τ_R is obtained as

$$\tau_R = R\phi + \frac{1}{8} \alpha^2 \phi' R^3 - \frac{1}{7} \alpha^2 \tau_y^{1/2} \phi' \phi^{-1/2} R^{5/2}
\tag{4.3.19}$$

The non – dimensional volumetric flow rate for the region $0 \leq r \leq R(z)$ is defined as

$$Q(z, t) = 4 \int_0^R r v_c dr$$

where $Q(z, t) = \frac{\bar{Q}(\bar{z}, \bar{t})}{\pi \bar{p}_0 \bar{R}_0^4 / 8 \bar{k}_c}$; $\bar{Q}(\bar{z}, \bar{t})$ being the dimensional volumetric flow rate.

Hence

$$\begin{aligned} Q = 2R^2v_s + \frac{2}{3}\tau_y R^3 + \frac{1}{2}R^4 \left(\phi + \frac{1}{6}\alpha^2\phi'R^2 - \frac{15}{77}\alpha^2\tau_y^{1/2}\phi'\phi^{-1/2}R^{3/2} \right) \\ - \frac{8}{7}\tau_y^{1/2}R^{7/2} \left(\phi^{1/2} + \frac{15}{176}\alpha^2\phi'\phi^{-1/2}R^2 \right. \\ \left. - \frac{1}{10}\alpha^2\tau_y^{1/2}\phi'\phi^{-1}R^{3/2} \right) \end{aligned} \quad (4.3.20)$$

4.3. Results and Discussion

The velocity profile for the axial velocity in the non – plug flow area has been obtained by equation (4.3.16). The graphical analysis of the results thus obtained are presented in Figs. 4.1(a) and 4.1(b).

Figure 4.1(a) describes the variations of the axial velocity versus axial distance for the different values of time t , stenosis height H , yield stress τ_y and slip velocity v_s taking fixed values $e = 0.1$ and $\alpha = 0.1$. The profile shows a natural pattern of fluid flow in a circular duct. There is an increase in velocity with the pulse while slip velocity increases the axial velocity of the fluid. It is found that the axial velocity decreases along the axial distance when time, yield stress and stenosis height increase.

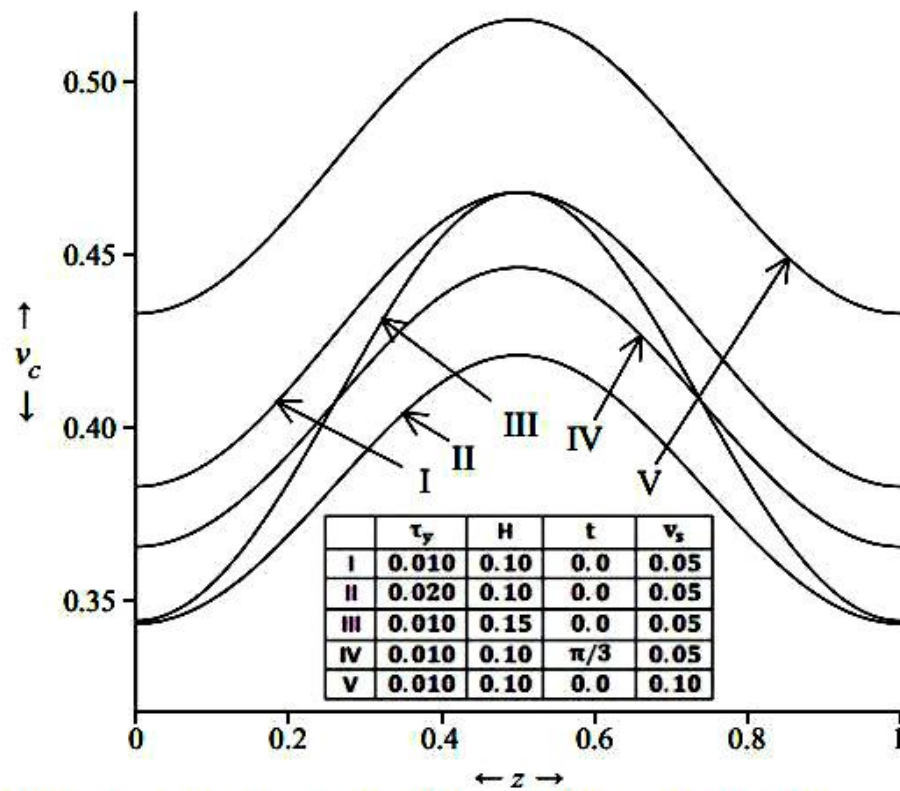


Figure 4.1 (a): Variation of Axial Velocity Along Axial Distance for Different Values of the Time t , Stenosis Height H , Yield Stress τ_y , and Slip Velocity v_s with Some Fixed Values $e = 0.1$ and $\alpha = 0.1$.

Figure 4.1(b) shows the variations of the axial velocity along radial distance for the various values of time t , yield stress τ_y and slip velocity v_s with some fixed values $e = 0.1$ and $\alpha = 0.1$. It is clear that the axial velocity slows down along the radial distance. Also the axial velocity increases when the time, yield stress and slip velocity increase. A similar graph is obtained showing the increments in the axial velocity with the increase in yield stress.

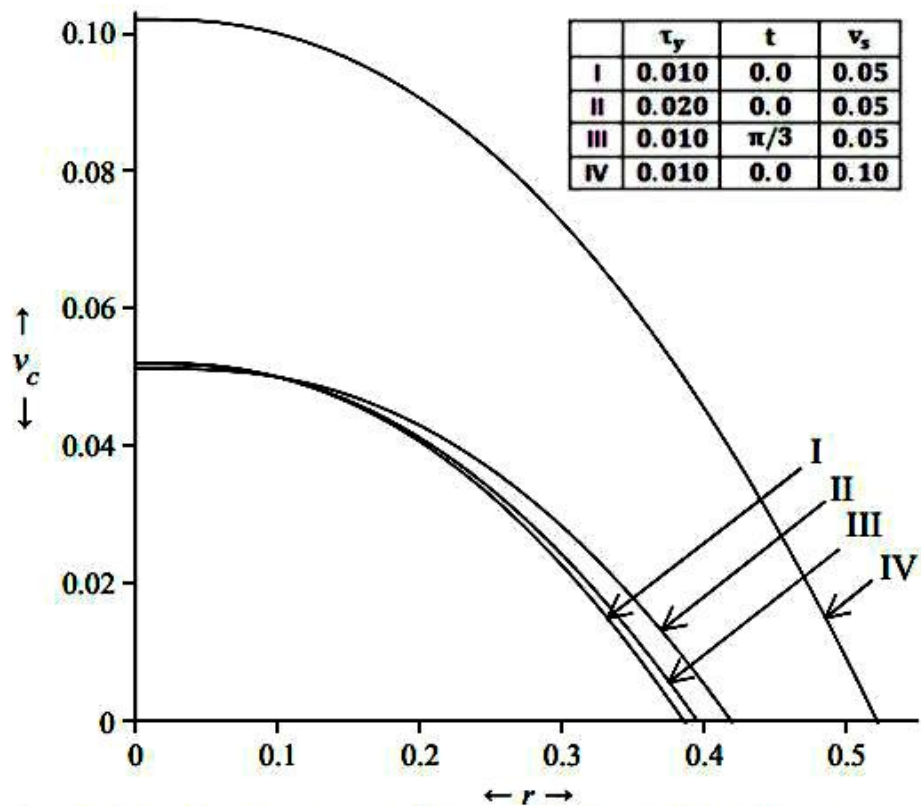


Figure 4.1 (b): Variation of Axial Velocity Along Radial Distance for Different Values of the Time t , Yield Stress τ and Slip Velocity v_s with Some Fixed Values $e = 0.1$ and $\alpha = 0.1$

The graphical analysis of the axial velocity for the plug flow area obtained through equation (4.3.17) has been described through Figs. 4.2(a) and 4.2(b). Figure 4.2(a) gives the variations in plug flow velocity along axial distance for the various values of time t , stenosis height H , yield stress τ_y and slip velocity v_s with some fixed values $e = 0.1$ and $\alpha = 0.1$. It shows that the plug flow velocity increases with the increase in axial distance, the stenosis height or slip velocity while it increases with the pulse. Also the plug flow velocity decreases as the yield stress and time increase.

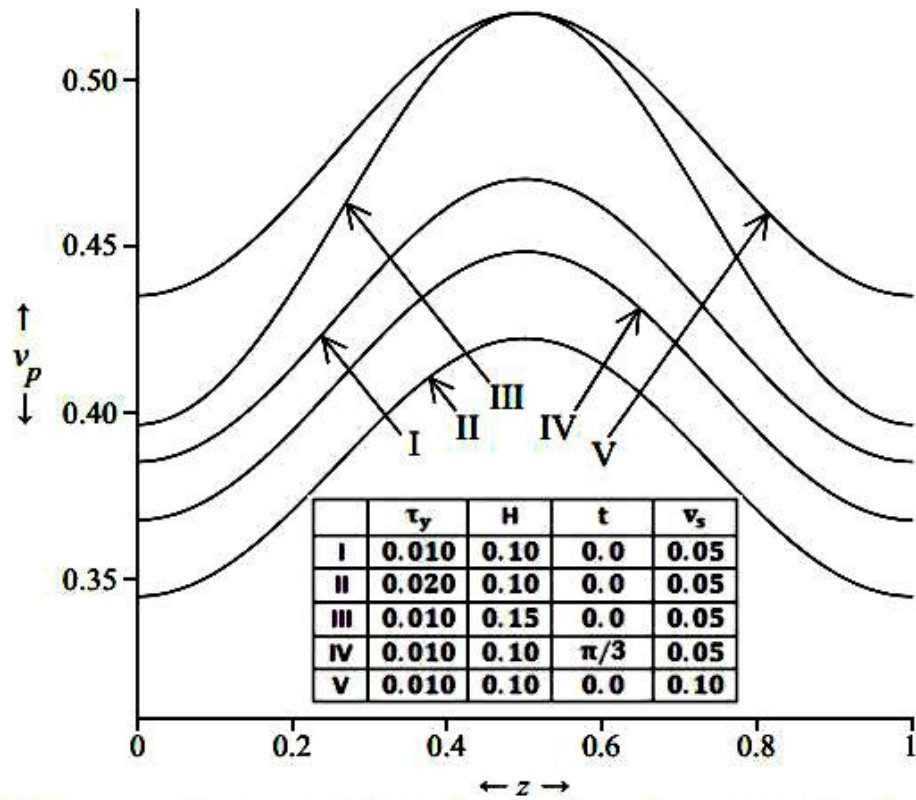


Figure 4.2 (a): Variation of Plug Flow Velocity Along Axial Distance for Different Values of the Time t , Stenosis Height H , Yield Stress τ_y and Slip Velocity v_s with Some Fixed Values $e = 0.1$ and $\alpha = 0.1$.

Figure 4.2(b) explains the changes in plug flow velocity versus radial distance for the different values of time t , yield stress τ_y and slip velocity v_s with some fixed values $e = 0.1$ and $\alpha = 0.1$. The graph shows that the plug flow velocity increases with increase in the radial distance and slip velocity but it decreases as the time and yield stress increase.

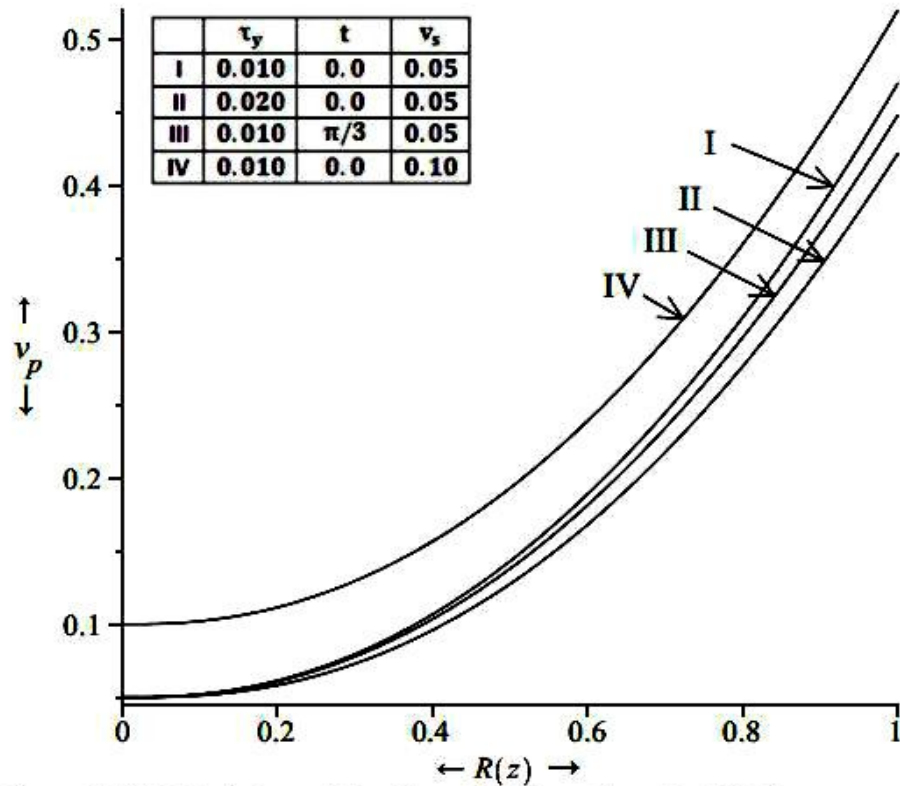


Figure 4.2 (b): Variation of Plug Flow Velocity Along Radial Distance for Different Values of the Time t , Yield Stress τ_y and Slip Velocity v_s with Some Fixed Values $e = 0.1$ and $\alpha = 0.1$

Figure 4.3(a) shows the changes in the wall shear stress derived through equation (4.3.19) along the axial distance for the different values of time t and the stenosis height H with some fixed values $e = 0.1$, $\tau_y = 0.010$ and $\alpha = 0.1$. It describes that the wall shear stress shows wave-like variations along the axial distance and it decreases when time and stenosis height increase.

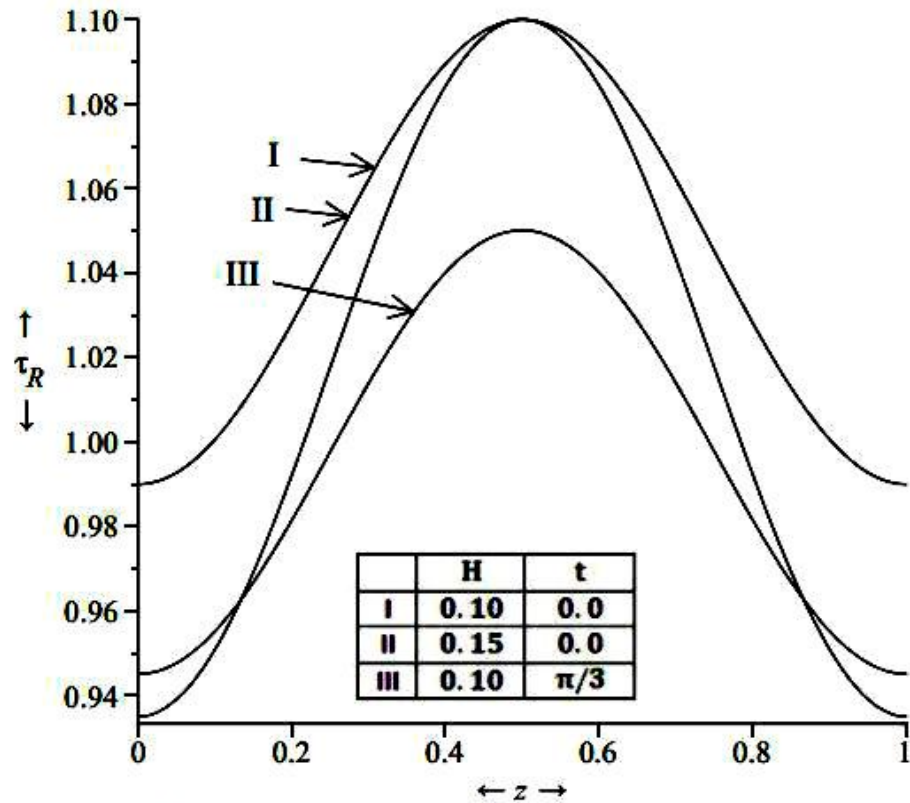


Figure 4.3 (a): Variation of Wall Shear Stress Along Axial Distance for Different Values of the Time t and Stenosis Height H with Some Fixed Values $e = 0.1$, $\tau_y = 0.010$ and $\alpha = 0.1$.

Figure 4.3(b) gives the variations of the wall shear stress along the radial distance for the different values of time t with some fixed values $e = 0.1$, $\tau_y = 0.010$ and $\alpha = 0.1$. It is observed that the wall shear stress increases along the radial distance but it decreases when the time increases.

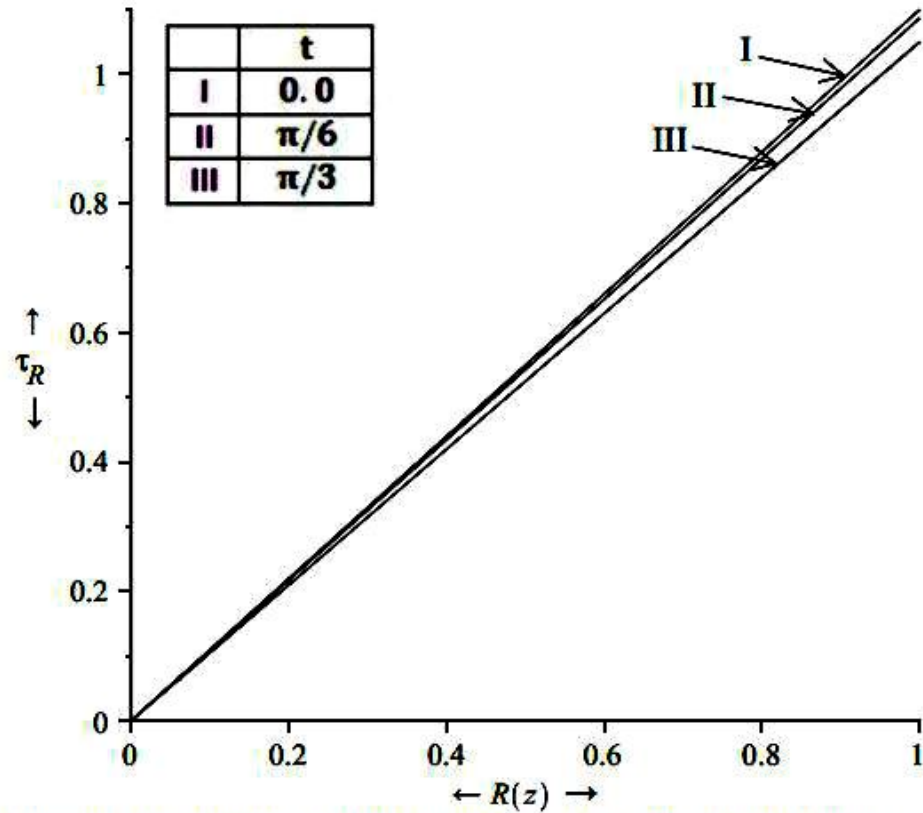


Figure 4.3 (b): Variation of Wall Shear Stress Along Radial Distance for Different Values of the Time t with Some Fixed Values $e = 0.1$, $\tau_y = 0.010$ and $\alpha = 0.1$

Figure 4.4(a) shows the variations of the volumetric flow rate obtained in equation (4.3.20) versus the axial distance for the different values of time t , stenosis height H , yield stress τ_y and slip velocity v_s taking fixed values $e = 0.1$ and $\alpha = 0.1$. It is observed that the volumetric flow rate fluctuates along the axial distance. The flow rate decreases with increase in time, yield stress or stenosis height but it increases when the slip velocity increases.

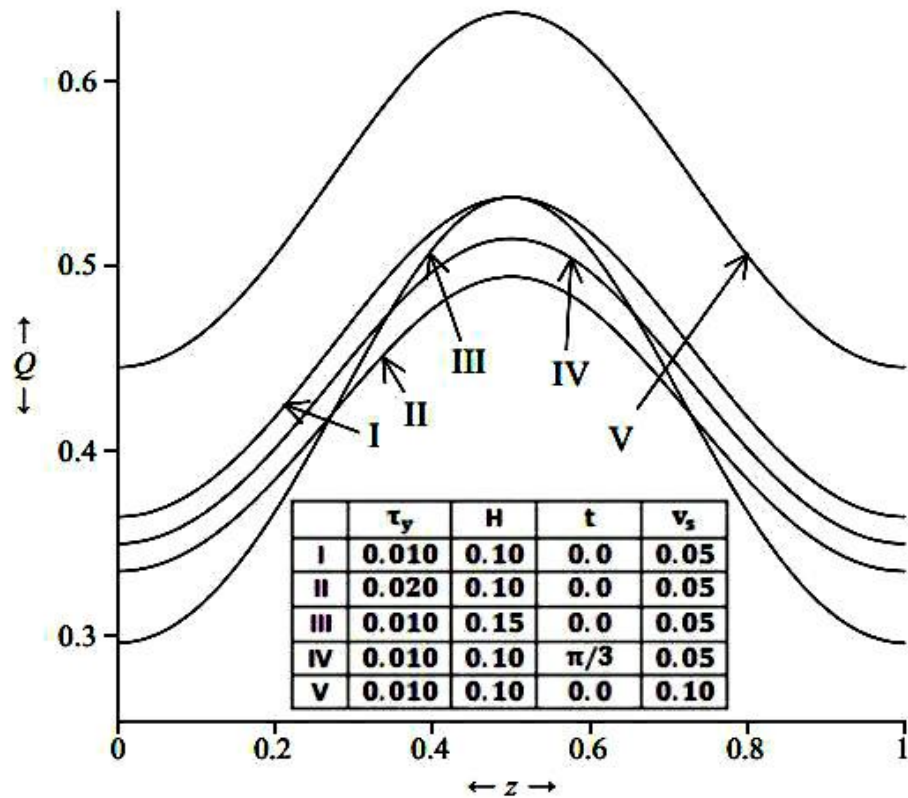


Figure 4.4 (a): Variation of Volumetric Flow Rate Along the Axial Distance for Different Values of the Time t , Stenosis Height and Slip Velocity v_s with Some Fixed Values $e = 0.1$ and $\alpha = 0.1$.

Figure 4.4(b) shows the variations of the volumetric flow rate along the radial distance for the different values of time t , stenosis height H , yield stress τ_y and slip velocity v_s with some fixed values $e = 0.1$ and $\alpha = 0.1$. The graph shows that the volumetric flow rate increases when the radial distance or slip velocity increases. Also it decreases when the time or yield stress increases.

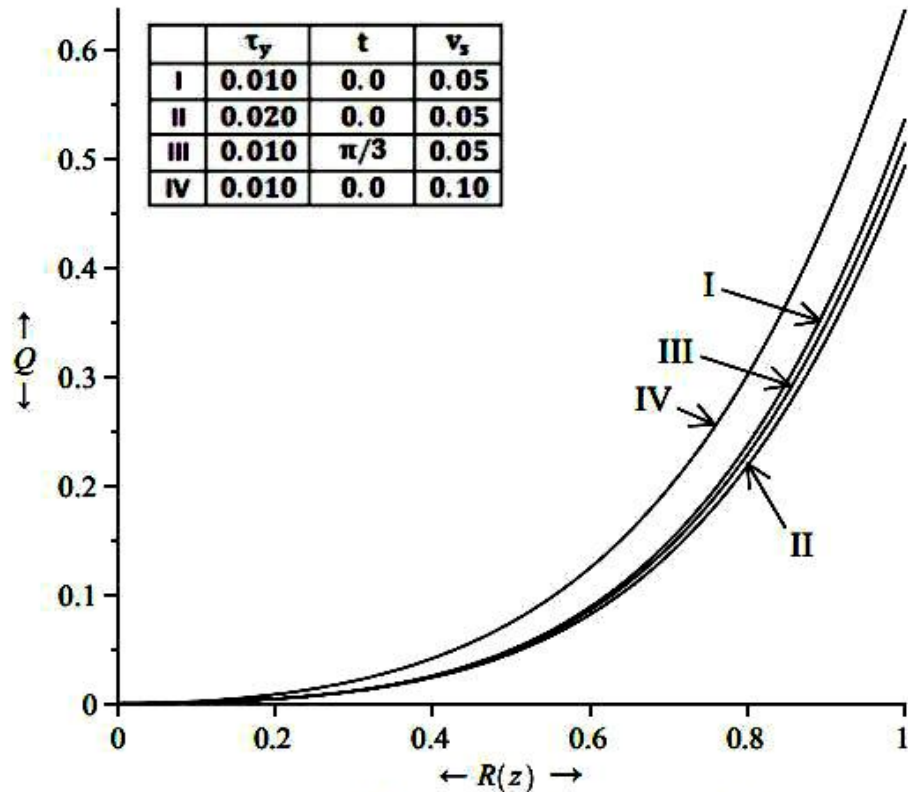


Figure 4.4 (b): Variation of Volumetric Flow Rate Along Radial Distance for Different Values of the Time t , Yield Stress τ_y , and Slip Velocity v_s with Some Fixed Values $e = 0.1$ and $\alpha = 0.1$.

4.5. Conclusion

In the present model where the Casson fluid is considered as a blood, the Womersley parameter α is taken less than one which is suitable for the small blood vessels like coronary arteries. The non – dimensional yield stress τ_y is taken from 0.01 to 0.03 for a normal state. The flow amplitude “e” is also taken less than one which is reasonable for physiological conditions in normal blood flow. Through the graphical analysis it is observed that the volumetric flow rate and the axial velocity in both plug flow and non – plug flow regions increase with pulse and slip velocity along axial distance but they decrease when time or yield stress increases. The axial velocity in non – plug flow region, flow flux and wall shear stress decrease but the plug flow velocity increases with increase in stenosis height. For $t = 0$ the model reduces to steady state situations which is verified by the author’s previous work in chapter 2. The wall shear stress decreases along axial distance when time increases. Also the plug flow velocity, wall shear stress and flow flux increase along radial distance and they decrease when yield stress or time increases. Non – plug flow velocity decreases with increase in radial distance but increases when time, yield stress or slip velocity increases.

CHAPTER - 5

**Biomagnetic Steady
Flow through an
Axisymmetric Stenosed
Artery**

BIOMAGNETIC STEADY FLOW THROUGH AN AXISYMMETRIC STENOSED ARTERY

5.1 Introduction

Many medical research works have so far proved this fact that the narrowing of the blood vessels is causing serious disorders in blood circulation which sometimes lead to the heart failures. It has been observed that the initial deposits of lipids at the sub-endothelial space and then extra addition of macrophages become fibrous in due course of time which creates the cardiovascular problems. So far a number of mathematical models taking different blood features have been proposed to study the rheology of blood. The magnetic aspect of blood has always been an interesting topic of research for the research workers. Since the hemoglobin present in the mature blood cells is a form of iron-oxides, therefore the blood behaves as a biomagnetic fluid. Some research workers have worked on the magnetic property of blood flow under stenotic conditions.

D.F. Young (1968) studied the effect of an axially symmetric time-dependent stenotic growth into the lumen of a tube of constant cross-section over the steady flow by taking the blood as a Newtonian fluid. P.K. Suri et al. (1981) presented a mathematical simulation of blood flow through branched arteries under transverse magnetic field and observed that the applied magnetic field reduces the strength of blockage at the apex of bifurcation. J.C. Misra et al. (1986) studied the flow through stenosed arteries. J.C. Mishra et al. (1989) used the momentum integral method to study flow characteristics of blood through stenosed vessel. K. Haldar et al. (1994) studied the effect of magnetic field on blood flow through indented tube in the presence of erythrocytes. V.P. Srivastava

(1995) dealt with the problem of stenotic blood flow taking blood as a particle-fluid suspension model and observed that the magnitudes of blood flow characteristics significantly increase with increase in red cell concentration. H.P. Mazumdar et al. (1996) investigated some flow characteristics of a Newtonian fluid under effect of magnetic field through a circular tube.

Y. Haik et al. (2001) studied the apparent additive viscosity of human blood because of a high static magnetic field and showed that the blood flow under gravity reduces by 30% when it is kept under high magnetic field of 10 T. J.C. Misra et al. (2007) gave a numerical model to study the effect of magnetic field on blood flow through an artery. S. Kenjeres (2008) analyzed blood flow numerically in realistic arteries subjected to strong non-uniform magnetic fields. L. Parmar et al. (2013) investigated the role of magnetic field intensity in Herschel – Bulkley blood flow through overlapping stenosed artery. In previous chapter 2 of this thesis, author discussed a Casson fluid model to study the steady flow through a stenosed blood vessel in which the author explained that the axial velocity, volumetric flow rate and pressure gradient increase with the increase in slip velocity and decrease with growth in yield stress. Author also studied the slip effects on steady flow through a stenosed blood artery and found that axial velocity, volumetric flow rate and pressure gradient decrease along the radial distance as the slip length increases but the wall shear stress increases with increase in slip length.

5.2 Mathematical Formulation

Let the blood flow be steady, laminar and incompressible through an axially symmetric stenosed cylindrical artery in z – direction.

The geometrical diagram of the stenosed artery is given in figure 2.0.

Let \bar{R}_0 be the radius of the normal tube and $\bar{R}(\bar{z})$ is the radius of the constricted area given by Young (1968):

$$\bar{R}(\bar{z}) = \begin{cases} \bar{R}_0 - \frac{\bar{h}}{2} \left[1 + \cos \frac{2\pi}{\bar{l}_s} (\bar{z}_1 + \bar{l}_s - \bar{z}) \right] & ; \bar{z}_1 \leq \bar{z} \leq \bar{z}_1 + \bar{l}_s \\ \bar{R}_0 & ; \text{otherwise} \end{cases} \quad (5.2.1)$$

Where \bar{l}_s is the length of the stenosis in the artery of the length \bar{l} , \bar{z}_1 is the location of the stenosis of maximum height \bar{h} . Also, let \bar{r} and \bar{z} be radial and axial coordinates.

Here the blood is considered to behave as a Casson fluid under the effect of an externally applied uniform transverse magnetic field which generates a motion due to which the fluid particles are attracted towards the magnetic field.

Under the above considerations, the equations of motion in the dimensional form are:

$$-\frac{\partial \bar{p}}{\partial \bar{z}} + \frac{1}{\bar{r}} \frac{\partial}{\partial \bar{r}} (\bar{r} \bar{\tau}_c) + \epsilon_0 M \frac{\partial \bar{B}}{\partial \bar{z}} = 0 \quad (5.2.2)$$

$$\frac{\partial \bar{p}}{\partial \bar{r}} = 0 \quad (5.2.3)$$

where \bar{p} denotes pressure at any point, ϵ_0 magnetic permeability, M magnetization and \bar{B} represents the magnetic field intensity. Also $\bar{\tau}_c$ denotes the shear stress of the fluid. Casson fluid has the following simplified constitutive equations:

$$F(\bar{\tau}_c) = -\frac{\partial \bar{v}_c}{\partial \bar{r}} = \frac{1}{k_c} (\bar{\tau}_c^{1/2} - \bar{\tau}_0^{1/2})^2 \quad \text{for } \bar{\tau}_c \geq \bar{\tau}_0 \quad (5.2.4)$$

$$\frac{\partial \bar{v}_c}{\partial \bar{r}} = 0 \quad \text{for } \bar{\tau}_c \leq \bar{\tau}_0 \quad (5.2.5)$$

where \bar{v}_c is the axial velocity of the blood, $\bar{\tau}_0$ represents the yield stress and k_c is the fluid viscosity.

The equations (5.2.2) to (5.2.5) are subject to the following boundary conditions:

$$\left. \begin{aligned} \bar{v}_c &= \bar{v}_s & \text{at } \bar{r} &= \bar{R}(\bar{z}) \\ \bar{\tau}_c &= \text{Finite value} & \text{at } \bar{r} &= 0 \end{aligned} \right\} \quad (5.2.6)$$

where \bar{v}_s denotes the slip velocity along z – axis.

Let us introduce the following non – dimensional variables as

$$\begin{aligned} R(z) &= \frac{\bar{R}(\bar{z})}{\bar{R}_0}, \quad z = \frac{\bar{z}_1 + \bar{l}_s - \bar{z}}{\bar{l}_s}, \quad r = \frac{\bar{r}}{\bar{R}_0}, \quad \tau_c = \frac{\bar{\tau}_c}{\bar{p}_0 \bar{R}_0 / 2}, \quad \tau_0 = \frac{\bar{\tau}_0}{\bar{p}_0 \bar{R}_0 / 2}, \\ v_c &= \frac{\bar{v}_c}{\bar{p}_0 \bar{R}_0^2 / 2k_c}, \quad v_s = \frac{\bar{v}_s}{\bar{p}_0 \bar{R}_0^2 / 2k_c}, \quad H = \frac{\bar{h}}{\bar{R}_0}, \quad B = \frac{\bar{B}}{\bar{B}_0}, \quad \frac{\partial p}{\partial z} = \frac{\partial \bar{p} / \partial \bar{z}}{\bar{p}_0} \end{aligned} \quad (5.2.7)$$

Here \bar{p}_0 is the steady – state amplitude and \bar{B}_0 represents the external transverse uniform constant magnetic field.

Under the above non – dimensional conditions, the radius of the stenotic area of the artery becomes

$$R(z) = \begin{cases} 1 - H \cos^2 \pi z & ; 0 \leq z \leq 1 \\ 1 & ; \text{otherwise} \end{cases} \quad (5.2.8)$$

The dimensionless forms of equations (5.2.2) to (5.2.5) are

$$-2 \frac{\partial p}{\partial z} + \frac{1}{r} \frac{\partial}{\partial r} (r \tau_c) - C \frac{\partial B}{\partial z} = 0 \quad (5.2.9)$$

$$\frac{\partial p}{\partial r} = 0 \quad (5.2.10)$$

$$-\frac{\partial v_c}{\partial r} = (\tau_c^{1/2} - \tau_0^{1/2})^2 \quad \text{for } \tau_c \geq \tau_0 \quad (5.2.11)$$

$$\frac{\partial v_c}{\partial r} = 0 \quad \text{for } \tau_c \leq \tau_0 \quad (5.2.12)$$

$$\text{where } C = \frac{2\epsilon_0 M \bar{B}_0}{\bar{p}_0 \bar{l}_s} \quad (5.2.13)$$

The non – dimensional boundary conditions are

$$\left. \begin{aligned} v_c &= v_s & \text{at } r &= R(z) \\ \tau_c &= \text{Finite value} & \text{at } r &= 0 \end{aligned} \right\} \quad (5.2.14)$$

Using condition (5.2.14) in equation (5.2.9), the shear stress τ_c and wall shear stress τ_R can be written as

$$\tau_c = \frac{r}{2} \left(2 \frac{\partial p}{\partial z} + C \frac{\partial B}{\partial z} \right) \quad (5.2.15)$$

$$\tau_R = \frac{R}{2} \left(2 \frac{\partial p}{\partial z} + C \frac{\partial B}{\partial z} \right) \quad (5.2.16)$$

From equations (5.2.15) and (5.2.16),

$$\frac{\tau_c}{\tau_R} = \frac{r}{R} \quad (5.2.17)$$

where $R = R(z)$

5.3 Method of Solution

Thus velocity in the region $r_p \leq r \leq R(z)$ is obtained by integrating equation (5.2.11) using conditions (5.2.14) and (5.2.15) where $r_p = \frac{r_p}{R_0}$ is the non – dimensional radius of the plug flow region, given as

$$v_c = v_s + \frac{1}{\left(2 \frac{\partial p}{\partial z} + C \frac{\partial B}{\partial z} \right)} \left[(\tau_R^{1/2} - \tau_0^{1/2})^4 + \frac{4}{3} \tau_0^{1/2} (\tau_R^{1/2} - \tau_0^{1/2})^3 - (\tau_c^{1/2} - \tau_0^{1/2})^4 - \frac{4}{3} \tau_0^{1/2} (\tau_c^{1/2} - \tau_0^{1/2})^3 \right] \quad (5.3.1)$$

Within plug flow region i.e. $0 \leq r \leq r_p$, $\tau_c = \tau_0$ at $r = r_p$, therefore the plug flow velocity is

$$v_p = v_s + \frac{1}{\left(2 \frac{\partial p}{\partial z} + C \frac{\partial B}{\partial z} \right)} \left[(\tau_R^{1/2} - \tau_0^{1/2})^4 + \frac{4}{3} \tau_0^{1/2} (\tau_R^{1/2} - \tau_0^{1/2})^3 \right] \quad (5.3.2)$$

Now the volumetric flow rate in the dimensionless form for the region $0 \leq r \leq R(z)$ can be obtained as

$$\begin{aligned} Q &= 4 \int_0^R r v(r) dr \\ &= 4 \int_0^{r_p} r v_p dr + 4 \int_{r_p}^R r v_c dr \end{aligned}$$

Hence

$$Q = 2R^2v_s + \frac{R^2}{\left(2\frac{\partial p}{\partial z} + C\frac{\partial B}{\partial z}\right)} \left[2(\tau_R^{1/2} - \tau_0^{1/2})^4 + \frac{8}{3}\tau_0^{1/2}(\tau_R^{1/2} - \tau_0^{1/2})^3 \right] - \frac{R^2}{\left(2\frac{\partial p}{\partial z} + C\frac{\partial B}{\partial z}\right)\tau_R^2} \left[\tau_R^4 - \frac{2}{3}\tau_R^2\tau_0^2 + \frac{8}{3}\tau_R^3\tau_0 - \frac{64}{21}\tau_R^{7/2}\tau_0^{1/2} + \frac{1}{21}\tau_0^4 \right] \quad (5.3.3)$$

If $\tau_0 \ll \tau_R$ i.e. $\frac{\tau_0}{\tau_R} \ll 1$, then equation (5.3.3) reduces to the form

$$Q = 2R^2v_s + \frac{R^2\tau_R}{\left(2\frac{\partial p}{\partial z} + C\frac{\partial B}{\partial z}\right)} \left(\tau_R - \frac{16}{7}\tau_0^{1/2}\tau_R^{1/2} + \frac{4}{3}\tau_0 \right) \quad (5.3.4)$$

which also gives us the wall shear stress for the stenosed artery as

$$\tau_R = \left[\frac{8}{7}\tau_0^{1/2} + \left\{ \frac{r(Q-2R^2v_s)}{R^3\tau_c} \left(2\frac{\partial p}{\partial z} + C\frac{\partial B}{\partial z} \right) - \frac{4}{147}\tau_0 \right\}^{1/2} \right]^2 \quad (5.3.5)$$

If there is no stenosis i.e. $R(z) = R_0$ then the wall shear stress for the non – constricted artery is given as

$$\tau_N = \left[\frac{8}{7}\tau_0^{1/2} + \left\{ \frac{r(Q-2R_0^2v_s)}{R_0^3\tau_c} \left(2\frac{\partial p}{\partial z} + C\frac{\partial B}{\partial z} \right) - \frac{4}{147}\tau_0 \right\}^{1/2} \right]^2 \quad (5.3.6)$$

5.4 Results and Discussion

The velocity profile for the axial velocity in the non – plug flow region has been obtained in equation (5.3.1) and the graphical discussions of the results are given in figures 5.1(a) and 5.1(b).

Figure 5.1(a) gives the variations of the axial velocity versus axial distance for the different values of the stenosis height H , pressure gradient $\frac{\partial p}{\partial z}$, magnetic field gradient $\frac{\partial B}{\partial z}$, yield stress τ_0 and slip velocity v_s with some fixed value $\tau_c = 0.030$. It is observed that the axial velocity first increases achieving a maximum value at the peak of the stenosis and then starts decreasing along the axial distance. Also the axial velocity increases with an increase in slip velocity, pressure gradient and magnetic field gradient but it decreases when the yield stress increases.

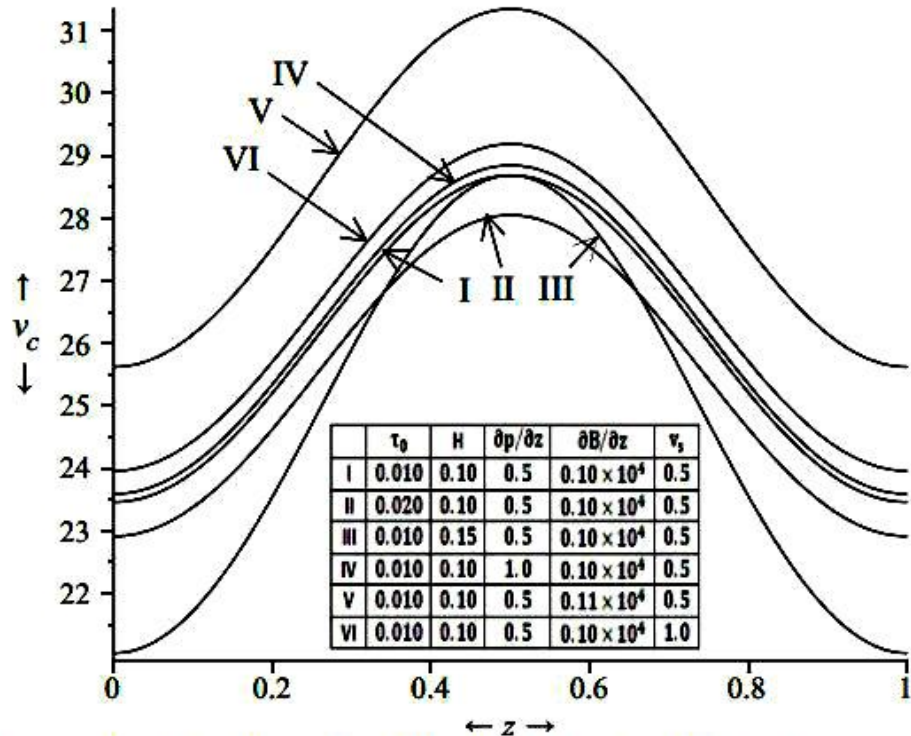


Figure 5.1 (a): Variation of Axial Velocity Along Axial Distance for Different Values of the Stenosis Height H , pressure gradient $\frac{\partial p}{\partial z}$, Magnetic Field Gradient $\frac{\partial B}{\partial z}$, Yield Stress τ_0 and Slip Velocity v_s .

Figure 5.1(b) shows the variations of the axial velocity along radial distance for the various values of the magnetic field gradient $\frac{\partial B}{\partial z}$, yield stress τ_0 and slip velocity v_s with some fixed value $\tau_c = 0.030$. When the magnetic field increases, the axial velocity starts increasing slowly but it increases fast as the radial distance increases. As the slip velocity increases, the axial velocity increases a little fast but grows slowly when the radial distance increases. The axial velocity decreases slowly when the yield stress increases along the radial distance.

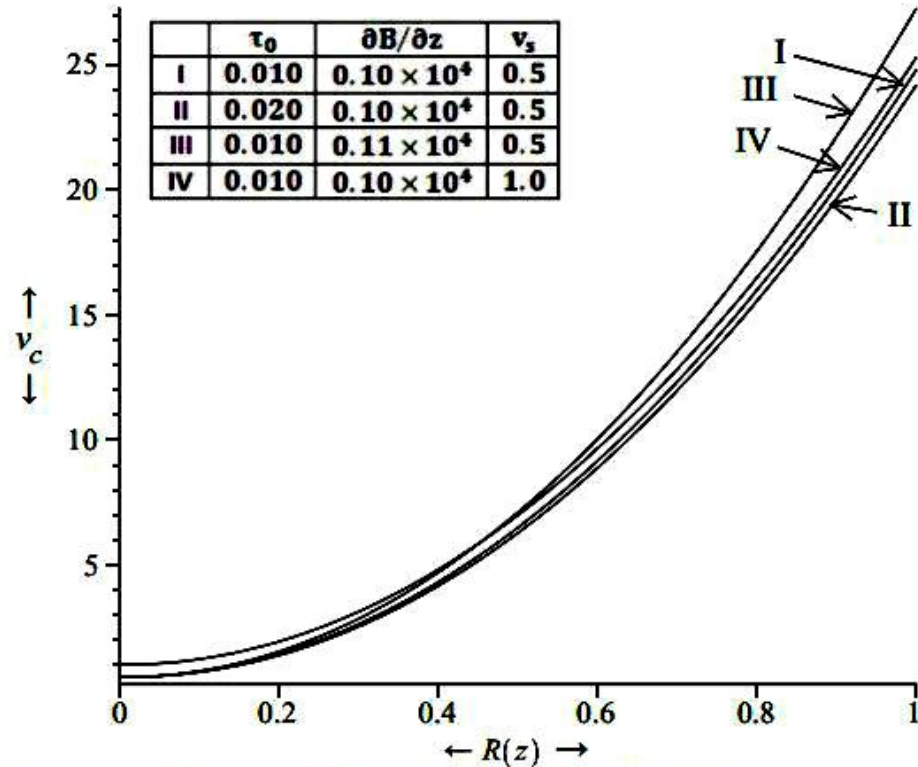


Figure 5.1 (b): Variation of Axial Velocity Along Radial Distance for Different Values of the Magnetic Field Gradient $\frac{\partial B}{\partial z}$, Yield Stress τ_0 and Slip Velocity v_s .

The graphical description of the axial velocity for the plug flow area obtained through equation (5.3.2) has been given in figures 5.2(a) and 5.2(b). Figure 5.2(a) describes the changes in plug flow velocity along axial distance for the different values of the stenosis height H , pressure gradient $\frac{\partial p}{\partial z}$, magnetic field gradient $\frac{\partial B}{\partial z}$, yield stress τ_0 and slip velocity v_s with a fixed value $\tau_c = 0.030$. The graph shows that the plug flow velocity first increases to get a maximum value at the peak of the stenosis along the axial distance and after a certain point it starts decreasing. The plug flow velocity increases greatly for smaller increments in magnetic field gradient along the axial distance. As the slip velocity increases, the plug flow velocity increases with pulse along the axial distance. When the pressure gradient increases, the plug flow velocity increases along the z – axis. The plug flow velocity decreases as the yield stress increases.

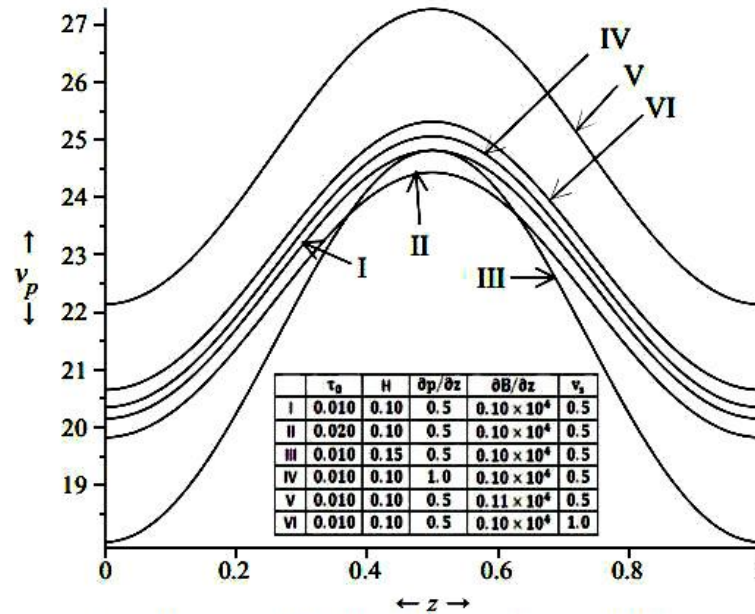


Figure 5.2 (a): Variation of Plug Flow Velocity Along Axial Distance for Different Values of the Stenosis Height H , pressure gradient $\frac{\partial p}{\partial z}$, Magnetic Field Gradient $\frac{\partial B}{\partial z}$, Yield Stress τ_0 and Slip Velocity v_s .

Figure 5.2(b) shows the variations in plug flow velocity versus radial distance for the different values of the pressure gradient $\frac{\partial p}{\partial z}$, magnetic field gradient $\frac{\partial B}{\partial z}$, yield stress τ_0 and slip velocity v_s with some fixed value $\tau_c = 0.030$. It clarifies that the plug flow velocity increases along the radial distance. As the magnetic field gradient increases, the plug flow velocity increases very slowly for smaller radial distance but it increases fast as the radial distance increases. When the slip velocity increases, the pug flow velocity increases fast for lower radial distance but it becomes slower along the radial distance. Also the plug flow velocity decreases as the yield stress increases.

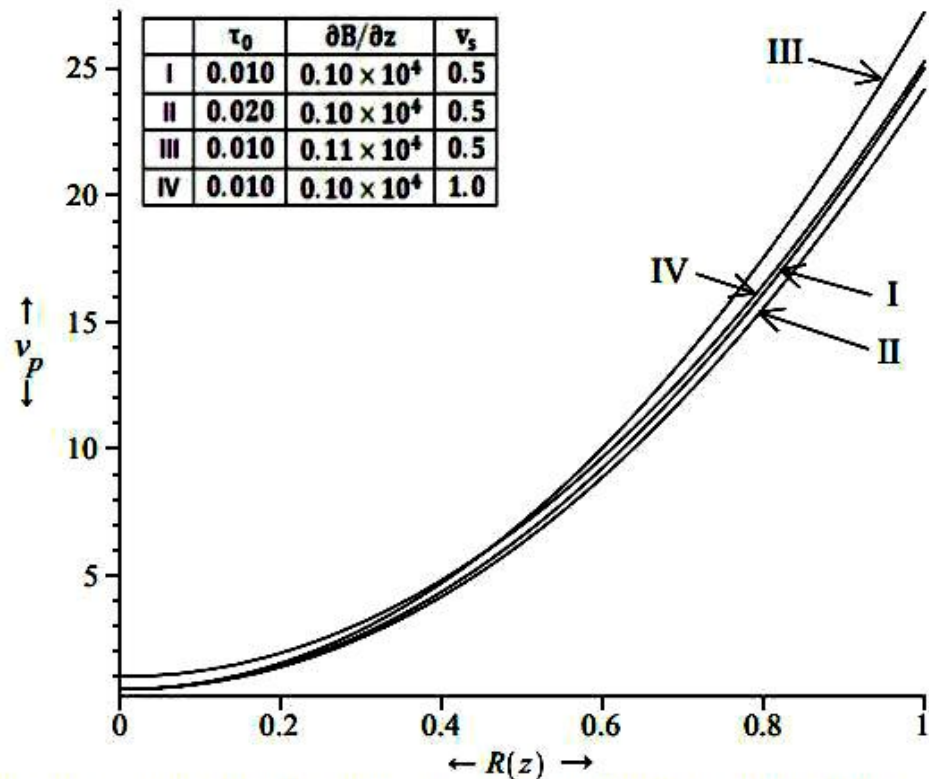


Figure 5.2 (b): Variation of Plug Flow Velocity Along Radial Distance for Different Values of the Magnetic Field Gradient $\frac{\partial B}{\partial z}$, Yield Stress τ_0 and Slip Velocity v_s .

The variations of the volumetric flow rate obtained through equation (5.3.4) are shown along the axial distance for the various values of the stenosis height H , pressure gradient $\frac{\partial p}{\partial z}$, magnetic field gradient $\frac{\partial B}{\partial z}$ and slip velocity v_s with a fixed value $\tau_c = 0.030$ in figure 5.3(a). It shows that the flow flux first increases and after getting a maximum value at the peak of the stenosis, it decreases. When the pressure gradient increases, the volumetric flow rate increases slowly with pulse along the axial distance. As slip velocity increases, the flow flux increases fast. The flow flux increases greatly for smaller increments in the magnetic field gradient along the axial distance. The volumetric flow rate decreases slowly with increment in the yield stress along the axial distance.

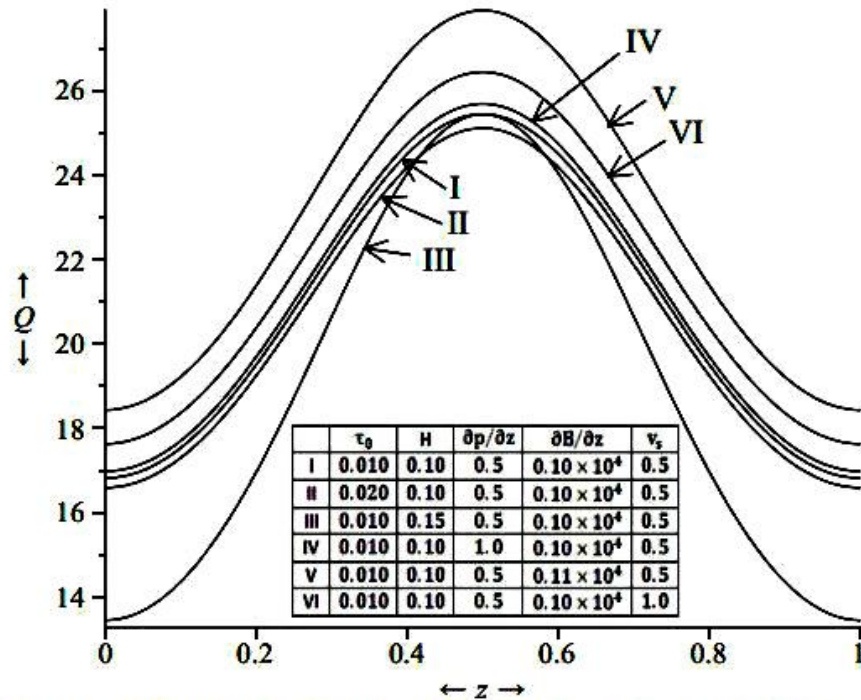


Figure 5.3 (a): Variation of Volumetric Flow Rate Along Axial Distance for Different Values of the Stenosis Height H , pressure gradient $\frac{\partial p}{\partial z}$, Magnetic Field Gradient $\frac{\partial B}{\partial z}$, Yield Stress τ_0 and Slip Velocity v_s .

Figure 5.3(b) shows the changes in the volumetric flow rate along the radial distance for the different values of the magnetic field gradient $\frac{\partial B}{\partial z}$ and slip velocity v_s with a fixed value $\tau_c = 0.030$. The volumetric flow rate keeps on growing along the radial distance. The flow flux increases very slowly for smaller increments in the magnetic field gradient along the radial distance. When the slip velocity increases, the volumetric flow rate slowly increases for lower radial distance but it increases fast as the radial distance increases.

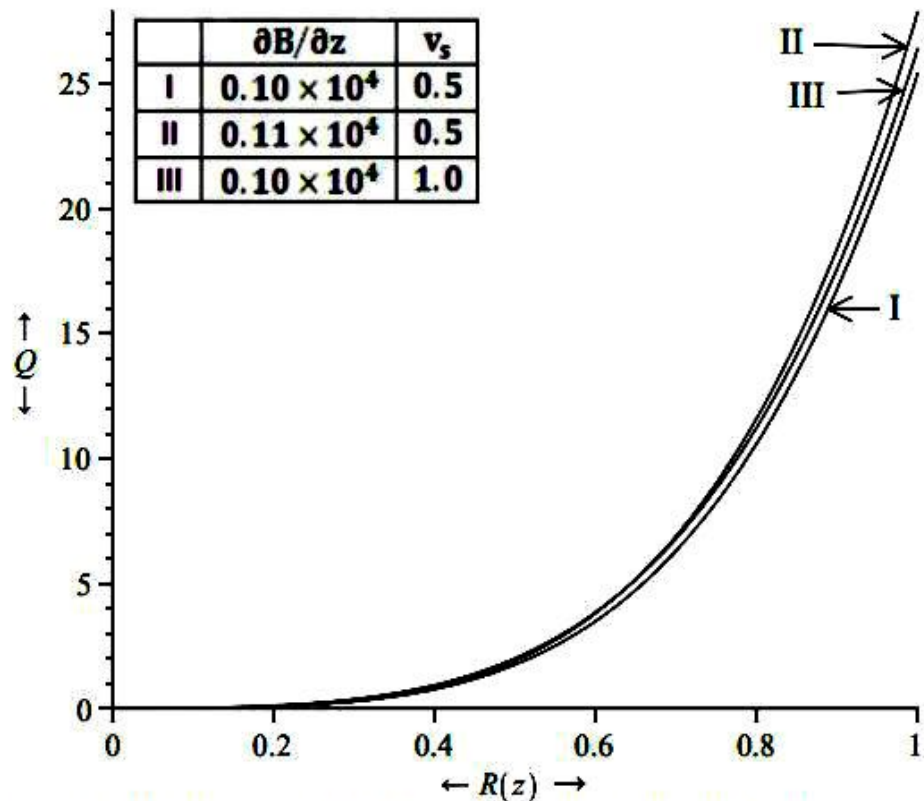


Figure 5.3 (b): Variation of Volumetric Flow Rate Along Radial Distance for Different Values of the Magnetic Field Gradient $\frac{\partial B}{\partial z}$ and Slip Velocity v_s .

Figure 5.4(a) shows the variations of the wall shear stress derived through equation (5.3.5) along the axial distance for the different values of the stenosis height H , pressure gradient $\frac{\partial p}{\partial z}$, magnetic field gradient $\frac{\partial B}{\partial z}$ and slip velocity v_s with a fixed value $\tau_c = 0.030$. The wall shear stress keeps on changing from high value to low value at the peak of the stenosis and then again to high value along the axial distance. When the pressure gradient increases, the wall shear stress shows slow increments along the axial distance. It almost coincides with the previous values of the wall shear stress. With increase in the magnetic field gradient, the wall shear stress increases. As the slip velocity increases, the wall shear stress increases greatly along the axial distance.

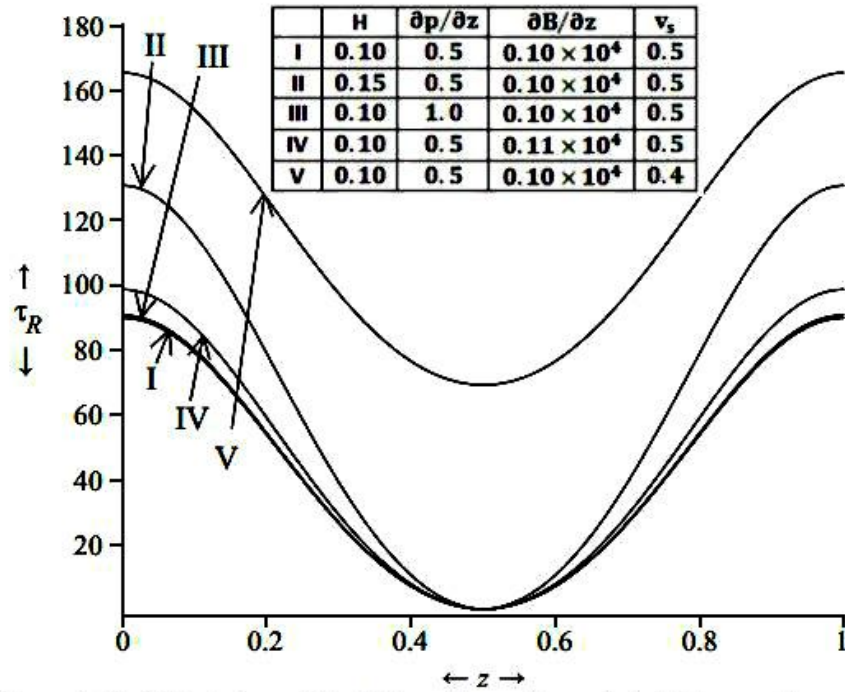


Figure 5.4 (a): Variation of Wall Shear Stress Along Axial Distance for Different Values of the Stenosis Height H , pressure gradient $\frac{\partial p}{\partial z}$, Magnetic Field Gradient $\frac{\partial B}{\partial z}$ and Slip Velocity v_s .

Figure 5.4(b) gives the changes in the wall shear stress versus the radial distance for the different values of the magnetic field gradient $\frac{\partial B}{\partial z}$ and slip velocity v_s with a fixed value $\tau_c = 0.030$. It is clear that the wall shear stress increases fast along the radial distance when the magnetic field gradient increases. Also the wall shear stress decreases very slowly along the radial distance as the slip velocity increases.

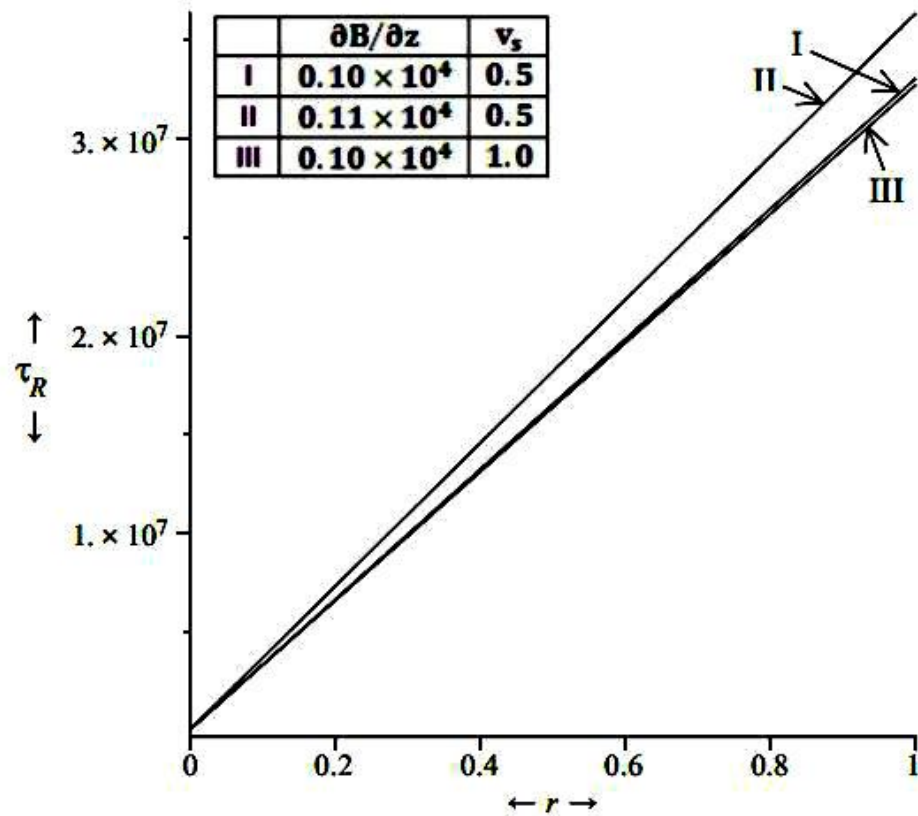


Figure 5.4 (b): Variation of Wall Shear Stress Along Radial Distance for Different Values of the Magnetic Field Gradient $\frac{\partial B}{\partial z}$ and Slip Velocity v_s .

The graphical representations of variations of some flow characteristics were not very clear due to the very small changes in the corresponding values. Therefore these variations are provided in tabulated forms.

The variations of axial and plug flow velocities versus pressure gradient along the radial distance are given in Table 5.1. It is clear from the table that the fluid velocities in both plug flow and non – plug flow regions are increasing with increase in the pressure gradient along the radial distance. The fluid velocity is also increasing when it enters from non – plug flow region to the plug flow region.

Table 5.1: Variation of Fluid Velocity in Plug Flow and Non-plug Flow Regions versus Pressure Gradient Along Radial Distance.

$\frac{\partial p}{\partial z}$	$R(z) = 0.0$		$R(z) = 0.5$		$R(z) = 1.0$	
	v_c	v_p	v_c	v_p	v_c	v_p
0.5	0.49999886	0.499999670	6.482	6.482	24.812	24.812
1.0	0.49999887	0.499999673	6.543	6.543	25.057	25.057
1.5	0.49999888	0.499999676	6.604	6.604	25.303	25.303

Table 5.2(a) shows the variations of the volumetric flow rate versus pressure gradient along the radial distance. When the pressure gradient increases, the flow flux increases along the radial distance.

Table 5.2(a): Variations of Volumetric Flow Rate versus Pressure Gradient Along Radial Distance.

$\frac{\partial p}{\partial z}$	Q		
	R = 0.0	R = 0.5	R = 1.0
0.5	0.0	1.757173	25.444514
1.0	0.0	1.772444	25.690503
1.5	0.0	1.787716	25.936512

Table 5.2(b) gives the changes in the volumetric flow rate versus pressure gradient along the radial distance. It is observed that the flow flux increases along the radial distance as the yield stress increases.

Table 5.2(b): Variations of Volumetric Flow Rate versus Yield Stress Along Radial Distance.

τ_0	Q		
	R = 0.0	R = 0.5	R = 1.0
0.010	0.0	1.757173	25.444514
0.015	0.0	1.728272	25.114776
0.020	0.0	1.706290	24.863310

The variations of the wall shear stress along axial and radial distances for different values of the yield stress are given in Table 5.3(a). The wall shear stress first decreases and after a minimum value it again starts increasing along axial distance. Also it increases with increase in the yield stress. The wall stress also increases along the radial distance when the yield stress increases.

Table 5.3(a): Variations of Wall Shear Stress versus Yield Stress Along Axial and Radial Distance.

τ_0	τ_R					
	z			r		
	0.1	0.4	1.0	0.1 ($\times 10^6$)	0.4 ($\times 10^7$)	1.0 ($\times 10^7$)
0.010	79.301	7.1852	89.8996	3.3037	1.321403	3.30343
0.015	79.759	7.3235	90.3872	3.3038	1.321421	3.30346
0.020	80.146	7.4410	90.7992	3.3038	1.321437	3.30348

Table 5.3(b) exhibits the changes in the wall shear stress versus pressure gradient along the radial distance. It is obvious that the wall shear stress increases along the radial distance when the pressure gradient increases.

Table 5.3(b): Variations of Wall Shear Stress versus Pressure Gradient Along Axial and Radial Distance.

$\frac{\partial p}{\partial z}$	τ_R		
	$r = 0.1$ ($\times 10^6$)	$r = 0.4$ ($\times 10^7$)	$r = 1.0$ ($\times 10^7$)
0.5	3.303715	1.321403	3.303431
1.0	3.307015	1.322723	3.306731
1.5	3.310315	1.324043	3.310031

5.5 Conclusion

The present model deals with the study of the magnetic feature of blood as a Casson fluid. The values of the different parameters used in the analysis have been taken from the chapter 2 of this thesis. The analysis of the study shows that the volumetric flow rate and the axial velocity increase along axial distance with pulse when the axial distance, pressure gradient, magnetic field gradient, yield stress and slip velocity increase and the axial velocity in plug flow region along radial distance decreases when yield stress increases but it rises with increase in magnetic field gradient and slip velocity. The axial velocity in both plug and non – plug flow regions and the flow flux decrease along the axial distance with increase in stenosis height. The axial and the plug flow velocity increase with increase in the pressure gradient along the radial distance. The flow flux in radial direction increases when the magnetic field gradient, pressure gradient and the slip velocity increase. The wall shear stress shows fluctuations along the axial distance from higher values to the minimum values and then again to higher values. It increases as the pressure gradient, magnetic field gradient, slip velocity and stenosis height increase in z – direction. Also the wall shear stress increases when magnetic field gradient increases but it decreases as the slip velocity increases. The wall shear stress increases along radial distance with increase in pressure gradient and the yield stress.

CHAPTER - 6

Steady Slip Blood Flow through a Stenosed Porous Artery

STEADY SLIP BLOOD FLOW THROUGH A STENOSED POROUS ARTERY

6.1 Introduction

It is believed that the abnormal and the unnatural deposits of the fatty and the fibrous tissues in arterial lumen obstruct the blood flow which gives rise to various cardiovascular and cerebral diseases. According to medical reports, the endothelial walls have the ultra – microscopic pores for filtration. Cholesterol increases the wall permeability when the arterial walls are damaged, inflamed or dilated. When the fatty and fibrous tissues are clotted in the wall lumen, its distribution acts like a porous medium. Many researchers have attempted to understand the different flow features by considering blood flow through a porous cylindrical tube under stenosis.

G.S. Beavers et al. (1967) studied the boundary conditions at a naturally permeable wall and suggested that the effect of boundary should be replaced with a slip velocity proportional to the exterior velocity gradient. D.F. Young (1968) investigated the effect of time dependent stenosis on blood flow through a tube taking blood as a Newtonian fluid. R.K. Dash et al. (1996) investigated the Casson fluid flow in a pipe filled with a homogeneous porous medium by applying the Brinkman model for the Darcy resistance shown by the porous medium. B.K. Mishra et al. (2007) studied the effect of porous parameter and stenosis height on the wall shear stress of human blood flow. S. Mishra et al. (2011) discussed the effects of the wall permeability through a stenosed artery. D. Jogie et al. (2012) studied the laminar flows of two immiscible fluids through permeable channel. A. Kumar et al. (2012) investigated the porous effects on two phase blood under magnetic field. S. Pramanik

(2014) used Casson fluid model to study the boundary layer fluid flow with heat transfer past an exponentially porous stretching surface under the thermal radiation and observed that the skin-friction increases when the suction parameter increases. Author in previous chapter 2, discussed a Casson fluid model for steady flow through a stenosed blood vessel in which author explained that the axial velocity, volumetric flow rate and pressure gradient increase with the increase in slip velocity and decrease with growth in yield stress. Author studied the slip effects on steady flow through a stenosed blood artery and found that axial velocity, volumetric flow rate and pressure gradient decrease along the radial distance as the slip length increases but the wall shear stress increases with increase in slip length. Author also analyzed the magnetic effects on steady blood flow through an artery under axisymmetric stenosis and concluded that the axial velocity and flow flux increase as the magnetic field gradient and slip velocity increase but they decrease with the stenosis height along axial distance.

6.2 Mathematical Formulation

Steady, laminar and incompressible flow of blood through an axially symmetric stenosed cylindrical artery in z – direction is considered.

The geometry of the stenosed artery is given in figure 2.0.

Let \bar{R}_0 be the radius of the normal tube and $\bar{R}(\bar{z})$ be the radius of the stenosed portion given by Young (1968) as:

$$\bar{R}(\bar{z}) = \begin{cases} \bar{R}_0 - \frac{\bar{h}}{2} \left[1 + \cos \frac{2\pi}{\bar{l}_s} (\bar{z}_1 + \bar{l}_s - \bar{z}) \right] & ; \bar{z}_1 \leq \bar{z} \leq \bar{z}_1 + \bar{l}_s \\ \bar{R}_0 & ; \text{otherwise} \end{cases} \quad (6.2.1)$$

where \bar{l}_s is the length of the stenosis in the artery of the length \bar{l} , \bar{z}_1 is the position of the stenosis of maximum height \bar{h} . Let \bar{r} and \bar{z} be radial and axial coordinates respectively.

The blood is considered to behave like Casson fluid passing through the artery having permeable walls of homogeneous and isotropic materials. Flow is considered to be governed by the Darcy's Law.

With above considerations, the equations of motion in the dimensional form are:

$$-\frac{\partial \bar{p}}{\partial z} + \frac{1}{\bar{r}} \frac{\partial}{\partial \bar{r}} (\bar{r} \bar{\tau}_c) = 0 \quad (6.2.2)$$

$$\frac{\partial \bar{p}}{\partial \bar{r}} = 0 \quad (6.2.3)$$

where \bar{p} is the pressure at any point and $\bar{\tau}_c$ be the shear stress of the Casson fluid with following simplified constitutive equations:

$$F(\bar{\tau}_c) = -\frac{\partial \bar{v}_c}{\partial \bar{r}} = \frac{1}{\bar{k}_c} (\bar{\tau}_c^{1/2} - \bar{\tau}_0^{1/2})^2 \quad \text{for } \bar{\tau}_c \geq \bar{\tau}_0 \quad (6.2.4)$$

$$\frac{\partial \bar{v}_c}{\partial \bar{r}} = 0 \quad \text{for } \bar{\tau}_c \leq \bar{\tau}_0 \quad (6.2.5)$$

where \bar{v}_c is the axial velocity of the blood, $\bar{\tau}_0$ be the yield stress and \bar{k}_c is the fluid viscosity.

The equations (6.2.2) to (6.2.5) are subject to the following boundary conditions (Beavers and Joseph, 1967):

$$\left. \begin{array}{l} \bar{\tau}_c = \text{Finite Value} \\ \bar{v}_c = \bar{v}_s \\ \frac{\partial \bar{v}_c}{\partial \bar{r}} = \frac{\alpha}{\bar{\epsilon}^{1/2}} (\bar{v}_s - \bar{v}_f) \end{array} \right\} \begin{array}{l} \text{at } \bar{r} = 0 \\ \text{at } \bar{r} = \bar{R}(\bar{z}) \\ \text{at } \bar{r} = \bar{R}(\bar{z}) \end{array} \quad (6.2.6)$$

where by Darcy's law,

$$\bar{v}_f = -\frac{\bar{\epsilon}}{\bar{k}_c} \frac{\partial \bar{p}}{\partial z} \quad (6.2.7)$$

Here \bar{v}_s represents the slip velocity in z – direction, \bar{v}_f is the filter velocity of fluid through the porous region known as the Darcy value, α be a non – dimensional quantity known as the slip

parameter which depends upon the material parameters characterizing the structure of porous material within the boundary region and $\bar{\epsilon}$ is the permeability of the wall material.

Introducing the following non – dimensional variables as

$$\begin{aligned} R(z) &= \frac{\bar{R}(z)}{\bar{R}_0}, \quad z = \frac{\bar{z}_1 + \bar{I}_s - \bar{z}}{\bar{I}_s}, \quad r = \frac{\bar{r}}{\bar{R}_0}, \quad \tau_c = \frac{\bar{\tau}_c}{\bar{p}_0 \bar{R}_0 / 2}, \quad \tau_0 = \frac{\bar{\tau}_0}{\bar{p}_0 \bar{R}_0 / 2}, \\ v_c &= \frac{\bar{v}_c}{\bar{p}_0 \bar{R}_0^2 / 2 \bar{k}_c}, \quad v_s = \frac{\bar{v}_s}{\bar{p}_0 \bar{R}_0^2 / 2 \bar{k}_c}, \quad v_f = \frac{\bar{v}_f}{\bar{p}_0 \bar{R}_0^2 / 2 \bar{k}_c}, \quad H = \frac{\bar{h}}{\bar{R}_0}, \quad \epsilon = \frac{\bar{\epsilon}}{\bar{R}_0^2}, \quad \frac{\partial p}{\partial z} = \frac{\partial \bar{p} / \partial \bar{z}}{\bar{p}_0} \end{aligned} \quad (6.2.8)$$

Here \bar{p}_0 denotes the steady – state amplitude.

With above non – dimensional scheme, the radius of the stenotic area of the artery becomes

$$R(z) = \begin{cases} 1 - H \cos^2 \pi z & ; 0 \leq z \leq 1 \\ 1 & ; \text{otherwise} \end{cases} \quad (6.2.9)$$

Non – dimensional forms of equations (6.2.2) to (6.2.5) are

$$-2 \frac{\partial p}{\partial z} + \frac{1}{r} \frac{\partial}{\partial r} (r \tau_c) = 0 \quad (6.2.10)$$

$$\frac{\partial p}{\partial r} = 0 \quad (6.2.11)$$

$$-\frac{\partial v_c}{\partial r} = (\tau_c^{1/2} - \tau_0^{1/2})^2 \quad \text{for } \tau_c \geq \tau_0 \quad (6.2.12)$$

$$\frac{\partial v_c}{\partial r} = 0 \quad \text{for } \tau_c \leq \tau_0 \quad (6.2.13)$$

The dimensionless slip boundary conditions are

$$\left. \begin{aligned} \tau_c &= \text{Finite Value} & \text{at } r &= 0 \\ v_c &= v_s & \text{at } r &= R(z) \\ \frac{\partial v_c}{\partial r} &= \frac{\alpha}{\epsilon^{1/2}} (v_s - v_f) & \text{at } r &= R(z) \end{aligned} \right\} \quad (6.2.14)$$

$$\text{where } v_f = -2 \epsilon \frac{\partial p}{\partial z} \quad (6.2.15)$$

Applying condition (6.2.14) in equation (6.2.10), the shear stress τ_c and wall shear stress τ_R are obtained as:

$$\tau_c = -r \frac{\partial p}{\partial z} \quad (6.2.16)$$

$$\tau_R = -R \frac{\partial p}{\partial z} \quad (6.2.17)$$

From equations (6.2.16) and (6.2.17),

$$\frac{\tau_c}{\tau_R} = \frac{r}{R} \quad (6.2.18)$$

where $R = R(z)$

6.3 Method of Solution

Integrating equation (6.2.12) under conditions (6.2.14) and using the result (6.2.15), the velocity in the region $r_p \leq r \leq R(z)$ where $r_p = \frac{\bar{r}_p}{R_0}$ being the non – dimensional radius of the plug flow region, is given as:

$$v_c = \frac{R}{2\tau_R} \left[(\tau_R^2 - \tau_c^2) - \frac{8}{3} \tau_0^{1/2} (\tau_R^{3/2} - \tau_c^{3/2}) + 2\tau_0 (\tau_R - \tau_c) \right] - \frac{\epsilon^{1/2}}{\alpha} (\tau_R^{1/2} - \tau_0^{1/2})^2 + \frac{2\epsilon\tau_R}{R} \quad (6.3.1)$$

Within plug flow region i.e. $0 \leq r \leq r_p$, $\tau_c = \tau_0$ at $r = r_p$, therefore the plug flow velocity is

$$v_p = \frac{R}{2\tau_R} \left[\tau_R^2 - \frac{1}{3} \tau_0^2 - \frac{8}{3} \tau_0^{1/2} \tau_R^{3/2} + 2\tau_0 \tau_R \right] - \frac{\epsilon^{1/2}}{\alpha} (\tau_R^{1/2} - \tau_0^{1/2})^2 + \frac{2\epsilon\tau_R}{R} \quad (6.3.2)$$

Now the volumetric flow rate in the dimensionless form for the region $0 \leq r \leq R(z)$ is obtained as:

$$\begin{aligned} Q &= 4 \int_0^R r v(r) dr \\ &= 4 \int_0^{r_p} r v_p dr + 4 \int_{r_p}^R r v_c dr \end{aligned}$$

Hence

$$Q = \frac{R^3}{2\tau_R^3} \left(\tau_R^4 - \frac{16}{7} \tau_0^{1/2} \tau_R^{7/2} + \frac{4}{3} \tau_0 \tau_R^3 - \frac{1}{21} \tau_0^4 \right) - \frac{2\epsilon^{1/2}}{\alpha} R^2 (\tau_R^{1/2} - \tau_0^{1/2})^2 + 4 \in R\tau_R \quad (6.3.3)$$

If $\tau_0 \ll \tau_R$ i.e. $\frac{\tau_0}{\tau_R} \ll 1$, then equation (6.3.3) becomes

$$Q = \frac{R^3}{2} \left(\tau_R - \frac{16}{7} \tau_0^{1/2} \tau_R^{1/2} + \frac{4}{3} \tau_0 \right) - \frac{2\epsilon^{1/2}}{\alpha} R^2 (\tau_R^{1/2} - \tau_0^{1/2})^2 + 4 \in R\tau_R \quad (6.3.4)$$

which gives us the wall shear stress for the stenosed artery as

$$\tau_R = \left[\frac{\phi_1}{2\phi_3} \tau_0^{1/2} + \left\{ \frac{42\alpha Q}{\phi_3} + \frac{(\phi_1^2 - 4\phi_2\phi_3)}{4\phi_3^2} \tau_0 \right\}^{1/2} \right]^2 \quad (6.3.5)$$

where

$$\left. \begin{aligned} \phi_1 &= 24R^2(2\alpha R - 7\epsilon^{1/2}) \\ \phi_2 &= 28R^2(\alpha R - 3\epsilon^{1/2}) \\ \phi_3 &= 21R(\alpha R^2 - 4R\epsilon^{1/2} + 8\alpha\epsilon) \end{aligned} \right\} \quad (6.3.6)$$

The pressure gradient is obtained by using equation (6.3.5) in equation (6.2.17) as:

$$\frac{\partial p}{\partial z} = -\frac{1}{R} \left[\frac{\phi_1}{2\phi_3} \tau_0^{1/2} + \left\{ \frac{42\alpha Q}{\phi_3} + \frac{(\phi_1^2 - 4\phi_2\phi_3)}{4\phi_3^2} \tau_0 \right\}^{1/2} \right]^2 \quad (6.3.7)$$

6.4 Results and Discussion

The velocity profile for the axial velocity in the non – plug flow region has been derived in equation (6.3.1) and the graphical discussions of the results are mentioned in figures 6.1(a) and 6.1(b).

Figure 6.1(a) shows the changes in the axial velocity along axial distance for the different values of the permeability ϵ , slip parameter α , stenosis height H and yield stress τ_0 with some fixed values $\tau_R = 0.070$ and $\tau_c = 0.030$. The axial velocity increases when the wall permeability increases but it decreases when slip parameter, stenosis height and the yield stress increase.

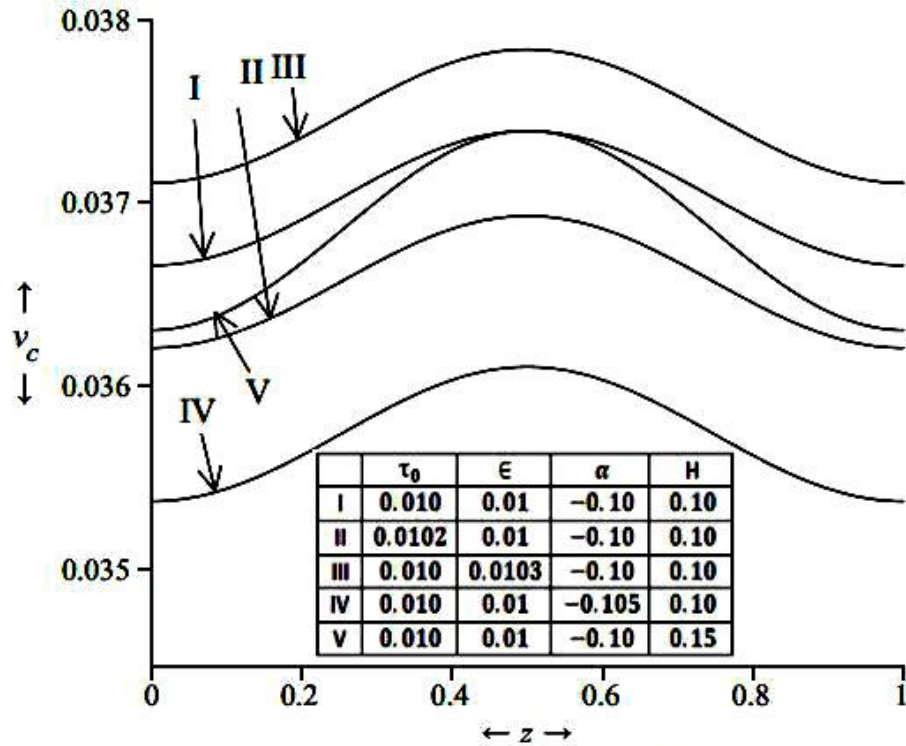


Figure 6.1 (a): Variation of Axial velocity Along Axial Distance for Different Values of the Permeability ϵ , Slip Parameter α , Stenosis Height H and Yield Stress τ_0 with Some Fixed Values $\tau_R = 0.070$ and $\tau_c = 0.030$

Figure 6.1(b) represents the variations of the axial velocity versus radial distance for the various values of the permeability ϵ , slip parameter α and yield stress τ_0 with some fixed values $\tau_R = 0.070$ and $\tau_c = 0.030$. The graph of axial velocity shows a fall up to the stenosis and then rise along the radius of the artery. The axial velocity increases with increase in wall permeability whereas it decreases as slip parameter and yield stress increase.

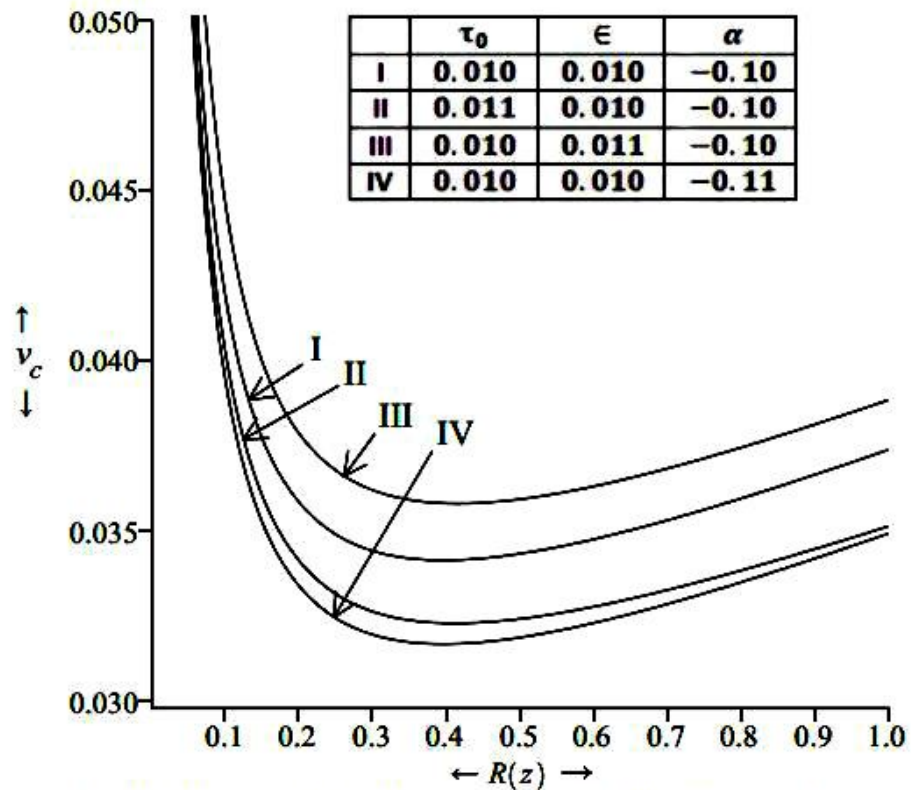


Figure 6.1 (b): Variation of Axial velocity Along Radial Distance for Different Values of the Permeability ϵ , Slip Parameter α , and Yield Stress τ_0 with Some Fixed Values $\tau_R = 0.070$ and $\tau_c = 0.030$.

The graphical details of the axial velocity for the plug flow area obtained through equation (6.3.2) has been shown in figures 6.2(a) and 6.2(b).

Figure 6.2(a) gives the variations in plug flow velocity along the arterial axis for different values of the permeability ϵ , stenosis height H and yield stress τ_0 with some fixed values $\tau_R = 0.070$ and $\tau_c = 0.030$. The plug flow velocity increases with increase in the wall permeability but it decreases when the yield stress, slip parameter and the stenosis height increase.

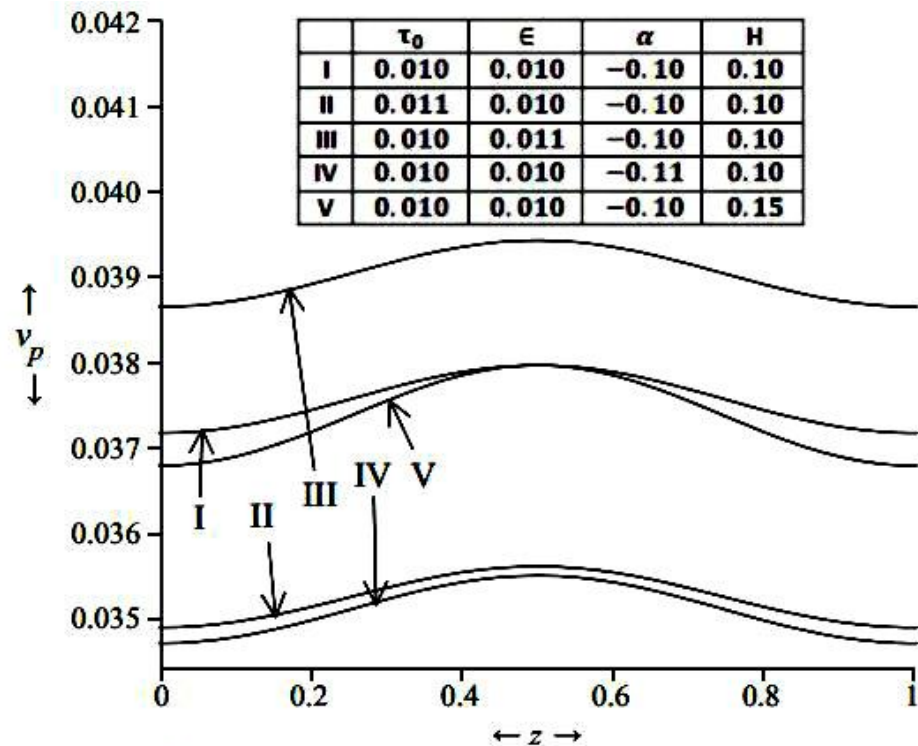


Figure 6.2 (a): Variation of Plug Flow Velocity Along Axial Distance for Different Values of the Permeability ϵ , Slip Parameter α , Stenosis Height H and Yield Stress τ_0 with Some Fixed Values $\tau_R = 0.070$ and $\tau_c = 0.030$.

Figure 6.2(b) shows the variations in plug flow velocity along radial distance for the various values of the permeability ϵ and yield stress τ_0 with some fixed values $\tau_R = 0.070$ and $\tau_c = 0.030$. The general behaviour of plug flow velocity is to decrease initially and then to increase with increments in radial distance. The plug flow velocity increases with the permeability but it decreases with the yield stress and slip parameter.

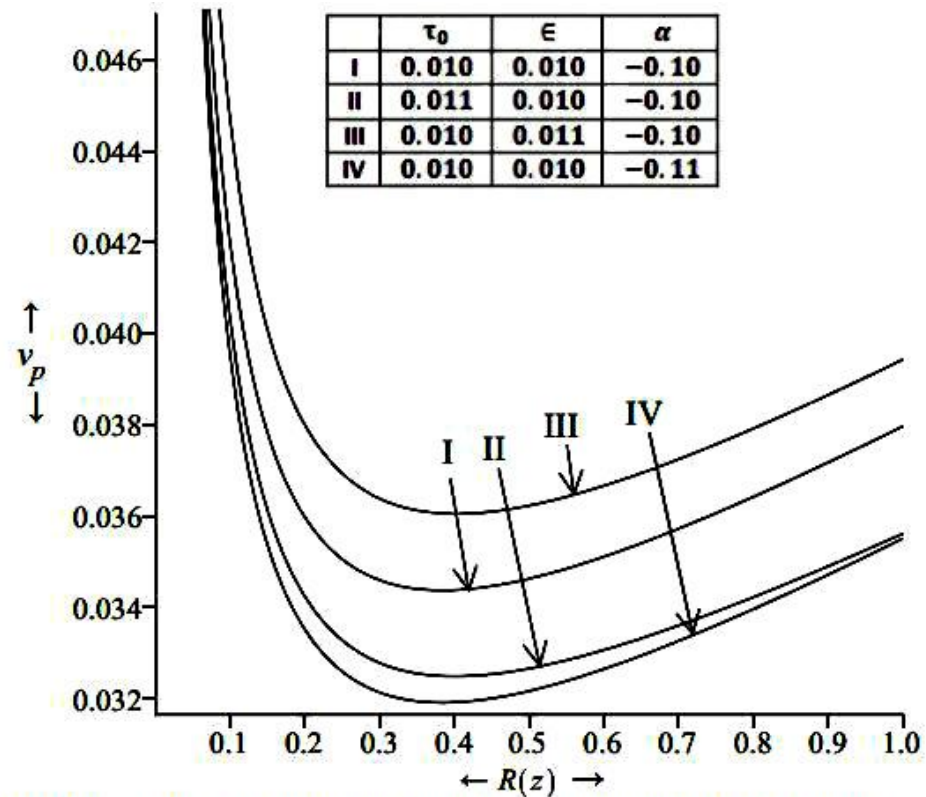


Figure 6.2 (b): Variation of Plug Flow Velocity Along Radial Distance for Different Values of the Permeability ϵ , Slip Parameter α and Yield Stress τ_0 with Some Fixed Values $\tau_R = 0.070$ and $\tau_c = 0.030$.

The variations of the volumetric flow rate obtained through equation (6.3.4) are plotted against the axial distance for the various values of the permeability ϵ , slip parameter α , stenosis height H and yield stress τ_0 with some fixed values $\tau_R = 0.070$ and $\tau_c = 0.030$ in figure 6.3(a). The figure shows that flow flux increases when the wall permeability increases but it decreases as the slip parameter, stenosis height and the yield stress increase.

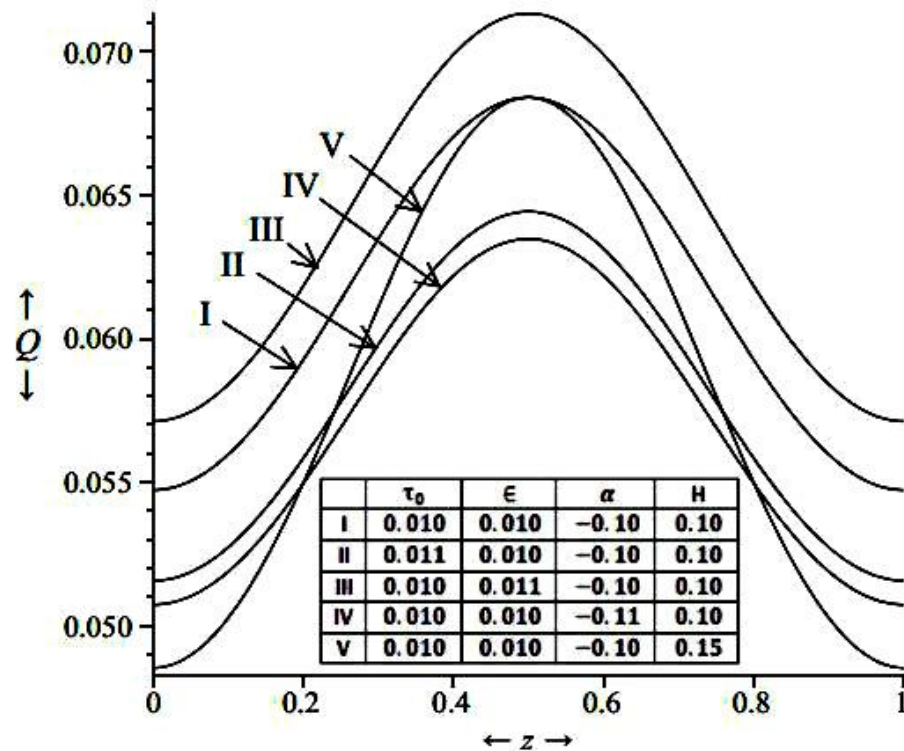


Figure 6.3 (a): Variation of Volumetric Flow Rate Along Axial Distance for Different Values of the Permeability ϵ , Slip Parameter α , Stenosis Height H and Yield Stress τ_0 with Some Fixed Values $\tau_R = 0.070$ and $\tau_c = 0.030$.

Figure 6.3(b) shows the variation in the volumetric flow rate versus the radial distance for the different values of the permeability ϵ , slip parameter α and yield stress τ_0 with some fixed values $\tau_R = 0.070$ and $\tau_c = 0.030$. The flow flux increases with increase in radial distance and the permeability and decreases with the increase in wall slip parameter and the yield stress.

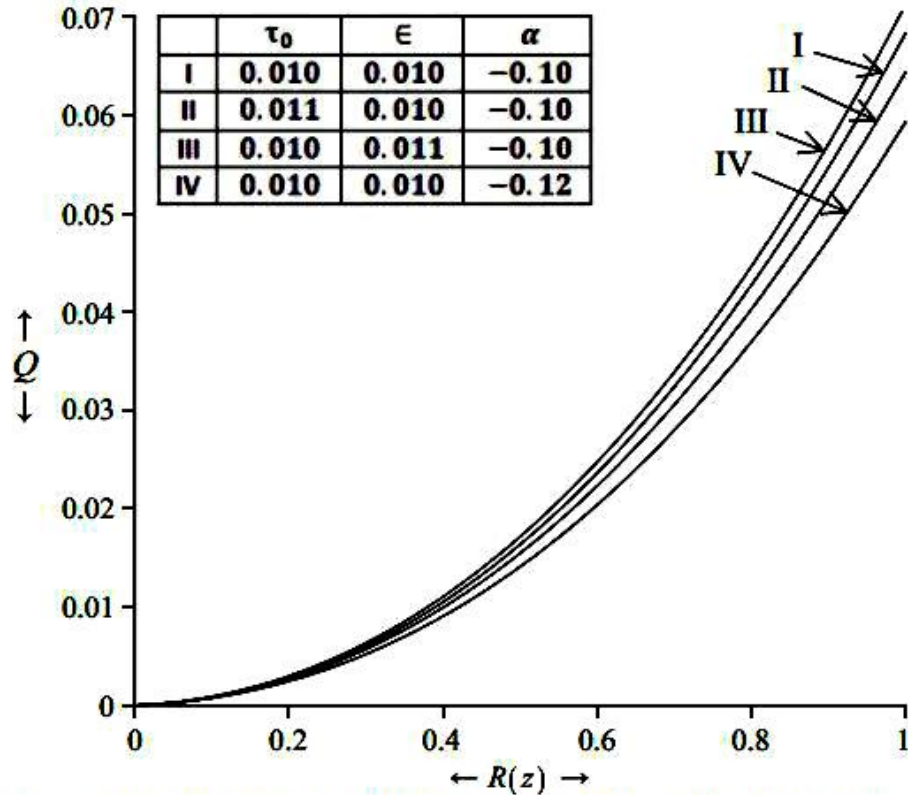


Figure 6.3 (b): Variation of Volumetric Flow Rate Along Radial Distance for Different Values of the Permeability ϵ , Slip Parameter α , and Yield Stress τ_0 with Some Fixed Values $\tau_R = 0.070$ and $\tau_c = 0.030$.

Figure 6.4(a) represents the variations of the wall shear stress obtained through equation (6.3.5) along axial distance for different values of the permeability ϵ , slip parameter α , stenosis height H and yield stress τ_0 with some fixed values $\tau_R = 0.070$, $\tau_c = 0.030$ and $Q = 1$. The wall shear stress increases with increase in the stenosis height, yield stress and the wall slip but it decreases as the wall permeability increases.

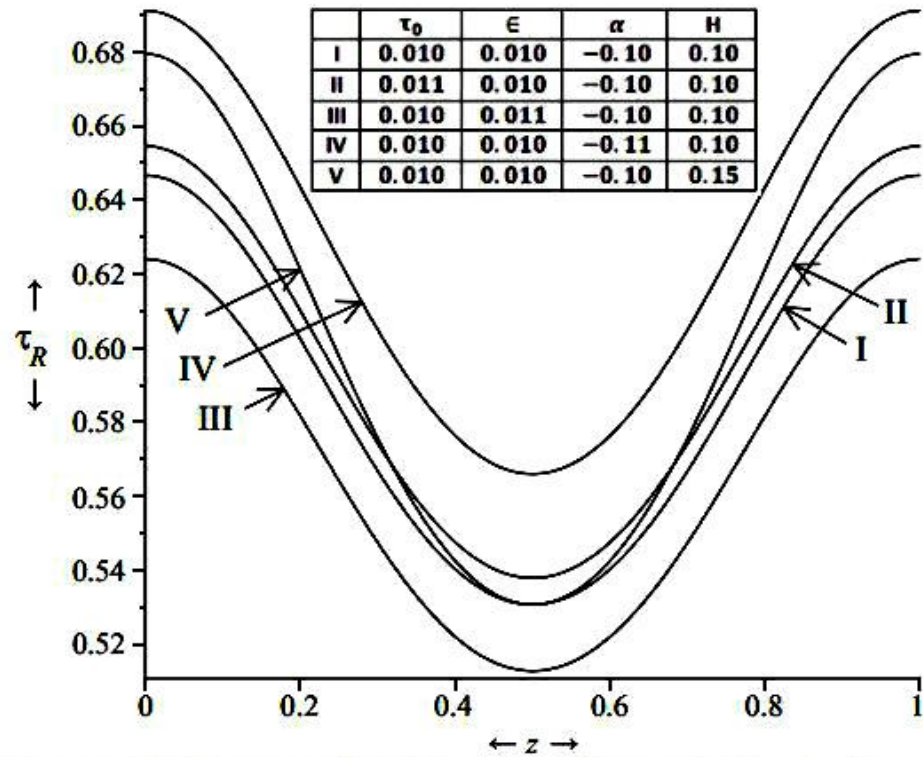


Figure 6.4 (a): Variation of Wall Shear Stress Along Axial Distance for Different Values of the Permeability ϵ , Slip Parameter α , Stenosis Height H and Yield Stress τ_0 with Some Fixed Values $\tau_R = 0.070$, $\tau_c = 0.030$ and $Q = 1$

Figure 6.4(b) shows the variation of wall shear stress along the radial distance for the different values of the permeability ϵ and slip parameter α with some fixed values $\tau_R = 0.070$, $\tau_c = 0.030$ and $Q = 1$. The wall shear stress decreases as the wall permeability increases while it increases when the wall slip increases.

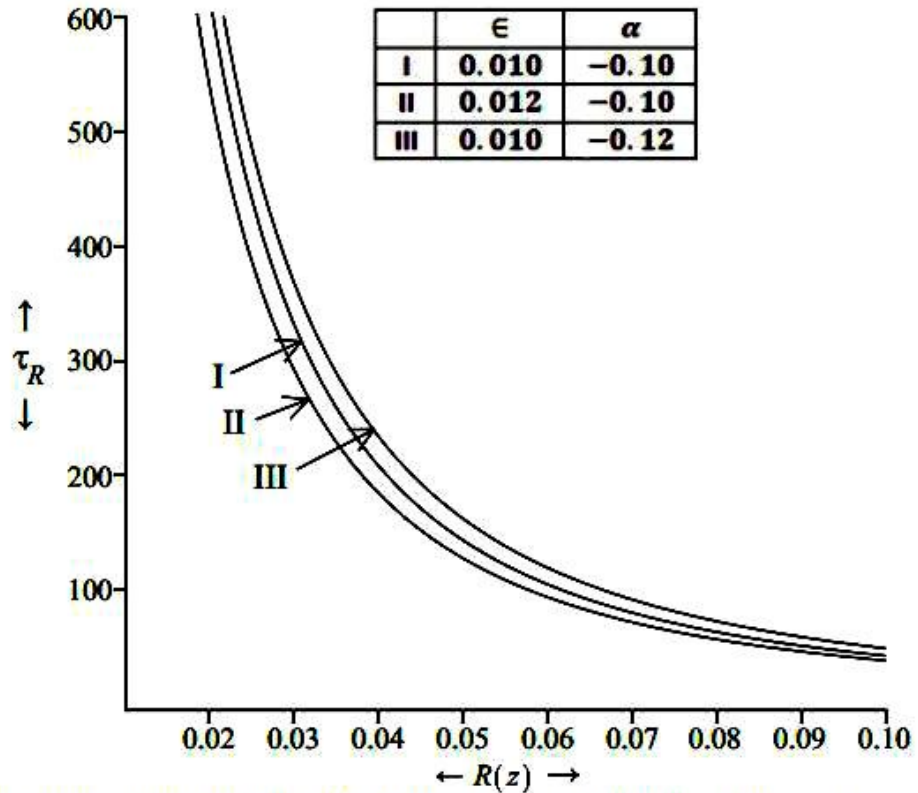


Figure 6.4 (b): Variation of Wall Shear Stress Along Radial Distance for Different Values of the Permeability ϵ and Slip Parameter α with Some Fixed Values $\tau_R = 0.070$, $\tau_c = 0.030$, $\tau_0 = 0.010$ and $Q = 1$.

Figure 6.5(a) shows the variations of the pressure gradient derived through equation (6.3.7) along the axial distance for the different values of the permeability ϵ , slip parameter α , stenosis height H and yield stress τ_0 with some fixed values $\tau_R = 0.070$, $\tau_c = 0.030$ and $Q = 1$. The figure shows that pressure gradient increases with increase in the wall permeability while it decreases as the slip parameter, yield stress and the stenosis height increase.

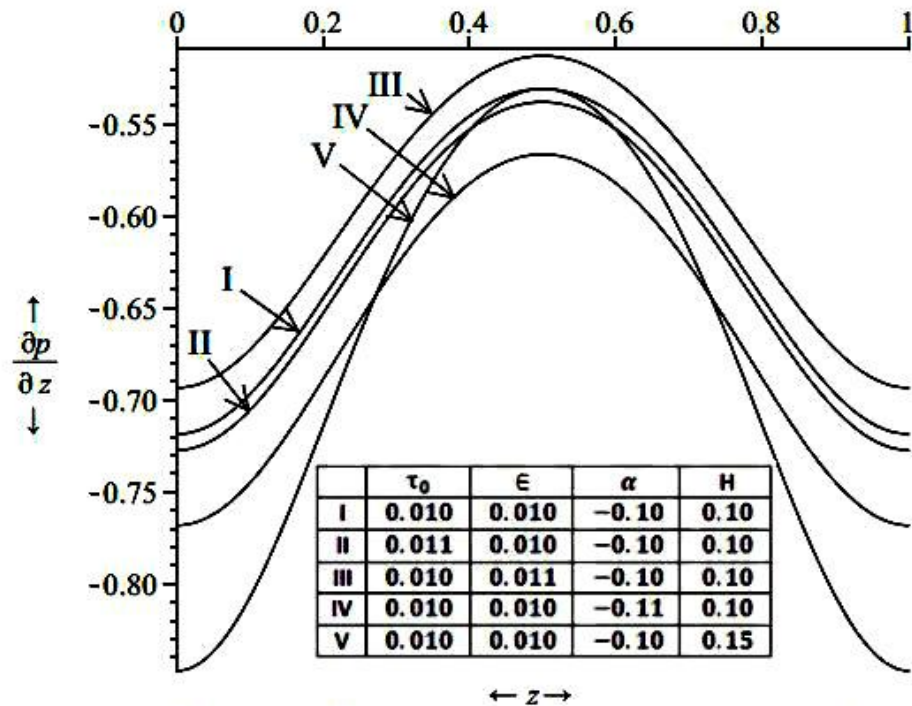


Figure 6.5 (a): Variation of Pressure Gradient Along Axial Distance for Different Values of the Permeability ϵ , Slip Parameter α , Stenosis Height H and Yield Stress τ_0 with Some Fixed Values $\tau_R = 0.070$, $\tau_c = 0.030$ and $Q = 1$.

Figure 6.5(b) represents variations of the pressure gradient versus the radial distance for the different values of the permeability ϵ , slip parameter α , stenosis height H and yield stress τ_0 with some fixed values $\tau_R = 0.070$, $\tau_c = 0.030$ and $Q = 1$. The pressure gradient exhibits increase along the arterial axis. It decreases with the increase in the permeability and the wall slip.

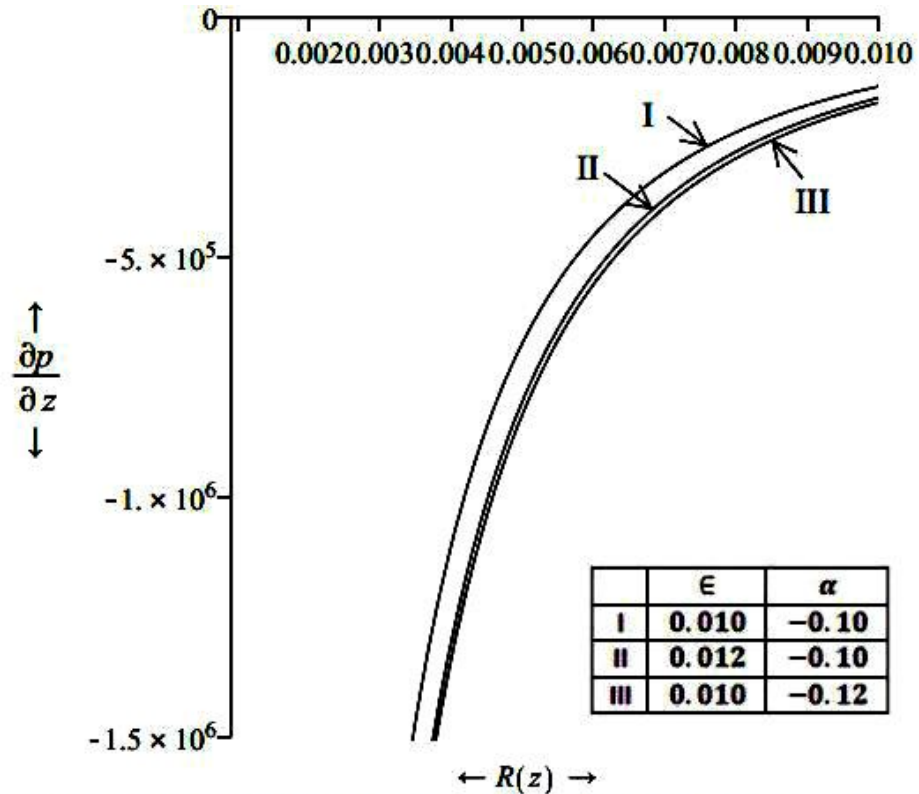


Figure 6.5 (b): Variation of Pressure Gradient Along Radial Distance for Different Values of the Permeability ϵ and Slip Parameter α with Some Fixed Values $\tau_R = 0.070$, $\tau_c = 0.030$, $\tau_0 = 0.010$ and $Q = 1$.

Table 6.1 shows the variations of the wall shear stress and the pressure gradient versus yield stress along the radial distance. It exhibits that the wall shear stress decreases with increase in radial distance but it increases as the yield stress increases. The pressure gradient increases with the increase in radial distance and decreases when the yield stress increases.

Table 6.1: Wall Shear Stress and Pressure Gradient versus Radial Distance and Yield Stress.

τ_0	R = 0.1		R = 0.5		R = 1.0	
	τ_R	$\frac{\partial p}{\partial z}$	τ_R	$\frac{\partial p}{\partial z}$	τ_R	$\frac{\partial p}{\partial z}$
0.010	41.894	- 418.948	1.9830	- 3.9458	0.5307	- 0.9770
0.015	42.138	- 421.387	2.0453	- 4.0600	0.5642	- 1.0223
0.020	42.344	- 423.448	2.0986	- 4.1558	0.5932	- 1.0614

6.5 Conclusion

The study shows that the axial velocity in both plug and non – plug flow regions, flow flux and the pressure gradient increase along axial and radial distances when the arterial wall becomes more porous. The wall shear stress decreases with increase in the wall porosity but it increases as the slip parameter along axial and radial distances increases. The skin friction decreases when the stenosis height increases along axial distance. The axial velocity, flow flux and the pressure gradient decrease along the axial distance when the slip parameter and the stenosis height increase. The axial velocity, plug flow velocity, flow flux decrease along axial distance when yield stress increases which verifies the author's previous work in chapter 2 of this thesis.

REFERENCES

REFERENCES

- [1] **Barbee, J. H. and Cokelet, G. R. (1971):** The Fahraeus effect, *Microvasc. Res.*, Vol. 34, pp. 6 – 21.
- [2] **Beavers, G. S. and Joseph, D. D. (1967):** Boundary conditions at a naturally permeable wall, *J. Fluid Mech.*, Vol. 30, No. 1, pp. 197 – 207.
- [3] **Biswas, D. and Laskar, R. B. (2011):** Steady flow of blood through a stenosed artery: A non – Newtonian fluid model, *Assam Univ. J. Sc. & Tech.*, Vol. 7, No. 11, pp. 144 – 153.
- [4] **Blair, G. W. S. (1959):** An equation for the flow of blood, plasma and serum through glass capillaries, *Nature*, Vol. 183, pp. 613 – 614.
- [5] **Burton, A. C. (1966):** Introductory text, *Physiology and Biophysics of Circulation*, Year Book Medical Publisher, Chicago, Il.
- [6] **Calo, V. M.; Brasher, N. F.; Bazilevs, Y. and Hughes, T. J. R. (2008):** Multiphysics model for blood flow and drug transport with application to patient specific coronary artery flow, *Comput. Mech.*, Vol. 43, Issue 1, pp. 161 – 177.
- [7] **Casson, N. (1959):** A flow equation for pigment oil suspensions of printing ink type, In *Rheology of Dispersed System* (Edited by Mill, C. C.), Pergamon Press, London, pp. 84 – 102.
- [8] **Chakravarty, S. (1987):** Effects of stenosis on the flow behaviour of blood in an artery, *Int. J. Engg. Sci.*, Vol. 25, pp. 1003 – 1016.

- [9] **Chakravarty, S. and Mandal, P. K. (1994):** Mathematical modelling of blood flow through an overlapping arterial stenosis, *Mathematical and Computer Modelling*, Vol. 19, No. 1, pp. 59 – 70.
- [10] **Charm, S. E. and Kurland, G. (1965):** Viscometry of human blood for shear rate of 0 – 100,000 sec⁻¹, *Nature*, Vol. 206, pp. 617 – 618.
- [11] **Chaturani, P. and D. Biswas (1983):** A theoretical study of blood flow through stenosed artery with velocity slip at the wall., *Proc. First Int. Symposium on Physiological Fluid Dynamics*, IIT Madras, India, pp. 23 – 26.
- [12] **Chaturani, P. and Palanisamy, V. (1990):** Casson fluid model of pulsatile flow of blood flow under periodic body acceleration, *Biorheology*, Vol. 27, Issue 5, pp. 619 – 630.
- [13] **Chaturani, P. and Samy, R. P. (1986):** Pulsatile flow of a Casson fluid through stenosed arteries with application to blood flow, *Biorheology*, Vol. 23, pp. 499 – 511.
- [14] **Chen, J. and Lu, X. Y. (2006):** Numerical investigation of the non – Newtonian pulsatile blood flow in a bifurcation model with a non-planar branch, *Journal of Biomechanics*, Vol. 39, Issue 5, pp. 818 – 832.
- [15] **Cho, Y. I. and Kensey, K. R. (1991):** Effects of the non-Newtonian viscosity of blood on flows in a diseased arterial vessel. Part 1: Steady Flows, *Biorheology*, Vol. 28, Issue 3 – 4, pp. 241 – 262.
- [16] **Das, B. and Batra, R. L. (1995):** Non-Newtonian flow of blood in an arteriosclerotic blood vessel with rigid permeable walls, *J. Theo. Biol.*, Vol. 175, Issue 1, pp. 1 – 11.

- [17] **Dash, R. K.; Mehta, K. N. and Jayaraman, G. (1997):** Effect of yield stress on the flow of a Casson fluid in a homogeneous porous medium bounded by a circular tube, *Applied Scientific Research*, Vol. 57, Issue 2, pp. 133 – 149.
- [18] **Dash, R. K; Mehta, K. N. and Jayaraman, G. (1996):** Casson fluid flow in a pipe filled with a homogeneous porous medium, *Int. J. Eng. Sc.*, Vol. 34, No. 10, pp. 1145 – 1156.
- [19] **Despande, M. D.; Giddens, D. P. and Mabon, R. F. (1976):** Steady laminar flow through modelled vascular stenosis, *J. Biomech.*, Vol. 9, pp. 165 – 174.
- [20] **Eldesoky, I. M. (2012):** Slip effects on the unsteady MHD pulsatile blood flow through porous medium in an artery under the effect of body acceleration, *International Journal of Mathematics and Mathematical Sciences*, Vol. 2012, Article ID 860239, 26 pages.
- [21] **Fahraeus, R. (1929):** The suspension stability of blood, *Physiol. Rev.*, Vol. 9, pp. 241 – 274.
- [22] **Fahraeus, R. and Lindqvist, T. (1931):** Viscosity of blood in narrow capillary tubes, *Am. J. Physiol.*, Vol. 96, pp. 562 – 568.
- [23] **Gupta, B. B.; Nigam, K. M. and Jaffrin, M. Y. (1982):** A three layer semi – empirical model for flow of blood and particular suspensions through narrow tubes, *Journal of Biomechanical Engineering*, Vol. 104, Issue 2, pp. 129 – 135.
- [24] **Haik, Y.; Pai, V. and Chen, C. J. (2001):** Apparent viscosity of human blood in a high static magnetic field, *J. Magnetism and Magnetic Material*, Vol. 225, No. 14, pp. 180 – 186.
- [25] **Haldar, K. (1985):** Effects of the shape of stenosis on the resistance to blood flow through an artery, *Bull. Math. Bio.*, Vol. 47, No. 4, pp. 545 – 550.

- [26] **Haldar, K. and Ghosh, S. N. (1994):** Effect of magnetic field on blood flow through indented tube in the presence of erythrocytes, *Ind. J. Pure Appl. Math.*, Vol. 25, No. 3, pp. 345 – 352.
- [27] **Haynes, R. H. and Burton, A. C. (1959):** Role of non – Newtonian behavior of blood in hemodynamics, *American Journal of Physiology*, Vol. 197, pp. 943 – 950.
- [28] **Huckaback, C. E. and Hahn, A. W. (1968):** A generalized approach to the modelling of arterial blood flow, *The Bull. Math. Biophys.*, Vol. 30, Issue 04, pp. 645 – 662.
- [29] **Huo, Y. and Kassab, G. S. (2006):** Pulsatile blood flow in the entire coronary arterial tree: Theory and experiment. *Am. J. Physiol. Heart Circ. Physiol.*, Vol. 291, Issue 3, pp. H1074 – H1087.
- [30] **Huyghe, J. M.; Arts, T.; Van Campen, D. H. and Reneman, R. S. (1992):** Porous medium finite element model of the beating left ventricle, *Am. J. Physiol.*, Vol. 262, Issue 4.2, pp. H1256 – H1267.
- [31] **Ishikawa, T.; Kawabata, N. and Imai, Y. (2007):** Numerical simulation of a low – hematocrit blood flow in a small artery with stenosis, *J. Biomechl. Sc. Engg.*, Vol. 2, No. 1, pp. 12 – 22.
- [32] **Jogie, D. and Bhatt, B. (2012):** Flow of immiscible fluids in a naturally permeable channel, *Int. J. Pure and Appl. Math.*, Vol. 78, No. 3, pp. 435 – 449.
- [33] **Jung, H.; Choi, J. W. and Park, C. G. (2004):** Asymmetric flows of non – Newtonian fluids in symmetric stenosed artery, *Korea-Australia Rhe. J.*, Vol. 16, No. 2, pp. 101 – 108.

- [34] **Jung, J.; Hassanein, A. and Lyczkowski, R. W. (2006):** Hemodynamic computation using multiphase flow dynamics in right coronary artery, *Ann. of Biomed. Eng.*, Vol. 34, Issue 3, pp. 393 – 407.
- [35] **Kenjeres, S. (2008):** Numerical analysis of blood flow in realistic arteries subjected to strong non – uniform magnetic fields, *Int. J. Heat and Fluid Flow*, Vol. 29, No. 3, pp. 752 – 764.
- [36] **Kumar, A.; Varshney, C. L. and Singh, V. P. (2012):** Performance modelling and study of blood flow in vessels with porous effects, *Appl. Math.*, Vol. 2, No. 5, pp. 166 – 170.
- [37] **Larson, R. E.; Higdon, J. J. L. (1986):** Microscopic flow near the surface of two-dimensional porous media. Part 1. Axial flow, *J. Fluid Mech.*, Vol. 166, pp. 449 – 472.
- [38] **Larson, R. E.; Higdon, J. J. L. (1987):** Microscopic flow near the surface of two-dimensional porous media. Part 2. Transverse flow. *Journal of Fluid Mechanics*, Vol. 178, pp. 119 – 136.
- [39] **Mandal, P. K. and Chakravarthy, S.; Mandal, A. and Amin, N. (2007):** Effect of body acceleration on unsteady pulsatile flow of non – Newtonian fluid through a stenosed artery, *Applied Mathematics and Computation*, Vol. 189 , Issue 1, pp. 766 – 779.
- [40] **Mazumdar, H. P.; Ganguly, U. N. and Venkatesan, S. K. (1996):** Some effects of magnetic field on flow of a Newtonian fluid through a circular tube, *Ind. J. Pure and Appl. Math.*, Vol. 5, pp. 519 – 524.
- [41] **Merrill, E. W.; Benis, A. M.; Gilliland, E. R.; Sherwood, T. K. and Salzman, E. W. (1965):** Pressure flow relations of human blood in hollow fiber at low flow rates, *J. Appl. Physiol.*, Vol. 20, pp. 954 – 967.

- [42] **Mernone, A.V. and Mazumdar, J. N. (2002):** A mathematical study of peristaltic transport of a Casson fluid, *Mathematical and Computer Modelling*, Vol. 35, pp. 895 – 912.
- [43] **Merrill, E. W.; Cokelet, G. C.; Britten, A. and Wells, R. E. (1963):** Non – Newtonian rheology of human blood: Effect of fibrinogen deduced by subtraction. *Circulation Research*, Vol. 13, pp. 48 – 55.
- [44] **Mishra, B. K. and Verma, N. (2007):** Effects of porous parameter and stenosis on the wall shear stress for the flow of blood in human body, *Res. J. Medicine and Medical Sc.*, Vol. 2, pp. 98 – 101.
- [45] **Mishra, B. K.; Pradhan, P. and Panda, T. C. (2008):** Effect of Resistance Parameter on uniform and non – uniform portion of artery for non – Newtonian fluid model of blood flow through an arterial stenosis, *Journal of modern Mathematics and Statistics*, Vol. 2, No. 6, pp. 203 – 206.
- [46] **Mishra, S.; Siddiqui, S.U. and Medhavi, A. (2011):** Blood flow through a composite stenosis in an artery with permeable wall, *Applications and Applied Math.*, Vol. 6, Issue 11, pp. 1798 – 1813.
- [47] **Misra, J. C. and Sahu, B. K. (1988):** Flow through blood vessels under the action of a periodic acceleration field: A mathematical analysis, *Comput. Math. Appl.*, Vol. 16, Issue 12, pp. 993 – 1016.
- [48] **Misra, J. C. and Chakravorty, S. (1986):** Flow in arteries in the presence of stenosis, *J. Biomech.*, Vol. 19, No. 11, pp. 1907 – 1918.
- [49] **Misra, J. C. and Kar, B. K. (1989):** Momentum integral method for studying flow characteristic of blood through stenosed vessel”, *Biorheology*, Vol. 26, No. 1, pp. 23 – 35.

- [50] **Misra, J. C. and Shit, G. C. (2007):** Effect of magnetic field on blood flow through an artery: A numerical model, *J. Comput. Tech.*, Vol. 12, No. 4, pp. 3 – 16.
- [51] **Misra, J. C. and Shit, G. C. (2007):** Role of slip velocity in blood flow through stenosed arteries: A non – Newtonian model, *Journal of Mechanics in Medicine and Biology*, Vol. 7, No. 3, pp. 337 – 353.
- [52] **Misra, J. C.; Patra, M. K. and Misra, S. C. (1993):** A non – Newtonian fluid model for blood flow through arteries under stenotic conditions, *Journal of Biomechanics*, Vol. 26, No. 9, pp. 1129 – 1141.
- [53] **Misra, J. C.; Sinha, A. and Shit, G. C. (2011):** Mathematical modelling of blood flow in a porous vessel having double stenoses in the presence of an external magnetic field, *Int. J. Biomath.*, Vol.4, Issue 2, pp. 207 – 225.
- [54] **Nardinocchi, P.; Pontrelli, G. and Teresi, L. (2005):** A one – dimensional model for blood flow in pre-stressed vessels. *Eur. J. mech. – A / Solids*, Vol. 24, pp. 23 – 33.
- [55] **Nubar, Y. (1971):** Blood flow, slip, and viscometry, *Biophysical Journal*, Vol. 11, No. 3, pp. 252 – 264.
- [56] **Parmar, L.; Kulshreshtha, S. B. and Singh, D. P. (2013):** The role of magnetic field intensity in blood flow through overlapping stenosed artery: A Herschel – Bulkley model, *Adv. Appl. Sci. Res.*, Vol. 4, Issue 6, pp. 318 – 328.
- [57] **Peskin, C. S. (1977):** Numerical Analysis of Blood Flow in the Heart, *Journal of Computational Physics*, Vol. 25, Issue 3, pp. 220 – 252.
- [58] **Pralhad, R. N. and Schultz, D. H. (2004):** Modelling of arterial stenosis and its applications to blood diseases, *Math. Biosc.*, Vol. 190, pp. 203 – 220.

- [59] **Pramanik, S. (2014):** Casson fluid flow and heat transfer past an exponentially porous stretching surface in presence of thermal radiation, *Ain Shams Eng. J.*, Vol. 5, pp. 205 – 214.
- [60] **Rodbard, S. (1966):** Dynamics of Blood Flow in Stenotic Lesions, *Am. Heart J.*, Vol. 72, Issue 5, pp. 698 – 704.
- [61] **Rudraiah, N. (1985):** Coupled parallel flows in a channel and a bounding porous medium of finite thickness, *Journal of Fluids Engineering*, Vol. 107, Issue 3, pp. 322 – 329.
- [62] **Saito, G. E. and Vander Werff, T. J. (1975):** The importance of viscoelasticity in arterial blood flow models, *J. Biomech.*, Vol. 8, Issue 3 – 4, pp. 237 – 245.
- [63] **Sankar, D. S.; Goh, J. and Ismail, A. I. M. (2010):** FDM analysis for blood flow through stenosed tapered arteries, *Boundary Value Problems*, Vol. 2010, Article ID 917067.
- [64] **Shukla, J. B.; Parihar, R.S. and Rao, B. R. P. (1980):** Effects of stenosis on non – Newtonian flow of the blood in an artery, *Bull. Math. Bio.*, Vol. 42, pp. 283 – 294.
- [65] **Siddiqui, S. U.; Verma, N. K. and Gupta, R. S. (2010):** A mathematical model for pulsatile flow of Herschel – Bulkley fluid through stenosed arteries, *E – Journal of Sc. Tech.*, Vol. 4, No. 5, pp. 49 – 66.
- [66] **Singh, B.; Joshi, P. and Joshi, B. K. (2010):** Blood flow through an artery having radially non – symmetric mild stenosis, *Applied Mathematical Sciences*, Vol. 4, No. 22, pp. 1065 – 1072.
- [67] **Sinha, A.; Shit, G. C. and Kundu, P.K. (2013):** Slip effects on pulsatile flow of blood through a stenosed arterial segment under periodic body acceleration, *ISRN Biomed. Engg.*, Vol. 2013, Article ID 925876.

- [68] **Smith, N.P.; Pullan, A. J. and Hunter, P. J. (2002):** An anatomically based model of transient coronary blood flow in the heart, *SIAM J. Appl. Math.*, Vol. 62, pp. 990 – 1018.
- [69] **Song, F.; Xu, Y. and Li, H. (2007):** Blood flow in capillaries by using porous media model, *Journal of Central South University of Technology*, Vol.14, Issue 1, pp. 46 – 49.
- [70] **Spaan, J.; Kolyva, C.; Van Den Wijngaard, J.; Ter Wee, R., Van Horsen, P.; Piek, J. and Siebes, M. (2008):** Coronary structure and perfusion in health and disease, *Philos. Trans. A. Math. Phys. Eng. Sci.*, Vol. 366, No. 1878, pp. 3137 – 3153.
- [71] **Srivastava, L.M. (1985):** Flow of couple stress fluid through stenotic blood vessels, *Journal of Biomechanics*, Vol. 18, No. 7, pp. 479 – 485.
- [72] **Srivastava, V. P. (1995):** Particle – fluid suspension model of blood flow through stenotic vessels, *Int. J. Biomed. Comp.*, Vol. 38, pp. 141 – 154.
- [73] **Srivastava, V. P. (2007):** A theoretical model for blood flow in small vessels, *Applications and Applied Mathematics*, Vol. 2, Issue 1, pp. 51 – 65.
- [74] **Sud, V. K. and Sekhon, G. S. (1985):** Arterial flow under periodic body acceleration, *Bull. Math. Biol.*, Vol. 47, pp. 35 – 52.
- [75] **Suri, P. K. Suri and Pushpa, R. (1981):** Effect of static magnetic field on blood flow in a branch, *J. Pure and Appl. Math.*, Vol. 12, No. 7, pp. 907 – 918.
- [76] **Tzirtzilakis, E. E. (2005):** A mathematical model for blood flow in magnetic field, *Physics of Fluids*, Vol. 17, Article ID 077103, pp. 1 – 15.

- [77] **Usha, R. and Prema, K. (1999):** Pulsatile flow of particle fluid suspension model of blood under periodic body acceleration, ZAMP, Vol. 50, Issue 2, pp. 175 – 192.
- [78] **Volokh, K. Y. (2006):** Stresses in growing soft tissues, Acta Biomaterialia, Vol. 2, pp. 493 – 504.
- [79] **Westerhof, N.; Boer, C.; Lamberts, R. R. and Sipkema, P. (2006):** Cross-talk between cardiac muscle and coronary vasculature. *Physiol. Rev.* Vol. 86, issue 4, pp. 1263 – 1308.
- [80] **Womersley, J. R. (1955):** Method for the calculation of velocity, rate of flow and viscous drag in arteries when the pressure gradient is known, *J. Physiol.* 127, pp. 553 – 563.
- [81] **Yadav, S. S. and Kumar, K. (2012):** Bingham Plastic characteristic of blood flow through a generalized atherosclerotic artery with multiple stenoses, *Advances in Applied Science Research*, Vol. 3, No. 6, pp. 3551 – 3557.
- [82] **Young, D. F. (1968):** Effect of time-dependent stenosis on flow through a tube. *J. Manuf. Sci. Eng.*, Vol. 90, Issue 2, pp. 248 – 254.

BOOKS

- [1] **Bayliss, L. E. (1952):** Rheology of Blood and Lymph, In Deformation and flow in Biological Systems. A. Frey – Wyssling (Ed.), North Holland Publ. Co. Amsterdam.
- [2] **Charm, S. E. and Kurland, G. S. (1965):** Blood Rheology and Cardiovascular Fluid Dynamics (Ed. D.H. Bergel), Academic Press, London.
- [3] **Cokelet, G. R. (1972):** The Rheology of Human Blood: In Biomechanics (Ed. Y.C. Fung et al.), Prentice Hall, Englewood Cliffs, New Jersey.
- [4] **Copley, A. L. and G. Stainsby (1960):** Flow Properties of Blood. Pergamon press, Oxford.
- [5] **Dhein, S.; Delmar, M. and Mohr, F. W. (2005):** Practical Methods in Cardiovascular Research, Springer – Verlag, New York. LLC.
- [6] **E.O. Attinger (1964):** Pulsatile Blood Flow, McGraw – Hill, New York.
- [7] **Fung, Y. C. (1981):** Biomechanics: Mechanical Properties of Living Tissues, Ch. 3, Springer, New York.
- [8] **Fung, Y. C. (1964):** Biomechanics: Its Scope, History and Some Problems of Continuum Mechanics in Physiology, Applied Mechanics Review 21, pp. 1 – 20.
- [9] **Fung, Y. C. (1993):** Biomechanics, Springer.
- [10] **Kapur, J. N. (1985):** Mathematical Models in Biology and Medicine, Affiliated East – West Press Pvt. Ltd., New Delhi.
- [11] **Landau, L. D. and Lifshitz, E. M. (1959):** Fluid Mechanics, Vol. 6, Pergamon Press Ltd.

- [12] **Lih, M. M. (1975):** Transport Phenomena in Medicine and Biology, Wiley, New York.
- [13] **Mazumdar, J. N. (1992):** Biofluid Mechanics, World Scientific Publishing Pvt. Ltd, Singapore.
- [14] **McDonald, D. A. (1974):** Blood Flows in Arteries, 2nd Edition, Ch. 2, Arnold, London.
- [15] **Nichols, W. W. and O'Rourke, M. F. (1990):** McDonald's Blood Flow in Arteries. Theoretical, Experimental and Clinical Principles, 3rd edition, Edward Arnold, London.
- [16] **Sherwood, L. (2010):** Human Physiology: From Cells to Systems, 7th Edition, Cengage Learning, Belmont.
- [17] **Waite, L. (2005):** Biofluid Mechanics in Cardiovascular Systems, McGraw – Hill Professional Publishing.